N 70-29475 NASA-CR-66953

DYNAMIC PROPERTIES OF MODELLING CLAY

Stephen H. Crandall Leonard G. Kurzweil Anant K. Nigam Paul J. Remington

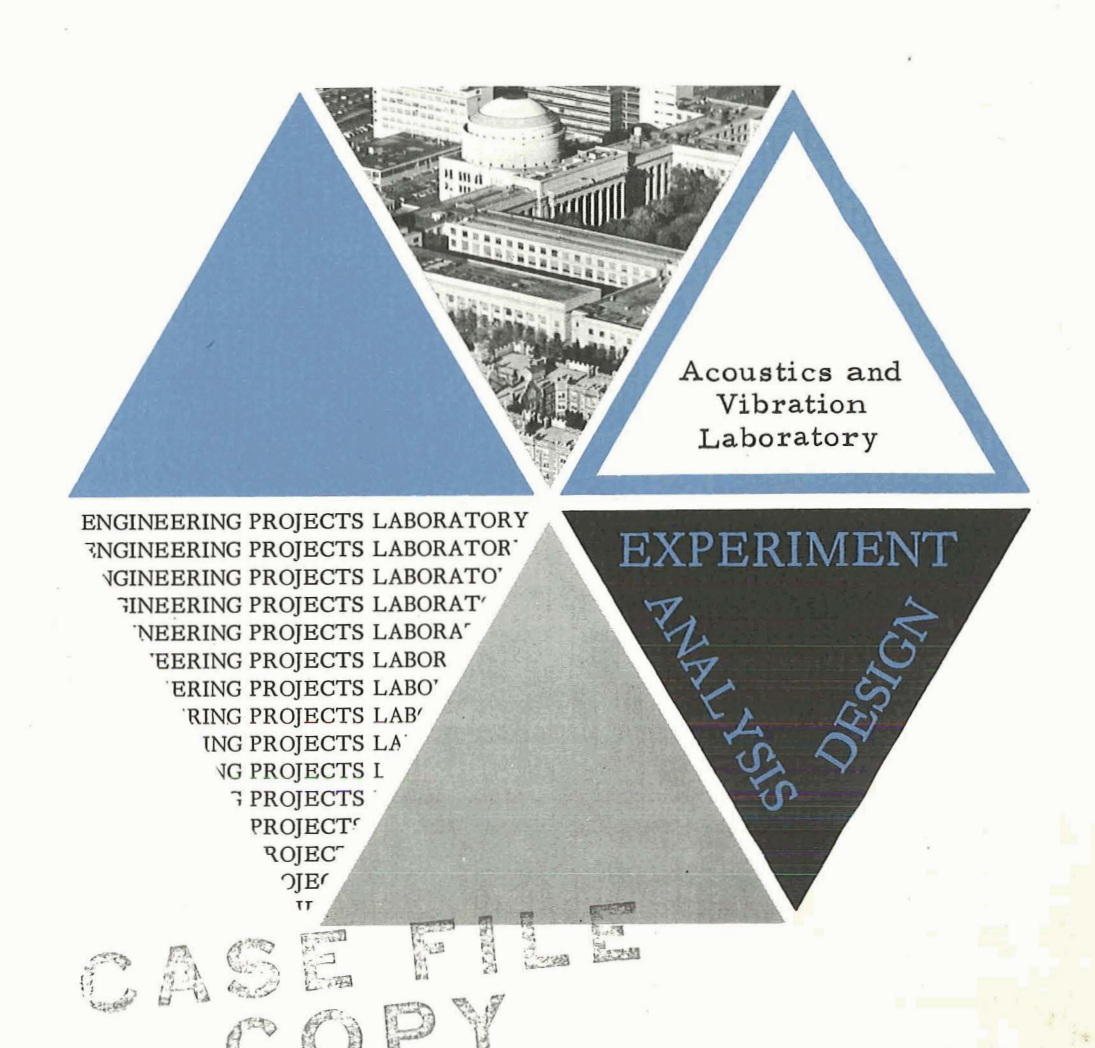
February 6, 1970

Report No. 76205-3

Grant No. NGR22-009-135

Acoustics and Vibration Laboratory
Massachusetts Institute of Technology
Cambridge, Massachusetts

This research was supported by the National Aeronautics and Space Administration



## TECHNICAL REPORT No. 76205-3

## DYNAMIC PROPERTIES OF MODELLING CLAY

by

Stephen H. Crandall
Leonard G. Kurzweil
Anant K. Nigam
Paul J. Remington

This research was supported by the National Aeronautics and Space Administration under Grant NGR-22-009-135.

February 6, 1970

Acoustics and Vibration Laboratory
Massachusetts Institute of Technology
Cambridge, Massachusetts
02139

## ABSTRACT

Dynamic Properties of Modelling Clay

by Stephen H. Crandall Leonard G. Kurzweil Anant K. Nigam Paul J. Remington

A number of dynamic characteristics of "Plasticine" have been measured for small strain simple harmonic oscillations in the frequency range 100 - 3000 Hz. In general the dynamic behavior of this material can be described by a simple linear isotropic viscoelastic model with complex moduli  $\overline{E}$  and  $\overline{G}$  where the values of  $\overline{E}$  and  $\overline{G}$  depend not only on frequency and temperature but also (due to thixotropy) on the prior history of large-strain deformation. Experimental limits on strain amplitude for validity of the linear model are given. Propagation velocities and loss factors for longitudinal waves in thin rods, plane dilational waves and simple shear waves are displayed. Poisson's ratio was determined by measuring both shear and dilational propagation velocities in the same specimen in a special sandwich configuration which permitted rapid changeover without introducing large strains. The measured properties of small samples are also used to predict the impedance of a rigid disk on the surface of a half-space of Plasticine and the predictions are compared with disk impedances measured on top of a large tub of Plasticine.

## Table of Contents

1.	Introduction	page	1
2.	Isotropic Viscoelastic Model		1
3.	Description of Tests on Rods		5
4.	Description of Dilational Tests		7
5.	Description of the Shear Tests		9
6.	Description of the Tests with Alternating		
	Dilation and Shear		11
7.	Test Results		15
8.	Temperature Effects		16
9.	Pressure Effects		20
10.	Nonlinear Effects		21
11.	Thixotropic Effects		22
12.	Dynamic Properties of Plasticine		27
13.	Predicted Admittance of a Disk on a Viscoelasti	c	
	Half-Space		35
14.	Measured Admittance of a Disk on the Surface of	1	
	a Large Tub of Plasticine		37
Acknowledgmen	<b>t</b>		39
References			41
Appendix A	Plane Waves in a Linear Viscoelastic Medium		A-1
Appendix B	Resonance-test relations for Uniform Rods		
	and Slabs of Linear Viscoelastic		
	Material		B-1
Appendix C	Resonance Test Relations for Sandwich Con-		
	figuration of Sec. 6		C-1
Captions for	Figures		
Figures			

by Stephen H. Crandall Leonard G. Kurzweil Anant K. Nigam Paul J. Remington

- Introduction. As part of an experimental study of noise transmission 1. between soil and building structures a model "soil" facility is desired. A possible candidate for the soil material is modelling clay which has many of the properties of natural clays. In addition, modelling clay appears to be homogeneous and relatively stable in its dynamic properties. This report describes the results of a number of tests that have been carried out on small samples of modelling clay in order to determine its dynamic behavior. The clay employed was white Plasticine manufactured by Harbutts, Bath, England. The precise composition is a trade secret but the main ingredients are undoubtedly fine kaolin clay mixed with mineral oil. Static strength properties of Plasticine have been reported by Baker [1] and the results of a wave propagation test along a thin rod of modelling clay have been reported by Calvit, Rader and Melville [2]. The dynamic tests described herein are chiefly resonance tests using thin rods or flat slabs of Plasticine. The frequencies used cover a range from 100 Hz to 3000 Hz.
- 2. <u>Isotropic Viscoelastic Model</u>. In order to interpret the results of our cests we have assumed that the dynamic behavior of Plasticine during a small strain oscillation at frequency  $\omega = 2\pi f$  can be represented by a linear isotropic viscoelastic model. With Re  $\{\sigma e^{i\omega t}\}$  and Re  $\{\tau e^{i\omega t}\}$  representing oscillating normal and shear stresses and Re  $\{\epsilon e^{i\omega t}\}$  and

Re  $\{\gamma e^{i\omega t}\}$  representing oscillating extensional and shear strains the constitutive relations for orthogonal axes x, y, and z are assumed to have the form

$$E(1 + i\eta)\varepsilon_{x} = \sigma_{x} - \nu(\sigma_{y} + \sigma_{z})$$

$$E(1 + i\eta)\varepsilon_{y} = \sigma_{y} - \nu(\sigma_{z} + \sigma_{x})$$

$$E(1 + i\eta)\varepsilon_{z} = \sigma_{z} - \nu(\sigma_{x} + \sigma_{y})$$

$$G(1 + i\eta)\gamma_{xy} = \tau_{xy}$$

$$G(1 + i\eta)\gamma_{yz} = \tau_{yz}$$

$$G(1 + i\eta)\gamma_{xz} = \tau_{xz}$$

$$(1)$$

where  $E(\omega)$  and  $G(\omega)$  are the real parts of complex tension and shear moduli  $\overline{E}$  and  $\overline{G}$ ,  $\eta(\omega)$  is a loss factor and  $\nu$  is a generalized Poisson's ratio. Since the loss factor for shear has been assumed to be the same as that for tension,  $\nu$  must be real and satisfy

$$G = \frac{E}{2(1+\nu)} \tag{2}$$

if the material is to be isotropic. Because of limitations and scatter in our data we cannot claim to have completely verified the validity of (1) and (2) as a model for Plasticine. We can only say that our results do not contradict the possibility that for small dynamic strains Plasticine can be represented by this model. The parameters in the model depend on the temperature and the prior large strain history of the sample as well as on the frequency of the oscillation.

A material satisfying (1) can support several types of attenuating plane waves. For propagation in the x-direction all stresses and strains in such waves would fluctuate in proportion to

Re 
$$\left\{e^{-\alpha x}e^{i\omega(t-\frac{x}{c})}\right\}$$
 (3)

where  $\alpha$  is an attenuation factor and c is a propagation velocity. The values of  $\alpha$  and c depend on the parameters in (1) and on the type of plane wave. For example, in the case of longitudinal motion in a thin uniform rod the relations are (see Appendix A)

$$c_{r} = \psi \sqrt{\frac{E}{\rho}} \qquad \qquad \alpha_{r} = \beta \frac{\omega}{c_{r}} \qquad (4)$$

where  $\rho$  is the mass density of the material and where the parameters  $\psi$  and  $\beta$  are functions of the loss factor  $\eta$ , given by

$$\psi^{2} = \frac{2(1+\eta^{2})}{\sqrt{1+\eta^{2}+1}}$$

$$\beta^{2} = \frac{\sqrt{1+\eta^{2}-1}}{\sqrt{1+\eta^{2}+1}}$$
(5)

Alternatively if the loss factor is interpreted as a loss tangent so that  $\eta$  = tan  $\delta$ , then

$$\psi^2 = \sec \delta \sec^2 \frac{\delta}{2} \qquad \beta = \tan \frac{\delta}{2}$$
 (6)

In the case of a plane dilational wave (the primary wave of seismology) the relations corresponding to (4) are

$$c_{p} = \psi \sqrt{\frac{G}{\rho} \frac{2(1-\nu)}{1-2\nu}} \qquad \alpha_{p} = \beta \frac{\omega}{c_{p}}$$
 (7)

with  $\psi$  and  $\beta$  given by (5) or (6). In the case of a simple transverse shear wave the corresponding relations are

$$\mathbf{c_s} = \psi \sqrt{\frac{G}{\rho}} \qquad \qquad \alpha_s = \beta \frac{\omega}{\mathbf{c_s}} \qquad (8)$$

where again  $\psi$  and  $\beta$  are given by (5) or (6).

Most of the dynamic tests described below lead to a simultaneous determination of a propagation speed and a loss factor at a single frequency for a single temperature and for a single state of previous large strain history. By using the appropriate relation (4), (7) or (8) it is possible to relate the measured propagation speed and loss factor to a value for the modulus E, 2G(1 - v)/(1 - 2v) or G, respectively. A limited study was made of the influence of frequency, temperature, pressure and large strain history on the small strain dynamic moduli and loss factors. effect of previous strain history was sufficiently large that nominally identical specimens could have a range of values for a small strain propagation velocity in which the extreme deviations from the mean were as much as 20% when tested under identical conditions. In most of the tests each specimen was subjected to only a single type of small strain motion: longitudinal motion in a rod, plane dilation or simple shear. These tests provided propagation speeds and loss factors for individual specimens with a particular type of motion but because of the differences in previous histories a meaningful comparison between the results for different types of motion could not be made. In order to accomplish

this last objective and thus to measure Poisson's ratio it was necessary to design a special test configuration in which the same specimen could alternately be excited in dilation and in shear with no intervening large strain.

3. <u>Description of Tests on Rods</u>. Thin rods of Plasticine were suspended from an impedance head driven by a shaker as shown in Fig. 1. The shaker excitation was a sinusoidal oscillation generated by a variable frequency oscillator and amplified by a power amplifier. The force and acceleration signals from the impedance head were amplified and the effective inertia force of the impedance head was subtracted from the force signal by a mass-cancellation circuit. The net force signal and the acceleration signal were observed on an oscilloscope and measured by a voltmeter. A block diagram of the instrumentation is shown in Fig. 2.

With any one rod, measurements were made at a number of resonant and antiresonant conditions. For a material satisfying (1) the resonances of a rod of length L occur for those frequencies where the wavelength  $\lambda_{\mathbf{r}} = \mathbf{c_r}/f = 2\pi\mathbf{c_r}/\omega \quad \text{of an attenuating wave of the form (3) is approximately equal to <math>2L/1$ , 2L/2, 2L/3, .... The antiresonances occur for those frequencies where  $\lambda_{\mathbf{r}}$  is approximately equal to 4L/1, 4L/3, 4L/5, .... More precisely the resonant and antiresonant conditions can be defined to occur when the net force and the acceleration are 90° out of phase with each other. Under these conditions (see Appendix B) the propagation velocity  $\mathbf{c_r}$  and the decay factor  $\beta$  of Eqs. 4, 5, and 6 are related to the force and acceleration amplitudes  $\mathbf{f_0}$  and  $\mathbf{a_0}$  by the pair of transcendental equations

$$\left| \frac{{\rm m_c a_o}}{{\rm f_o}} \right| = \phi_{\rm r} \frac{(1 + \beta^2) \sinh 2\beta \phi_{\rm r}}{\cosh 2\beta \phi_{\rm r} - \cos 2\phi_{\rm r}}$$
(9)

$$\sin 2\phi_{\mathbf{r}} = -\beta \sinh 2\beta\phi_{\mathbf{r}} \tag{10}$$

where  $m_{c}$  is the mass of the rod and

$$\phi_{\mathbf{r}} = \frac{\omega \mathbf{L}}{\mathbf{c}_{\mathbf{r}}} \tag{11}$$

The roots of (10) for  $\phi_r$  near  $\pi/2$ ,  $3\pi/2$ ,  $5\pi/2$  ... represent antiresonances and the roots near  $\pi$ ,  $2\pi$ ,  $3\pi$  ... represent resonances. The number of real roots for  $\phi_r$  depends on the magnitude of the loss factor  $\eta$  (there are at least three distinct resonances and three distinct antiresonances for  $0 < \eta < 0.3$ ).

In the test procedure the oscillator frequency was varied while the Lissajous pattern between the net force and acceleration signals was observed on the oscilloscope. At the 90° phase condition (represented by a circle when the signals were appropriately scaled) the force and acceleration amplitudes were measured. From the measured values of  $\omega$ , a and f Eqs. 9, 10, and 11 were used to calculate c and  $\beta$ . Finally the loss factor  $\eta$  was obtained from Eq. 5 or 6.

The Plasticine rods were of square cross section, 1/2 in. by 1/2 in., and varied in length from 3 in. to 15 in. The rods were made by working Plasticine into the collapsible mold shown in Fig. 3 using a screwdriver to tamp the material firmly into the mold and then removing the excess material by sliding a wooden block across the top of the mold. Sections about two feet long were removed from the mold and permitted to "cure" for

about a week at room temperature on a flat surface before being cut into smaller lengths for testing. The rods were attached to the impedance head by means of a stud with a 10 - 24 thread screwed into a hole in the Plasticine.

As an illustration of the type of results obtained from these tests, Fig. 4 shows the rod propagation velocity and loss factor derived from three anti-resonances and three resonances of a rod with L = 9 inches at T = 75° F. Similar results were obtained for a total of 15 rods ranging in length from L = 3 inches to L = 15 inches. These results are discussed in Sec. 12. Similar tests were performed with the specimen hanging in a temperature controlled box (see Sec. 8) and in a pressure chamber (see Sec. 9) to investigate the effects of ambient temperature and pressure. The same set-up was also used to investigate the effect of large strain bending on the small strain dynamic parameters (see Sec. 11).

4. <u>Description of the Dilational Tests</u>. Flat slabs of Plasticine were sandwiched between two aluminum disks which were vibrated axially. From the dynamic response of the combination the dilational wave speed and loss factor of the Plasticine were estimated. One disk, called the base mass, was suspended by soft rubber bands and excited axially by an impedance head driven by an electromagnetic shaker. The other disk, called the suspended mass, was designed so that additional aluminum disks could be fastened to it as shown in Fig. 5. All disks were 5 inches in diameter. The base mass was fixed at a value close to 2 lbm while, by using different combinations of the additional disks, the suspended mass could be set at values close to 2, 3, 4 or 5 lbm. The accelerations of both masses were observed on an oscilloscope and measured at those frequencies for which there was 90° phase difference between the motions of the

masses. A block diagram of the instrumentation is shown in Fig. 6.

Under the assumption that the aluminum masses remain rigid and that there is plane wave dilation in the clay (edge effects at the perimeter are neglected) the propagation velocity  $c_p$  and the loss factor  $\eta$  of Eqs. 7, 5 and 6 are related (see Appendix B) to the measured acceleration amplitude of the base mass  $a_b$  and the measured acceleration amplitude of the suspended mass  $a_b$  at the frequency  $\omega = 2\pi f$  for which there is a 90° phase difference between the accelerations by the following pair of transcendental equations:

$$\frac{m_{c}}{m_{s}} = \phi_{p} \tan \phi_{p} - \beta \phi_{p} \tanh \beta \phi_{\tilde{p}}$$
(12)

where  $\mathbf{m}_{\mathbf{c}}$  is the mass of the clay,  $\mathbf{m}_{\mathbf{s}}$  is the mass of the rigid suspended mass and

$$\phi_{\mathbf{p}} = \frac{\omega \mathbf{h}}{\mathbf{c}_{\mathbf{p}}} \tag{13}$$

where h is the thickness of the clay slab. From the measured values of  $a_s$ ,  $a_b$  and  $\omega$  Eq. 12 can be used to calculate  $\phi_p$  and  $\beta$  from which  $c_p$  and  $\eta$  follow from Eqs. 13, 5 and 6.

The test specimen was prepared by placing a large mass of clay between the aluminum disks and squeezing the assembly in a vice.

Excess clay forced out around the rim was trimmed off. The clay sandwich was then instrumented as shown in Fig. 5 and measurements were

made at the lowest frequency with 90° phase difference for each of the four possible values of the suspended mass magnitude. The frequency range available was limited to frequencies below about 1200 Hz by the requirement of rigidity for the aluminum disks. (When the base mass alone was excited by the impedance head the fundamental resonance occured at 3150 Hz).

As an illustration of the type of results obtained for these tests Fig. 7 shows the dilational propagation velocity and the loss factor obtained from a clay sandwich 0.7 inches thick at 75° F. The results  $\Lambda$  were obtained immediately after forming the specimen in the vice while the results B were obtained on the same specimen two days later.

Plasticine was sandwiched between the surface of a horizontal slip table and a sheet glass cover which acted as a suspended mass. The slip table was then excited horizontally which caused the clay slab to vibrate with a predominately shearing deformation. From measurements of the dynamic response of the system at resonance the shear wave propagation velocity and loss factor of the Plasticine were estimated.

The clay slab measured 9 x 16 inches and was 1/2 inch thick. Its mass was 5.31 lbm. The clay was pounded into a collapsible frame placed on the slip table and excess material was removed by sliding a straight edge over the top. The suspended mass was initially a glass sheet 1/16 inch thick pressed onto the top of the clay. A uniformly distributed dead load of 144 lbs. was left on the glass for 24 hours to assure good contact. The initial suspended mass weighed 0.901 lb. After testing

this combination, the suspended mass was increased by cementing a second glass sheet to the first using Eastman 910 adhesive. This process was repeated so as to obtain test results for five different values of suspended mass: 0.901 lbm, 2.55 lbm, 4.16 lbm, 6.55 lbm and 9.94 lbm.

The tests were resonance tests in which the slip table was vibrated horizontally and the horizontal accelerations of the slip table and the suspended mass were observed. Two different excitation schemes were employed. For small amplitude motions a small shaker (50 lb capacity) was attached to the slip table and the exciting force was developed by the inertial reaction from a 5-pound mass driven by the shaker. See Fig. 8. For large amplitude motions the slip table was driven by a large shaker (1500 lb. capacity) as shown in Fig. 9.

The frequency range for the shear tests was limited by resonances in the nominally rigid slip table (the first bending resonance of the slip table occured at 400 Hz, well below the test range of 600-1300 Hz). In an attempt to minimize the effect of nonuniform motion of the slip table and the suspended cover plate a survey of their horizontal motions was made at the locations indicated in Fig. 10. The magnitudes of the suspended masses were selected so that at the test frequencies the horizontal motions of the slip table were substantially of the same phase. In performing the tests the excitation frequency was adjusted until the signals from acceleratometers at locations T-1 and B-2 in Fig. 10 were 90° out of phase. The signals from these accelerometers were also taken to represent the effective amplitudes of the horizontal motions of the suspended mass and the slip-table base. A block diagram of the instrumentation employed is shown in Fig. 11.

Under the assumption that the slip table and the suspended glass cover plate remain rigid and that there is a plane shear wave in the clay (end effects at the edges of the clay slab are neglected) the shear wave propagation velocity  $c_s$  and the loss factor  $\eta$  are related to the measured acceleration amplitudes  $a_b$  and  $a_s$  of the slip table base and suspended cover plate at the frequency  $\omega=2\pi f$  for which there is a 90° phase difference between accelerations by equations of the same form as Eqs. 12 and 13 for the dilation tests. The only difference is that the subscript p (for primary wave) must everywhere be replaced by the subscript s (for shear wave); compare Eq. 8 with Eq. 7. By using five different values of the suspended mass for each sample of clay it was possible to use this test to estimate  $c_s$  and  $\eta$  for five different frequencies.

As an illustration of the type of results obtained from these tests Fig. 12 shows the shear propagation velocity and the loss factor obtained from a 1/2 inch thick clay slab at 75° F. These tests were used to study the effects of temperature and amplitude on the dynamic parameters. See Secs. 8, 10, and 11.

order to permit testing the same clay sample under fundamentally different types of deformation, under the same conditions of previous large strain history, a special test configuration was designed which essentially joined together the dilation test of Sec. 4 and the shear test of Sec. 5. A symmetrical sandwich consisting of two clay slabs between three metal slabs was assembled as shown in Fig. 13. The sandwich was then attached to a shaker-driven impedance head by a threaded stud in one of the two positions shown in Fig. 14. In the

configuration of Fig. 14(a) the oscillatory deformation of the clay is primarily tensile and compressive. If the edge effects are neglected it can be assumed that the clay undergoes plane-wave dilation. In the configuration of Fig. 14(b) the oscillatory deformation of the clay is primarily that of shear. If the end effects are neglected it can be assumed that the clay undergoes plane-wave shear deformation.

The sandwich was tested by observing the first antiresonance and first resonance in the position of Fig. 14(a). This provided data from which the dilational propagation velocity and loss factor could be estimated at two frequencies. The sandwich was then carefully disconnected and reconnected in the position of Fig. 14(b). Again the first antiresonance and the first resonance were observed and the data used to estimate the shear wave propagation velocity and loss factor at two frequencies. The entire process was then repeated. If the second set of estimated dynamic parameters were the same as the first it could be assumed that no increment of large strain had occurred and that the dilation and shear parameters obtained applied to the same large strain history. The dilation and shear parameters could then be inserted in Eqs. 7, and 8 to obtain an estimate for Poisson's ratio (see Sec. 12 and Eq. 20).

Each of the slabs in the sandwich was two inches square. The aluminum end slabs were 3/4 inch thick and the central steel slab was 1/2 inch thick. The clay slabs were 0.395 inch thick. At the test frequencies (under 3000 Hz for dilation and under 1300 Hz for shear) the metal slabs were essentially rigid (the first resonance of an aluminum end plate alone on the impedance head in the dilation configuration was at 9,500 Hz, and the first resonance of the central steel plate alone on the impedance head in the shear configuration was at 6,700 Hz).

The test procedure and instrumentation were essentially similar to those used in the tests on rods as described in Sec 3. The force signal from the impedance head was corrected to account for the inertia of the impedance head in front of the force gage by a mass cancellation Resonances and antiresonances were located at frequencies for circuit. which there was a 90° phase difference between the corrected force signal and the acceleration signal. In addition to manually recording the magnitudes of the signals under these conditions, we also extended the instrumentation so as to obtain continuous records of the corrected force and acceleration signal amplitudes, together with the phase angle between the signals, as functions of frequency. To simplify the presentation the input level to the shaker amplifier was servocontrolled so as to maintain a constant level of corrected force amplitude. A block diagram of the instrumentation is shown in Fig. 15. Typical x-y plots obtained in a dilation test are shown in Figs. 16 and 17. In Fig. 16 the corrected force and acceleration amplitudes are displayed for the frequency range 100 to 4000 Hz. Note the acceleration minimum at 1250 Hz and the acceleration maximum at 2650 Hz. Fig. 17 shows the phase angle between the corrected force signal and the acceleration. Note that the 90° phase condition occurs at 1320 Hz (antiresonance) and 2460 Hz (resonance). Corresponding x-y plots for a shear test are shown in Figs. 18 and 19.

In order to interpret the test results the clay sandwich shown in Fig. 13 was represented by the lumped parameter models of Fig. 20. The metal slabs are represented by rigid masses and the clay slabs are represented by springs with complex spring constants. The effect of the clay's distributed inertia was estimated by carrying out the data

reduction for two extreme cases. In the first, the clay mass was neglected altogether, and in the second, the mass of each clay slab was apportioned equally to the two adjoining metal slabs. For the dilational model of Fig. 20(a) the spring constant  $k_d$  was taken as

$$k_{\rm d} = \frac{2(1-\nu)}{1-2\nu} \frac{GA}{h}$$
 (14)

while for the shear model of Fig. 20 (b) the spring constant  $\mathbf{k}_{\mathbf{S}}$  was taken as

$$k_{s} = \frac{GA}{h} \tag{15}$$

where A is the area and h is the thickness of the clay slab. These results assume uniform strain fields in the clay (bulging at the edges is neglected). Improvements could be made at this point if three-dimensional elasticity solutions for k<sub>d</sub> and k<sub>s</sub> were available. If at a resonance or an antiresonance (defined by 90° phase angle between the net force and the driving point acceleration) the force and acceleration amplitudes and the frequency are recorded, it is possible (see Appendix C) to estimate the loss factor and spring constant of the clay at that frequency. Then using Eq. 14 or Eq. 15 together with Eqs. 5 to 8 one can estimate the dilational or shear wave propagation speed in the clay. Finally if both the dilational and shear speeds can be estimated at the same frequency then Poisson's ratio for this frequency can be determined from Eqs. 7 and 8.

As an illustration of the results obtained from these tests Fig. 21 shows how the shear propagation velocity corresponding to the first

antiresonance increased with time. Here the clay was molded into the sandwich, the plates were squeezed slightly and the excess clay trimmed off at t = 0. After this no further large strains were applied to the clay. The entire sandwich was gently alternated between the dilational and shear configurations where it was subjected to controlled low-level sinusoidal excitation. Fig. 21 shows that there is a systematic difference of about 7% between the results calculated by the two extreme procedures for accounting for the inertia of the clay. The same percentage discrepancy also appears in the dilational propagation speed with the result that the estimate for Poisson's ratio is substantially unaffected by the choice of procedure for accounting for the inertia of the clay. For simplicity all further results from the sandwich tests are reported only on the basis of the procedure B: the entire mass of each clay slab is apportioned equally to the adjacent metal slabs.

7. Test results. In most of the tests the data obtained for computing propagation velocities and loss factors were consistent and repeatable provided that the interval between tests was short and that the specimen remained undisturbed between tests. The dynamic response was linear provided that the oscillatory strain amplitude was small enough. In general propagation velocities were more precisely determined than loss factors. Unaccounted scatter in loss-factor determinations was an order of magnitude greater than the corresponding scatter in propagation velocities.

It soon became apparent however that there was considerable discrepancy in the values of propagation velocity when nominally identical specimens were tested or when the same specimen was tested on different days. Considerable effort was expended in tracking down the causes of these

measured. It was found that fluctuations of a few degrees Fahrenheit have a marked (but predictable) effect on propagation velocities.

Ambient pressure changes of a few psi have much smaller influence. It was found that one of the primary reasons for variations in values of propagation velocity was differences in the large-strain history of specimens. Immediately after remolding a specimen its propagation velocities are low. If no subsequent large strain occurs the propagation velocities increase monotonically, rapidly at first and then more and more slowly. If the specimen undergoes a large strain at any time there usually is a simultaneous drop in its propagation velocities followed by a gradual increase.

A detailed description of these results appears in Secs. 8-11 which follow.

Remperature Effects. The effects of ambient temperature on propagation velocity and loss factor were observed for a rod specimen and for a shear specimen. In the rod test a 3" rod was suspended as shown in Fig. 1 in a temperature controlled chamber. The tests were performed as described in Sec. 3 at temperatures ranging from 70° F. to 120° F. At each temperature the dynamic properties were measured at frequencies corresponding to the first antiresonance, the first resonance, the second antiresonance and the second resonance. In the shear test the clay slab with suspended mass of 9.94 lbm was tested as described in Sec. 5 at temperatures ranging from 66° F. to 82° F. The temperatures were obtained by changing the room temperature in the laboratory. The tests were performed after the internal temperature of the clay reached equilibrium with the surrounding air temperature. At

each temperature the dynamic properties were measured at the frequency corresponding to 90° phase difference between the acceleration of the base and the acceleration of the suspended mass. In both the rod and the shear tests the excitation level was kept sufficiently low that the dynamic response remained in the linear range.

The rod tests provided values of the rod propagation velocity  $c_r$  and the loss factor  $\eta$  for more than two dozen combinations of frequency and temperature ranging from 300 to 3000 Hz and from 70° F. to 120° F. In this range (and for this single specimen) the propagation velocity  $c_r$  was strongly dependent on temperature but only weakly dependent on frequency. For example, at a constant temperature the extreme values of  $c_r$  over a two-octave range of frequency seldom differed by more than 10% while, at a constant frequency, a decrease of about 4° F (in the neighborhood of 75° F) resulted in a 10% increase in  $c_r$ . This is illustrated in Fig. 22 which shows the approximate location of contour lines for constant levels of the rod propagation velocity  $c_r$  in the frequency—temperature plane. The contour lines were interpolated from measurements at 10° F intervals for the four frequencies indicated. Note the relatively systematic dependence of rod propagation speed on temperature and frequency represented by Fig. 22.

The corresponding values of the loss factor  $\eta$  showed no such systematic dependance. The approximate location of contour lines for constant levels of  $\eta$  is sketched in Fig. 23. Because of uncertainties in determining  $\eta$  it is not clear how much of the pattern in Fig. 23 represents experimental noise and how much represents a bona fide constitutive relation. The evidence suggests that for this specimen there is little (if any) correlation between loss factor and temperature but that there may be a correlation between loss factor and frequency.

Returning to the rod propagation velocity contours displayed in Fig. 22, we describe a simple condensation of the data. When, along each of the four modes indicated the ratio of the propagation velocity at temperature T to the propagation velocity for that mode at the reference temperature of 75° is plotted against the temperature T, the curves for all four modes turn out to be nearly identical. The average of the four curves is shown in Fig. 24. The individual deviations from the average are hardly visible on the scale of Fig. 24. For most temperatures and most modes the deviations are under one percent. Only five individual deviations are greater than one percent. Three of these are under two percent and the greatest individual deviation is less than four percent.

For operation in the neighborhood of  $75^{\circ}$  F. it is convenient to approximate the average curve of Fig. 24 by its tangent at T = 75. This tangent has the following analytical representation

$$\frac{c_r(T)}{c_r(75)} = \exp\{-0.024(T - 75)\}$$
 (16)

The divergence between the tangent (16) and the average curve of Fig. 24 is less than one percent within the temperature range from 68° F to 82° F. where most of the room temperature testing of rods was performed.

The shear tests provided values of the shear wave propagation velocity  $c_s$  and loss factor  $\eta$  for a single mode of vibration over a temperature range from 66° F to 82° F. The temperature dependence of  $c_s$  is displayed in Fig. 25. At most temperatures three independant determinations of  $c_s$  were made. The points plotted in Fig. 25 are the averages of the three values obtained. The deviations of the individual values from the average are hardly visible at the scale of Fig. 25. The straight line drawn through

the plotted points in Fig. 25 has the analytical representation

$$\frac{c_s(T)}{c_s(75)} = \exp\{-0.020(T - 75)\}\tag{17}$$

The corresponding values of loss factor are displayed in Fig. 26. For most temperatures the plotted points again represent averages of three independent determinations. Here, however, the individual deviations are considerable. The standard deviation for all determinations is 0.012 which is about 7 percent of the mean value of  $\eta$ . The averaged points plotted in Fig. 26 exhibit a comparable residual scatter.

Based on these results we have reduced all room-temperature measurements of propagation velocity to equivalent velocities at 75° F. For rod measurements Eq. 16 was used, and for shear measurements Eq. 17 was used. No direct measurements were made of the effect of temperature on the dilational wave propagation velocity  $\mathbf{c}_{\mathbf{p}}$ . It was, however, assumed that the temperature dependence of dilational wave propagation velocities was similar to that for rod and shear waves. Furthermore since the discrepancy between (16) and (17) is less than 2% in the temperature range from 70° to 80° F. it was assumed that either formula could be used to reduce the room-temperature measurements of  $\mathbf{c}_{\mathbf{p}}$  to equivalent velocities at 75° F. No temperature corrections were applied to measurements of the loss factor  $\mathbf{q}$ . The observed correlations of  $\mathbf{q}$  with temperature displayed in Figs. 23 and 26 are too weak to materially affect the unaccountable scatter in the loss factor measurements.

9. Pressure effects. In the proposed soil model facility the clay at the bottom of an 18" deep tub will be under a pressure of 1.24 psi above atmospheric. To investigate the effects of ambient pressure on the dynamic properties of clay a 3" rod of Plasticine was suspended as shown in Fig. 1 in a pressure controlled chamber. Tests were performed as described in Sec. 3 at pressures up to 30 psig. The tests were conducted at 72° F. and the propagation velocities measured were reduced to equivalent values at 75° F. by using Eq. 16. It was discovered that pressure of these magnitudes caused little permanent change in the rod propagation velocity c<sub>r</sub>. An interesting transient effect due to abrupt changes in pressure was however observed. A typical example is shown in Fig. 27 where a pressure loading history with sudden jumps is shown below and the resulting time history of c<sub>r</sub> in the first anti-resonant mode is shown above. Similar results were observed for other modes.

Note that in Fig. 27 a sudden change in pressure (either an increase or a decrease) is generally accompanied by a sudden decrease in  $c_r$  followed by a gradual return toward the original value. If the small strain dynamic properties of Plasticine are used to deduce the change in extensional strain due to a 10 psi change in pressure the strain change obtained is of the order of 2 x  $10^{-4}$ . As will be seen in Sec. 11 this much strain is sufficient to initiate thixotropic behavior and must be considered to be a large strain.

Note in Fig. 27 that the instantaneous decreases in  $c_r$  due to the step changes in pressure are as large as 10 percent for pressure jumps of 20 and 30 psi but that more than half of any such decrease is recovered in 10 minutes time if no additional large strain occurs. It may be concluded that a steady static pressure loading of 1.24 psi will not materially alter the small-strain dynamic properties of plasticine.

Nonlinear effects. In a linear viscoelastic material the wave propagation velocities and loss factor are independent of the amplitude of sinusoidal excitation. The linearity of a specimen under test can be checked by observing the effect of a change in excitation level on the measured propagation velocity. A number of such observations were made during the tests on rod specimens, as described in Sec. 3, and during the shear tests, as described in Sec. 5. In all cases it was found that beneath a certain threshold level of excitation the propagation velocities were independent of the excitation level. For excitation levels above the threshold the propagation velocities decreased with increasing amplitude of excitation. No systematic change in loss factor was observed.

Several representative results are displayed in Figs. 28 and 29. The excitation level is characterized by the level of strain in the specimen. For the rod tests the strain level adopted is the rms longitudinal strain  $\varepsilon$  at the driven end of the rod. This strain is related to the stress by the constitutive relation (1). Inserting Eqs. 4 and 5 we eventually obtain

$$\varepsilon = \frac{\epsilon_0}{\rho A c_r^2} \frac{2}{\sqrt{1 + \eta^2 + 1}}$$
 (18)

where  $f_o$  is the rms amplitude of the net exciting force driving the specimen,  $\rho$  is the mass density of the clay, A is the specimen crosssection and  $c_r$  and  $\eta$  are the measured rod propagation velocity and loss factor. In Fig. 28 the rod propagation velocity measured at strain level  $\epsilon$  is normalized by dividing it by the value of  $c_r$  corresponding to the smallest strain level  $\epsilon_{\min}$ . The normalized rod propagation velocity is plotted against the strain level  $\epsilon$ . The data shown in Fig. 28 are for the first antiresonant modes of four Plasticine rods.

One specimen had a length of 9" (circled points) while the other three each had a length of 3". Figure 28 indicates a threshold strain level for nonlinearity in the neighborhood of  $\varepsilon = 10^{-5}$ .

For the shear tests the strain level adopted is the rms average shear strain  $\gamma$  in the clay slab obtained by dividing the rms displacement d of the suspended mass by the thickness h of the clay slab. The displacement d is inferred from the measured acceleration a of the suspended mass so that

$$\gamma = \frac{d_s}{h} = \frac{a_s}{m_h^2} \tag{19}$$

In Fig. 29 the shear wave propagation velocity measured at strain level  $\gamma$  is normalized by dividing it by the value of  $c_s$  corresponding to the smallest strain level  $\gamma_{min}$ . The normalized shear wave propagation velocity is plotted against the strain level  $\gamma$ . The data shown in Fig. 29 apply to the five different values of suspended mass described in Sec. 5 (in order of increasing mass the results are indicated by diamonds, squares, circles, triangles pointing down and triangles pointing up.) Fig. 29 indicates a threshold strain level for nonlinearity in the neighborhood of  $\gamma = 3 \times 10^{-5}$ .

Thixotropic Effects. Thixotropy describes a complex rheological property of materials which involves changes in microscopic structure with time and stress. The word was first applied [3] to describe the isothermal reversible gel-sol transformation in colloidal suspensions. It was later generalized to apply [4] to any isothermal decrease in viscosity due to increasing rate of shear. More recently thixotropy

has been defined [5] as a process of softening caused by remolding, followed by a time-dependent return to the original harder strength. In soil mechanics the word thixotropy is commonly used to describe [6] the "age-hardening" or time-dependent strength gain of soils.

In our tests on Plasticine specimens we find that the small-strain dynamic properties depend on the large-strain history of the specimens. At the risk of further confusing an overworked word we have used the term thixotropy to describe this phenomenon. The general pattern of behavior is parallel to that usually associated with thixotropy although the strain levels involved are an order of magnitude smaller than those customarily encountered. In the previous section it was indicated that the strain threshold for nonlinearity was in the vicinity of  $10^{-5}$ . Here we shall see that the strain threshold for observable thixotropic effects is in the neighborhood of  $10^{-4}$ .

For soils the usual aspect of thixotropy is the time-dependent gain of strength of undisturbed soil where "strength" is measured quantitatively by the yield stress in a standardized compression test. Our tests have shown that after remolding, the propagation velocities of a specimen of Plasticine increase with time providing the strain levels remain below  $10^{-4}$ . See Fig. 21 for a typical example. Here the "strength" of the clay is represented by its propagation velocity or by its small-strain dynamic modulus. Our tests indicate that as long as the strain levels in the small-strain dynamic tests are less than  $10^{-6}$  there is no interference with the thixotropic process; i.e., the time-dependent increase in propagation speed is neither accelerated nor retarded by the presence of the small-strain oscillations. The small-strain oscillations thus provide a non-destructive probe for thixotropic phenomena.

The increase in propagation velocity with time after remolding is also indicated in Fig. 7 where the dilational wave propagation velocity  $c_p$  has increased about 17% during a two-day curing period. Fig. 7 also indicates that there is no significant effect of thixotropy on the loss factor  $\eta$ .

To illustrate the effect of subsequent large strains a 6" rod specimen was tested as described in Sec. 3. The specimen was then manually bent back and forth and re-straightened at A in Fig. 30. The rod propagation velocity c<sub>r</sub> immediately dropped nearly 30% and then gradually increased until after 18 hours it had almost regained its initial value. At this time the specimen underwent a calibrated bending B in which the 6" rod was bent into the arc of a circle of 16" diameter and then restraightened. The maximum bending strain in the extreme fibers was about 0.033. There was a sudden drop of about 15% in c<sub>r</sub> due to the initial application of B followed by a time-dependent increase. The calibrated bending B was repeated three more times after intervening periods of 100 minutes duration with results as shown in Fig. 30. Twenty one hours after the final large-strain application the propagation velocity had returned to within 3% of its initial value.

A similar time history of  $c_r$  for a 3" Plasticine rod is shown in Fig. 27 where the large-strains are due to changes in ambient pressure. Here the time intervals are shorter and the magnitudes of the large-strains are smaller. The largest drop in  $c_r$  (about 10%) is due to a pressure increase of 30 psi which involves an extensional strain somewhat less than 0.0006.

In Fig. 31 the frequency dependence of  $c_r$  for a 3" Plasticine rod which had not been exposed to large strain for a two-week period is shown at B (before bending). The rod was then bent in the arc of a circle until

the bending strain was 0.07. The rod was straightened, bent the same amount in the opposite direction and finally straightened and left for a three hour period. The frequency dependence of  $c_r$  at that time is shown in Fig. 31 at A (after bending). Note that there has been about 32% decrease in  $c_r$  throughout the frequency range examined.

Another aspect of thixotropy can be demonstrated by measuring the propagation velocity as the strain level of steady state oscillation is increased up to some maximum level and then is subsequently decreased. If the maximum level is under the thixotropic threshold then the propagation velocity measured at any strain level is independent of the strain history. If however the maximum level exceeds the thixotropic threshold, then the propagation velocity at a lower strain level measured when the oscillation amplitude is decreased to the lower level is less than the propagation velocity measured at this same level prior to the excursion over the thixotropic threshold. This test was carried out with the Plasticine slab excited in shear as described in Sec. 5. The results are displayed in Fig. 32. The dashed-line curve in Fig. 32 is the same as that in Fig. 29 showing the nonlinear effect of strain level  $\gamma$  on the shear wave propagation velocity  $c_{\epsilon}$ . The data for the dashed curve were obtained under conditions of monotonically increasing strain amplitude (the frequencies involved for the different suspended masses are indicated in Fig. 12). In Fig. 32 the solid lines are drawn through measurements made as the strain level was decreased from various maximum levels. The curve beginning at A was generated by decreasing the strain level from a maximum level of  $2 \times 10^{-4}$ . In this case the solid curve (decreasing amplitude) coincided with the dashed curve (increasing amplitude). The curve beginning at B is drawn through the results of two tests (the coding of the points in Fig. 32 is the same as that in

Fig. 29) in which the strain level was decreased from a maximum level in the neighborhood of 4 x  $10^{-4}$ . Here there is measurable "hysteresis" between the solid and dashed curves. Similarly the curve beginning at C was generated by decreasing the strain level from a maximum level of  $5.8 \times 10^{-4}$ .

In performing these tests the system was oscillated continuously as shown in Fig. 9 for about half an hour at the maximum levels B and C. The energy dissipated in the clay at these large amplitudes caused the clay temperature to rise about 5 or 6° F. All values of  $c_s$  in Fig. 32 have however been reduced to an equivalent propagation velocity at 75° F. by use of Eq. 17. In decreasing the amplitude of oscillation below a strain level of 2 x  $10^{-4}$  it was necessary to change the excitation configuration from that of Fig. 9 to that of Fig. 8. A time delay of about 10 minutes was required for the changeover. The "hysteresis" indicated in Fig. 32 thus represents the residual thixotropic decrease in  $c_s$  after 10 minutes "healing" time.

These results do not provide an exhaustive study of the thixotropic properties of Plasticine. They do however indicate the usefulness of small-strain dynamic measurements as a tool to study the phenomenon of thixotropy. Earlier studies [7, 8] of thixotropy in clay have utilized cyclic loading. The strain levels employed were of the order 0.01 or larger and the frequencies employed ranged from 0.01 to 0.33 Hz. There still remains a large gap between such large-strain, low-frequency studies and our small-strain, high-frequency investigations.

12. Dynamic Properties of Plasticine. A large number of resonance tests have been performed on rods and slabs of Plasticine. Using simple dynamic models (e.g. uniform thin rods with ideal fixed and free ends) and assuming that the clay could be represented as a linear viscoelastic material as described in Sec. 2, we have converted direct measurements of frequencies and amplitudes into "measured" values of propagation speeds and loss factors. Combining these with the measured density (119 lbs/cu. ft.) we obtain "measured" values of the moduli G, E and  $2G(1 - \nu)/(1 - 2\nu)$ .

Although individual measurements can usually be repeated within a percent or two, there is considerable variation in the results of tests on different samples. One source of variation is the ambient temperature. The effect of temperature on propagation velocity was sufficiently consistent that we have converted all values to a standard temperature of 75° F. as described in Sec. 8. The results described in this section were all obtained at atmospheric pressure for ambient temperatures within ±10° F. of the standard temperature. In our opinion the major source of variation is the effect of prior large strain history as described in Sec. 11. Because of thixotropy two nominally identical specimens can have quite different small-strain dynamic properties and a nominally homogeneous member can have quite different local properties at different points within the member.

In general there was small scatter in the measured values of propagation velocities and these values usually exhibited definite trends under variation of temperature, pressure or frequency. There was greater scatter in the measured values of loss factor and the values obtained did not usually appear to be correlated with any other variable.

The effect of frequency on propagation speed was generally small.

The widest frequency ranges explored on single samples without introducing

intervening large strains were those used in the rod tests. In these tests the higher frequency data are obtained by exciting the higher modes. In almost every case the rod propagation velocity increased by 5 to 10% over a frequency range of one to three octaves. See Figs. 4 and 22 for typical examples. In the shear tests described in Sec. 5 the frequency was lowered by increasing the suspended mass. Generally a day passed between tests as each increment of mass was glued in place. It is therefore not clear whether the frequency effect shown in Fig. 12 is actually due to frequency or due to thixotropic stiffening with time.

Poisson's ratio. If the small-strain dynamic properties of the clay had remained fixed, independently of the large strain history, it would have been possible to obtain Poisson's ratio v by measuring two different propagation velocities (e.g., shear and dilation velocities or shear and rod velocities). Furthermore the consistency of the model could have been checked by measuring all three propagation velocities. In most of our results the fluctuations from sample to sample were sufficiently great that a meaningful determination of Poisson's ratio was impossible.

The one exception was in the tests described in Sec. 6 where a special triple decker sandwich was used which permitted alternating from shear to dilation without introducing any intervening large strain. In these tests resonances and anti-resonances for both shear and dilation were measured at intervals during a period of 120 hours immediately after forming the specimen. The individual measurements were made sufficiently quickly that all four determinations could be made and repeated in a matter of minutes. From these determinations we derived two values of shear velocity  $\mathbf{c}_{\mathbf{S}}$  (at two frequencies) and two values of dilational velocity  $\mathbf{c}_{\mathbf{S}}$  (at two other frequencies). By assuming that

the propagation speeds varied linearly with frequency between the measured frequencies we established equivalent shear and dilation velocities at common frequencies and from these we calculated Poisson's ratio from the relation

$$v = \frac{2 - (c_p/c_s)^2}{2[1 - (c_p/c_s)^2]}$$
 (20)

which follows from Eqs. 7 and 8. We found that at any fixed time the variation of V with frequency was under one percent. Even more interesting it was found that throughout the 120 hour period while the propagation velocities themselves were increasing by more than 20% the individual values of V never deviated by more than one percent from their average value v = 0.434. This suggests that Poisson's ratio is unaffected by the thixotropic stiffening and that it is frequency independent in the twooctave range of frequencies (700 to 2800 Hz) included in these tests. numerical value of V obtained does depend on the dynamic model employed as described in Sec. 6. One approximation involves the treatment of the clay mass. As noted in Sec. 6 the choice of approximation here can affect the values of the individual propagation velocities by as much as 7 percent but the ratio of the two propagation velocities, and hence Poisson's ratio, is substantially unaffected. Another approximation whose effects remain unknown involves the neglect of edge effects in the slab models for relating the slab stiffness to the material modulus. Exact solutions or good numerical approximations from the theory of elasticity would be helpful here.

Rod velocity and loss factor. A wide range of conditions were explored in the rod tests. The rod propagation velocity  $c_{\mathbf{r}}$  and the loss factor  $\eta$  were measured on Plasticine rods from 3 to 15 inches long, in temperatures

ranging from 70° F. to 120° F., at pressures ranging from atmospheric to 30 psig, and at frequencies ranging from 100 to 3000 Hz. The measured values of  $c_r$  (reduced to 75° F.) ranged from 340 ft/sec for a 6" rod immediately after major bending to 750 ft/sec for a 3" rod which had not been disturbed for several days. The measured values of  $\eta$  ranged from 0.14 to 0.34.

In a systematic test involving fifteen rods all fabricated and tested in a nominally identical manner a total of 77 individual measurements were made (see Fig. 4 where six of these measurements are displayed). At the time these tests were run the importance of previous history was not appreciated and the effects of small bending (as demonstrated in Fig. 30) had not been discovered. The resulting scatter of the 77 measurements is considerable. The average value of  $c_r$  is 575 ft/sec with a standard deviation of 63 ft/sec (11%). The average value of the loss factor  $\eta$  is 0.222 with a standard deviation of 0.040 (18%).

Dilational velocity and loss factor. Dilational tests were run as described in Sec. 4 and also in connection with the measurement of Poisson's ratio as described in Sec. 6. The former tests were chiefly of value in alerting us to problems of resonance limitations of the impedance head-disk combination. This was helpful in the subsequent design of the sandwich configuration described in Sec. 6. The former tests also provided evidence of the time-dependent nature of the dynamic properties of Plasticine: see Fig. 7. The dilational velocity c increased from about 650 ft/sec to about 750 ft/sec due only to the passage of time. The first set of measurements was made shortly after molding the specimen. The second was made two days later. The loss factor, ranging from 0.20 to 0.16 over the frequency range from 600 to 1000 Hz did not change appreciably during this time. In these tests the high frequency points

were measured first and the lower frequencies were obtained sequentially by politing on increments of suspended mass. After the lowest frequency measurements were complete the mass increments were removed and the high frequency measurements repeated to verify that there had been no appreciable drift in the small strain dynamic properties during the test.

In the tests described in Sec. 6 dilational velocities and loss factors at two frequencies (the first antiresonance and the first resonance) were measured at intervals during a period of 120 hours immediately after the formation of the specimen. The dilational velocities at the two frequencies increased about 20 per cent during the period but they remained substantially in a fixed proportion corresponding to an increase in  $c_p$  of 6.3 percent per octave (at the antiresonance  $c_p$  increased from 801 to 905 ft/sec as the frequency increased from 1226 to 1468 Hz while at the resonance  $c_p$  increased from 850 to 1015 ft/sec as the frequency increased from 2280 to 2772 Hz). The loss factor remained within 4 percent of the value  $\eta$  = 0.227 for all the antiresonant measurements and within 6 percent of the value  $\eta$  = 0.251 for all the resonant measurements.

Shear velocity and loss factor. Shear tests were run as described in Sec. 5 and also in connection with the measurement of Poisson's ratio as described in Sec. 6. Fig 12 shows typical results for the former tests.

In these tests the measurements began with the highest frequency and proceeded to the lower frequencies as increments of suspended mass were glued in place. The passage of time between measurements and the introduction of strains large enough to cause thixotropic changes during the measurements both act to complicate the interpretation of Fig. 12 as a representation of the effect of frequency alone. From a total of 114 individual measurements on three different specimens the average of the measured values of the

shear velocity is  $c_s$  = 286 ft/sec with a standard deviation of 23 ft/sec (8%) while the average of the measured values of the loss factor is  $\eta$  = 0.225 with a standard deviation of 0.065 (29%).

In the tests described in Sec. 6 shear velocities and loss factors at the first antiresonance and the first resonance were measured at intervals during the 120 hour period following formation of the specimen. The shear velocities of the two frequencies increased about 23 per cent during the period but they remained in a fixed proportion corresponding to an increase in  $c_s$  of 6.5 percent per octave (at the antiresonance  $c_s$  increased from 258 to 319 ft/sec as the frequency increased from 728 to 896 Hz while at the resonance  $c_s$  increased from 266 to 327 ft/sec as the frequency increased from 993 to 1220 hz). The loss factor remained within 3 percent of the value  $\eta$  = 0.239 for all the antiresonant measurements and within 2 percent of the value  $\eta$  = 0.239 for all the resonant measurements.

Dynamic moduli. The measured values of propagation velocity and loss factor can be converted to values of dynamic moduli by using Eqs. 4, 7, or 8 along with Eqs. 5 or 6. For example, putting the average values  $c_r = 575$  ft/sec and  $\eta = 0.222$  obtained from the 77 measurements on 15 rods in Eqs. 4, and 5 we find E = 8,200 psi. The accompanying standard deviation is 1,950 psi (24%). Similarly, putting  $c_s = 236$  ft/sec and  $\eta = 0.225$  obtained from the 114 measurements on 3 shear slabs in Eqs 8 and 5 we find G = 2,020 psi. The accompanying standard deviation is 344 psi (17%).

The average values of E and G just calculated are averages over frequency and states of previous large strain history for many different samples. As such they do not necessarily represent values which could simultaneously be observed on any one specimen. In fact, these values for E and G do not satisfy Eq. 2 unless Poisson's ratio takes the impossible value of  $\nu = 1.03$  (in the linear viscoelastic model of Eqs. 1 and 2 the

value of Poisson's ratio cannot be greater than v = 0.5 for stability).

In the one case where care was taken to measure shear and dilation under the same state of large strain history Poisson's ratio appeared to be independent of frequency and thixotropic stiffening. To demonstrate the potential consistency of our data with the assumed model we have used the measured value  $\nu = 0.434$  to convert direct measurements of  $c_p$  to corresponding values of  $c_s$  using Eq. 20. Similarly we have converted direct measurements of  $c_r$  to corresponding values of  $c_s$  using Eq. 2 in conjunction with Eqs. 4 and 8. The extreme ranges of resulting values of equivalent shear propagation velocity in our tests on rods and slabs are then as shown in Table 1.

Table 1. Equivalent shear velocity ranges in the various tests

Type of Test	Equivalent c (ft/sec)
Rod tests (Sec. 3)	200 to 412
Shear tests (Sec. 5)	263 to 309
Sandwich tests (Sec. 6)	258 to 327

Note that there is a central overlap range from 263 to 309 ft/sec common to all three tests. Note also the wider range in the rod tests as compared to the slab tests. This may be due simply to the fact that more different rod specimens were tested or it may be due to the fact that the rods were more exposed to large strains. There is also some indication that the time scale for thixotropic recovery is more rapid for rods than slabs.

For the central overlap range of Table 1 the corresponding ranges of values for the rod propagation velocity  $c_r$ , the dilational propagation velocity  $c_p$  and the moduli E and G all computed on the basis of  $\nu=0.434$  are given in Table 2.

Table 2. Range of dynamic parameters of Plasticine common to three types of tests

Parameter	Range
c <sub>s</sub>	263 to 309 ft/sec 446 to 524 ft/sec 771 to 908 ft/sec
e p E G	4,910 to 6,770 psi 1,710 to 2,360 psi

The corresponding values of loss factor  $\eta$  had an even wider range of variation throughout the tests although the average values for each type of test were quite close together. For the rod tests the average value was  $\eta$  = 0.222. For the shear tests of Sec. 5 the average value was  $\eta$  = 0.225 and for the sandwich test of Sec. 6 the average value was  $\eta$  = 0.234.

Summary. For strain levels smaller than  $10^{-5}$  the linear viscoelastic model of Eqs. 1 and 2 provides a useful representation for Plasticine. The parameters depend (weakly) on frequency and (strongly) on temperature and (intermediately) on the large strain history of the specimen. We believe that the major effects of temperature have been accounted for in our results. The primary source of uncertainty is due to the effects of large strain history which we have ascribed to thixotropy. These effects have not yet been completely explored. A promising start has been made by the tests described in Sec. 6 where the large strain history was strictly controlled during the 5 day period of testing.

Comparison with other results. The modulus E for modelling clay has been measured previously by other investigators. Under static compressive loading of unconfined cylinders of Plasticine [1] the highest modulus obtained was 925 psi. From wave motions excited by small explosive charges at the ends of clay rods [2] the modulus was estimated to be 650,000 psi. The values of E that we measured for small steady state oscillations cover a range well between these two extremes. The range of equivalent modulus common to three different types of test (see Table 2) is 4,910 to 6,770 psi. If we consider the entire range of all our tests the equivalent modulus E ranges from 2,840 to 13,800 psi. Our smallest modulus is more than three times larger than the static measurement [1] and our largest modulus is smaller than the wave propagation measurement [2] by a factor of forty-seven!

13. Predicted Admittance of a Disk on a Viscoelastic Half-Space. To illustrate the application of the results obtained on small samples of Plasticine we predict the admittance of a rigid disk on a viscoelastic half space liaving parameters equal to those previously measured and compare the results with direct measurements on a large tub of Plasticine. We consider vertical motion of a rigid disk of radius r and mass m excited by an oscillating force whose amplitude is P and whose frequency is  $\omega$ . The disk remains in contact with a viscoelastic half space governed by Eqs. 1 and 2 with the parameters  $\rho$ , G,  $\nu$  and  $\eta$ . The system is sketched in Fig. 33(a). The problem is to predict the acceleration admittance  $a_z/P$  where  $a_z$  is the complex amplitude of the steady state acceleration of the disk.

The solution is obtained in two steps. In fig. 33(b) the half space alone is considered subject to a distributed vertical loading whose resultant is the interaction force  $P_{i}$ . An approximate solution to this problem has

been obtained by Lee [9] on the assumption that the distribution of P<sub>i</sub> is uniform. In this assumption the resulting acceleration of the half space is not strictly uniform under the disk. The acceleration at the center of the disk is arbitrarily taken to represent the acceleration of the entire interface. This approximation is a familiar one for elastic half-space problems. See for example [10-13]. For the half-space alone the solution [9] for the acceleration admittance is

$$\frac{\mathbf{a_z}}{\mathbf{P_i}} = \frac{1}{\rho \mathbf{r}^3} \left(\frac{\omega \mathbf{r}}{c_s}\right)^2 (\mathbf{g_1} + i\mathbf{g_2}) \tag{21}$$

where the dimensionless viscoelastic half-space functions  $g_1$  and  $g_2$  depend on Poisson's ratio  $\nu$ , the loss factor  $\eta$  and the dimensionless frequency parameter  $\omega r/c_s$ . For  $\nu=0.5$  and  $\eta=0.2$  (which are nearest to the measured values for Plasticine) the functions  $g_1$  and  $g_2$  as given by [9] are plotted in Fig. 34 as functions of the frequency parameter  $\omega r/c_s$ .

In Fig. 33(c) the rigid disk is shown under the influence of the external excitation P and the interaction force  $P_i$ . The equation of motion for steady state vibration is

$$P - P_{i} = ma_{z}$$
 (22)

Elimination of the interaction force  $P_{i}$  between (21) and (22) leads to the desired admittance function

$$\frac{a_z}{P} = \frac{1}{m} \left[ 1 + \frac{\rho r^3}{m} \left( \frac{c_s}{\omega r} \right)^2 \frac{1}{g_1 + ig_2} \right]^{-1}$$
 (23)

For fixed values of the half space parameters, the dimensionless admittance  $ma_z/P$  depends only on the frequency parameter  $\omega r/c_s$  and the mass ratio  $m/\rho r^3$ . In general the admittance has real and imaginary parts which are both frequency dependent.

Measured Admittance of a Disk on the Surface of a Large Tub of Plasticine. 14. The acceleration admittance of a small lucite disk resting on the surface of a tub of clay was directly measured and the result compared with a prediction based on the theory outlined in Sec. 13. The tub is square, 35" on a side, and is filled to a depth of 15" with 1270 lbm of white Plasticine. The disk is 0.84" in diameter and has a mass of 0.0145 lbm. (6.6 grams). The disk is excited by a shaker driving through an impedance head as shown in Fig. 35. The instrumentation chain employed (shown in Fig. 36) permitted the direct recording of the real and imaginary parts of the acceleration admittance as functions of frequency. The oscillator generates a sinusoidal signal which is slowly swept from 200 to 2000 Hz. The level of the excitation is servo-controlled so as to provide a constant level of oscillating force (0.0015 1bf) through the impedance head. Under this condition the output of the co-channel of the co-quad analyzer is proportional to the real part of the acceleration admittance and the output of the quad-channel of the co-quad analyzer is proportional to the imaginary part of the acceleration admittance. These outputs are recorded directly on an x-y plotter as a function of frequency ( the oscillator provides a signal proportional to the logarithm of the sweeping frequency). The tracking filters with bandwidth are included to remove background noise effects.

The system was calibrated by first shaking the disk alone, away from the clay. The acceleration admittance  $a_{\rm Z}/P$  under these conditions should be 1/m; i.e., real, positive and independent of frequency. In actuality

the result was substantially independent of frequency from 200 to 1400 Hz but showed minor undulations (up to 15 percent) due to extraneous resonances in the range from 1400 to 2000 Hz. The value of m here is the mass of the disk plus the mass of that part of the impedance head which is ahead of the force gauge. The total mass is 0.063 lbm (28.6 grams).

After calibration the disk and shaker assembly was gently placed on the clay surface in the middle of the tub and allowed to rest there under its own weight. The oscillator was set to sweep from 200 to 2000 Hz and the acceleration admittance curves indicated by the solid lines in Fig. 37 were recorded. These results are to be compared with the dashed predictions based on the theory of Sec. 13 in which the viscoelastic half-space parameters are taken as

v = 0.5

 $\eta = 0.2$ 

 $c_s = 278 \text{ ft/sec}$ 

and the mass ratio m/pr<sup>3</sup> is taken as 12.2 corresponding to

m = 0.063 1bm

r = 0.035 ft.

 $\rho = 119 \text{ lbm/ft}^3$ 

The correspondence between the prediction based on the idealized half-space model with parameters obtained from tests on small specimens and the direct measurements in the tub is quite good, in the frequency range from 200 to 1400 Hz. Subsequent tests at other locations in the tub showed that the apparent shear wave velocity of the clay was not uniform (variations of 10 to 15 percent are common). Good agreement between measured and predicted admittance curves could, however, be obtained by selecting the half-space shear wave velocity used in the prediction so as to match the admittances at resonance (90° phase). The predictions based on an infinite

half space were in good agreement with the measurements as long as the disk was located more than  $8^{\prime\prime}$  from the nearest edge of the tub.

Acknowledgment. This research was supported by a grant from the National Aeronautics and Space Administration.

## References

- 1. A.B. Mason, "Influence of Anisotropic Properties of Clay Deposits on Settlements", Ph.D. Thesis, Harvard University, May, 1939. See Chapter 9. Tests on Plasticine, pp. 94-114.
- 2. H.H. Calvit, D. Rader and J. Melville, "Some Wave Propagation Experiments in Plasteline Clay Rods", Experimental Mechanics 8, 418-423 (1968).
- 3. H. Freundlich, Thixotropy, Hermann and Cie., Paris, 1935.
- 4. C.F. Goodeve, "A General Theory of Thixotropy and Viscosity", <u>Trans.</u>
  Faraday Soc. 35, 342-358 (1939).
- 5. J.M. Burgers and G.W. Scott Blair, "Report on the Principles of Rheological Nomenclature", Proc. Internatl. Rheologic Congress,
  Amsterdam, 1948.
- J.K. Mitchell, "Fundamental Aspects of Thixotropy in Soils",
   J. Soil Mech. and Foundtns. Div., Proc. ASCE 86, 19-52 (1960).
- 7. H.B. Seed and C.K. Chan, "Thixotropic Characteristics of Compacted Clays", J. Soil Mech. and Foundtns. Div., Proc. ASCE 83, 1427-1 to 1427-35 (1957).
- 8. N.F. Astbury and F. Moore, "Torsional Hysteresis in Plastic Clay and its Interpretation", Materials Res. and Stds. 5, 178-183 (1965).

- 9. T.M. Lee, "Near Field Study of Surface Loadings on a Semi Infinite Viscoelastic Medium", Unpublished Technical Memorandum, Army Cold Regions Research and Engineering Laboratory, Hanover, N.H., August, 1967.
- 10. E. Reissner, "Stationare Axialsymmetrische, durch eine shuttelende Masse erregte, Schwingungen eines homogenen elastischen Halbraums",
  Ingenieur-Archiv, 7, 381-396 (1936).
- 11. T.Y. Sung, "Vibrations in SemiInfinite Solids due to Periodic Surface Loadings", Am. Soc. Test. Matls, STP, 156, 35-63 (1953).
- 12. R.N. Arnold, G.N. Bycroft and G.B. Warburton, "Forced Vibrations of a Body on an Infinite Elastic Solid", J. Appl. Mech., 22, 391-400 (1955).
- 13. T.K. Hsieh, "Foundation Vibrations", Proc. Instn. Civil Engrs., 22, 211-255 (1962).

## Appendix A

## Plane Waves in a Linear Viscoelastic Medium

We consider three types of plane harmonic waves in a medium satisfying Eqs. 1 and 2. In every case propagation takes place in the x-direction and all variables are independent of y and z. For <u>longitudinal</u> waves in a rod the only non-zero stress component is  $\sigma_{\rm x}$  and Eq. 1 reduces to

$$E(1 + i\eta)\epsilon_{x} = \sigma_{x} \tag{A-1}$$

with  $\varepsilon_y = \varepsilon_z = -v\varepsilon_x$ . If  $\text{Re}\{v_x e^{i\omega t}\}$  represents the oscillating component of velocity parallel to x and  $\rho$  is the mass density of the medium, the momentum equation is

$$\frac{d\sigma_{x}}{dx} = i\omega\rho v_{x} \tag{A-2}$$

and the geometric compatibility requirement is

$$\frac{d\mathbf{v}_{\mathbf{x}}}{d\mathbf{x}} = \mathbf{i}\omega\varepsilon_{\mathbf{x}} \tag{A-3}$$

Elimination of  $\mathbf{v}_{\mathbf{x}}$  and  $\boldsymbol{\sigma}_{\mathbf{x}}$  between Eqs. A-1, A-2 and A-3 leads to

$$E(1 + i\eta) \frac{d^2 \varepsilon_x}{dx^2} = -\omega^2 \rho \varepsilon_x$$
 (A-4)

as the governing equation for the strain distribution in a harmonic plane longitudinal wave.

$$\mathbb{E}(1+i\eta) \frac{1-\nu}{(1+\nu)(1-2\nu)} \varepsilon_{x} = \sigma_{x}$$
 (A-5)

with  $\sigma_y = \sigma_z = v\sigma_x/(1-v)$ . An alternative to (A-5) is obtained by eliminating E between (A-5) and Eq. 2 to get

$$G \frac{2(1-v)}{1-2v} (1+i\eta)\varepsilon_{x} = \sigma_{x}$$
 (A-6)

Combining (A-6) with the momentum equation (A-2) and the compatibility equation (A-3) we find

$$\mathbf{G} \frac{2(1-\nu)}{1-2\nu} (1+i\eta) \frac{\mathrm{d}^2 \varepsilon_{\mathbf{x}}}{\mathrm{d} \mathbf{x}^2} = -\omega^2 \mathbf{\rho} \varepsilon_{\mathbf{x}}$$
 (A-7)

as the governing equation for strain distribution in a harmonic plane dilational wave.

For plane shear waves with motion parallel to y the only non-zero stress component is  $\tau_{xy}$  (the only non-zero strain component is  $\gamma_{xy}$ ) and Eq. 1 reduces to

$$G(1 + i\eta)\gamma_{xy} = \tau_{xy}$$
 (A-2)

If  $\text{Re}\{v_ye^{i\omega t}\}$  represents the oscillating component of velocity parallel y, the momentum equation is

$$\frac{\mathrm{d}\tau}{\mathrm{d}x} = \mathrm{i}\omega \rho v_{y} \tag{A-9}$$

and the geometric compatibility requirement is

$$\frac{dv}{dx} = i\omega v_{xy} \tag{A-10}$$

Elimination of  $v_y$  and  $\tau_{xy}$  among Eqs. A-8, A-9 and A-10 leads to

$$G(1 + i\eta) \frac{d^2 \gamma_{xy}}{dx^2} = -\omega^2 \rho \gamma_{xy}$$
 (A-11)

as the governing equation for strain distribution in a harmonic plane shear wave.

Equations A-4, A-7 and A-11 all have the form

$$a^{2}(1 + i\eta) \frac{d^{2}f}{dx^{2}} = -\omega^{2}f$$
 (A-12)

where f represents the appropriate strain amplitude and the constant  $a^2$  takes the value

$$a^2 = \frac{E}{\rho}$$
,  $a^2 = \frac{G}{\rho} \frac{2(1-\nu)}{1-2\nu}$  or  $a^2 = \frac{G}{\rho}$  (A-13)

respectively. In order for the strain waves to have the form of Eq. 3 the strain amplitude f must be proportional to

$$e^{-CX}e^{-i(t)X/C}$$
 (A-14)

where  $\alpha$  and c are (real) decay and propagation velocity parameters. To find the connection between  $\alpha$  and c and the parameters  $\eta$  and a in Eq. A-12 we insert (A-14) for f in Eq. A-12 to get

$$a^{2}(1 + i\eta)(\alpha + i\omega/c)^{2} = -\omega^{2}$$
 (A-15)

Then by treating the real and imaginary parts of (A-15) separately it is possible to obtain the desired relations. A convenient device for accomplishing this is to set

$$1 + i\eta = \psi^2 \frac{(1 + i\beta)^2}{(1 + \beta^2)^2}$$
 (A-16)

thereby defining the two new (real) parameters  $\psi$  and  $\beta.$  Then the square root of (A-15) is

$$a\psi \frac{1+i\beta}{1+\beta^2} (\alpha + i\omega/c) = i\omega \qquad (\Lambda-17)$$

Separating real and imaginary terms yields

$$\alpha = \beta \omega/c$$
(A-18)
 $c = \psi a$ 

and it remains only to identify  $\psi$  and  $\beta$  from Eq. A-16. Separating real and imaginary parts in (A-16) leads to

$$\dot{\psi}^2 = \frac{(1+\beta^2)^2}{1-\beta^2} \qquad \eta = \frac{2\beta}{1-\beta^2} \qquad (A-19)$$

from which follows

$$\beta = \frac{\sqrt{1 + \eta^2} - 1}{n}$$
 (A-20)

as well as the alternative forms given in Eqs. 5 and 6. Equations 4, 7 and 8 in Section 2 are the particular forms assumed by (A-18) when specialized to longitudinal waves in a rod, dilational waves and shear waves respectively.

Λ-6

Resonance-test relations for uniform rods and slabs of linear viscoelastic material

The resonance relations derived herein apply to a uniform viscoelastic rod or slab of length L in the x-direction which is excited at the end x = 0 and which carries a suspended rigid mass m<sub>g</sub> at the end x = L. To simplify the exposition the discussion is restricted to the case of a thin rod with longitudinal motion. The results, however, can be immediately extended to uniform dilation or uniform shear of a slab by making substitutions corresponding to the parallel treatment of the three types of waves in Appendix A (e.g., see Eq. A-13). In the first part, general expressions are obtained for the complex amplitudes of the accelerations at the ends of the rod and the amplitude of the driving force when the rod undergoes steady harmonic oscillation at frequency  $\omega$ . In the second part these general expressions are particularized to resonance (or antiresonance) conditions where there is a 90° phase difference between two of these expressions. The resulting relations provide means for converting experimentally determined amplitudes and frequencies into "measured" values of propagation velocity and loss factor.

Consider a uniform viscoelastic rod of length L and cross-sectional area A. At frequency  $\omega$  let the acceleration amplitude  $i\omega v_{x}(x)$  be denoted by  $a_{0}$  (or  $a_{b}$ ) at x=0 and by  $a_{s}$  at x=L. In terms of the stress amplitude  $\sigma_{x}(x)$  introduced in Appendix A the force amplitude driving the rod at x=0 is

$$f_{O} = -A\sigma_{X}(0) \tag{B-1}$$

and the terminal acceleration amplitudes are

$$\mathbf{a}_{o} = \frac{1}{\rho} \frac{d\sigma_{\mathbf{x}}}{d\mathbf{x}} \Big|_{\mathbf{0}}$$

$$\mathbf{a}_{s} = \frac{1}{\rho} \frac{d\sigma_{\mathbf{x}}}{d\mathbf{x}} \Big|_{\mathbf{L}}$$
(E-2)

The desired quantities thus follow as soon as  $\sigma_{_{\rm X}}({\rm x})$  is known. In Appendix A it was shown that the viscoelastic medium supports strain waves which decay as they propagate. Because of the assumed linearity stress waves will have the same form. The wave represented by Eq.  $\Lambda$ -14 propagates (and decays) to the right. In a finite rod the general solution also includes a wave which propagates to the left. Thus, for arbitrary values of  ${\rm C}_1$  and  ${\rm C}_2$  the medium will support a stress in the rod of the form

$$\sigma_{\mathbf{x}} = C_1 e^{-\phi (\beta + \mathbf{i})\mathbf{x}/L} + C_2 e^{\phi (\beta + \mathbf{i})\mathbf{x}/L}$$
(B-3)

where  $\phi = \omega L/c$ , with c and  $\beta$  given by Eqs. A-18 and A-19. To evaluate the constants  $C_1$  and  $C_2$ , we introduce the boundary conditions. At x=0 we take  $a_0$  to be specified and at x=L the terminal force must be just large enough to impart the acceleration  $a_S$  to the suspended mass  $m_S$ . These conditions, expressed in terms of  $\sigma_x$ , are

$$\frac{d\sigma_{x}}{dx}\Big|_{0} = \rho a_{0} \qquad -\Lambda \sigma_{x}(L) = \frac{m_{s}}{\rho} \frac{d\sigma_{x}}{dx}\Big|_{L} \qquad (B-4)$$

Insertion of (B-3) in (B-4) leads to a pair of simultaneous equations from which we obtain  $C_1$  and  $C_2$ . Substituting these back into Eq. B-3

and evaluating Eqs. B-1 and B-2 leads, after considerable algebra, to

$$\frac{f_o}{m_{c,o}} = \frac{1}{\phi(\beta + i)} \frac{H}{D}$$
 (B-5)

$$\frac{a_{s}}{a_{0}} = \frac{1}{0} \tag{B-6}$$

where we have set  $m_c$  =  $\rho AL$  for the mass of the clay and N and D stand for complex functions of  $\phi$ ,  $\beta$  and  $m_s/m_c$ . Their real and imaginary parts are listed below.

$$D_{\text{real}} = \cos \phi \cosh \beta \phi + \frac{m_{s}}{m_{c}} \phi (\beta \cos \phi \sinh \beta \phi - \sin \phi \cosh \beta \phi)$$

$$D_{\text{imag}} = \sin \phi \sinh \beta \phi + \frac{m_{s}}{m_{c}} \phi (\beta \sin \phi \cosh \beta \phi + \cos \phi \sinh \beta \phi)$$

$$(B-7)$$

$$N_{real} = \cos \phi \sinh \beta \phi + \frac{m_s}{m_c} \phi (\beta \cos \phi \cosh \beta \phi - \sin \phi \sinh \beta \phi)$$
(B-8)

$$N_{imag} = \sin \phi \cosh \beta \phi + \frac{m_s}{m_c} \phi (\beta \sin \phi \sinh \beta \phi + \cos \phi \cosh \beta \phi)$$

Suppose that in a resonance test the suspended mass acceleration  $a_s$  and the base acceleration  $a_b$  =  $a_o$  are monitored. The two accelerations will have a 90° phase difference when  $D_{real}$  vanishes. Setting  $D_{real}$  equal to zero leads to the requirement

$$1 + \frac{m_s}{m_c} \phi(\beta \tanh \beta \phi - \tan \phi) = 0$$
 (B-9)

which is equivalent to the first of Eqs. 12 in the text. When (b-9) is satisfied the magnitude of the acceleration ratio is simply the reciprocal of D  $_{\rm imag}$  or

$$\left|\frac{\frac{a_s}{a_b}}{a_b}\right| = \frac{1}{\sinh \beta \phi \left[\sin \phi \left(1 + \frac{m_s}{m_c} \beta \phi \coth \beta \phi\right) + \frac{m_s}{m_c} \cos \phi\right]}$$
(B-10)

which is equivalent to the second of Eqs. 12 in the text. For a given mode and a fixed value of  $m_s/m_c$  there is a unique set of values for  $\beta$  and  $\phi$  which satisfy both (B-9) and (B-10) for each measurement of the amplitude ratio  $\left|a_s/a_b\right|$  at the 90° phase condition. The loss factor  $\eta$  then follows from  $\beta$  (e.g., by use of Eq. A-20) and the propagation velocity c follows from  $\phi = \omega L/c$  and the measured frequency at the 90° phase condition.

When the suspended mass  $m_s$  vanishes, as in the tests described in Sec. 3, the reciprocal of the ratio (B-5) reduces to

$$\frac{{}^{m}c^{a}_{o}}{f_{o}} = \phi(\beta + i) \frac{\cos \phi \cosh \beta \phi + i \sin \phi \sinh \beta \phi}{\cos \phi \sinh \beta \phi + i \sin \phi \cosh \beta \phi}$$

$$= \phi \frac{\beta \sinh 2\beta \phi + \sin 2\phi + i(\sinh 2\beta \phi - \beta \sin 2\phi)}{\cosh 2\beta \phi - \cos 2\phi}$$
(B-11)

The driving point acceleration and force will be 90° out of phase whenever

the real part of (B-11) vanishes; i.e., when

$$\beta \sinh 2\beta \phi + \sin 2\phi = 0 \qquad (E-12)$$

which is equivalent to Eq. 10 in the text. When Eq. B-12 is satisfied the ratio (6-11) takes on the value

$$\frac{{}^{\text{m}}c^{a}\sigma}{f} = i\phi \frac{(1+\beta^{2})\sinh 2\beta\phi}{\cosh 2\beta\phi - \cos 2\phi}$$
 (E-13)

which is equivalent to Eq. 9 in the text. For a given mode there is a unique set of values for  $\beta$  and  $\phi$  which satisfy both (B-12) and (B-13) for each measurement of the magnitude  $\left| \mathbf{m_c a_o} / \mathbf{f_o} \right|$  at the 90° phase condition. From the values of  $\beta$  and  $\phi$  together with the measured frequency at the 90° phase condition, the loss factor  $\eta$  and the propagation velocity c follow from Eq. A-20 and the relation  $\phi = \omega L/c$ .

Resonance test relations for sandwich configuration of Sec. 6

The equations connecting the material modulus and loss factor with the measured amplitudes and frequency at a resonance (or antiresonance) for the lumped parameter models of Fig. 20 are derived herein. We consider first the shear test configuration of Fig. 20(b) where the exciting force is applied to the center mass. Under steady state vibration at frequency  $\omega$  with oscillating displacements represented by  $\text{Re}\{xe^{i\omega t}\}$  and the oscillating force represented by  $\text{Re}\{fe^{i\omega t}\}$  the equations of motion are

$$k_s(1 + i\eta)(x_2 - x_1) + \omega^2 mx_1 = 0$$

$$-k_{s}(1 + i\eta)(x_{2} - x_{1}) + k_{s}(1 + i\eta)(x_{3} - x_{2}) + \omega^{2}m_{o}x_{2} = -f$$
 (C-1)

$$-k_s(1 + i\eta)(x_3 - x_2) + \omega^2 mx_3 = 0$$

Denoting the driving point acceleration amplitude by  $a_2 = -\omega^2 x_2$  we obtain the driving point response ratio  $f/m_0 a_2$  by eliminating  $x_1$  and  $x_3$  from (C-1). Setting  $\phi = \omega^2 m/k_s$  and  $\mu = m/m_0$  we find, after some algebra,

$$\frac{f}{{m_0}a_2} = \frac{\phi^2 - 2\phi(1+\mu) + (1+\eta^2)(1+2\mu) - i2\eta\phi\mu}{2}$$

$$(C-2)$$

There will be a 90° phase difference between the driving point force and acceleration when the real part of (C-2) vanishes; i.e., when

$$\phi = 1 + \mu\{1 \pm [1 - \eta^2(1 + 2\mu)/\mu^2]^{1/2}\}$$
 (C-3)

If the loss factor is not too great, there are two real roots for  $\phi$ : the plus sign corresponding to the resonance and the minus sign corresponding to the antiresonance. In either case the response ratio reduces to

$$\frac{f}{m_0 a_2} = \frac{-i2\eta\phi\mu}{2}$$

$$(C-4)$$

$$(1 - \phi) + \eta^2$$

Measured amplitudes and frequencies at the 90° phase conditions can be related to the complex shear modulus  $G(1+i\eta)$  of the clay by using Eqs. C-3 and C-4. For a fixed value of  $\mu = m/m_0$  there is a unique pair of values for  $\eta$  and  $\phi$  which simultaneously satisfy both (C-3) and (C-4) for each measurement of the magnitude  $\left| f/m_0 a_2 \right|$ . The measured frequency together with the relation  $\phi = \omega^2 m/k_s$  yield the shear spring constant  $k_s$  which leads by way of Eq. 15 to the real modulus G.

For the dilation test configuration of Fig. 20(a) the equations of motion are

$$k_d(1 + i\eta)(x_2 - x_1) + m\omega^2 x_1 = -f$$

$$-k_{d}(1 + i\eta)(x_{2} - x_{1}) + k_{d}(1 + i\eta)(x_{3} - x_{2}) + m_{o}\omega^{2}x_{2} = 0$$
 (C-5)

$$-k_d(1 + i\eta)(x_3 - x_2) + m\omega^2 x_3 = 0$$

Denoting the driving point acceleration amplitude by  $a_1 = -\omega^2 x_1$  we obtain the driving point response ratio  $f/ma_1$  by eliminating  $x_2$  and  $x_3$  from (C-5).

Setting  $\phi = \omega^2 m/k_d$  and  $\mu = m/m_o$  we find

$$\frac{f}{ma_1} = \frac{\phi^4 + r_3\phi^3 + r_2\phi^2 + r_1\phi + r_0 - i\eta\phi(\phi^2 + s_1\phi + s_0)}{[\phi^2 - \phi(1 + 2\mu) + (1 - \eta^2)\mu]^2 + \eta^2[\phi(1 + 2\mu) - 2\mu]^2}$$
(C-6)

where the coefficients in the real part of the numerator are

$$r_{3} = -(3 + 4\mu)$$

$$r_{2} = 3 + 9\mu + 4\mu^{2} + \eta^{2}(1 + 3\mu + 4\mu^{2})$$

$$r_{1} = -(1 + \eta^{2})(1 + 6\mu + 6\mu^{2})$$

$$r_{0} = (1 + \eta^{2})^{2}\mu(1 + 2\mu)$$
(C-7)

and the coefficients in the imaginary part of the numerator are

$$s_1 = -2(1 + \mu)$$
  
 $s_0 = (1 + \eta^2)(1 + 2\mu + 2\mu^2)$  (C-8)

For this configuration if the loss factor is not too large there are four real values of  $\phi = \omega^2 m/k_d$  for which the real part of (C-6) vanishes: two resonances and two antiresonances. At any one of these 90° phase conditions the magnitude of the response ratio reduces to

$$\left|\frac{\mathbf{f}}{ma_1}\right| = \frac{\eta \phi \left[\phi^2 - 2\phi(1+\mu) + (1+\eta^2)(1+2\mu+2\mu^2)\right]}{\left[\phi^2 - \phi(1+2\mu) + (1-\eta^2)\mu\right]^2 + \eta^2 \left[\phi(1-2\mu) - 2\mu\right]^2}$$
(C-9)

For fixed  $\mu=m/m_0$  there is a unique pair of values for  $\eta$  and  $\phi$  which simultaneously cause the real part of (C-6) to vanish and satisfy (C-9) for a measured value of the response ratio obtained when the phase difference is 90°. As before, the value of  $\phi=\omega^2m/k_d$  together with the measured frequency yield the dilational spring constant  $k_d$  which in turn provides the dilational modulus by way of Eq. 14.

## Captions for Figures

- Fig. 1 Suspension configuration for longitudinal vibration of clay rods.
- Fig. 2 Instrumentation chain for longitudinal vibration of rods.
- Fig. 3 Frame for forming clay rods.
- Fig. 4 Propagation velocity and loss factor for clay rod with L = 9 in. at 75° F.
- Fig. 5 Suspension configuration for determining dilational wave parameters of clay disk. Suspended mass can be increased by bolting on additional disks.
- Fig. 6 Instrumentation chain for determining dilational wave parameters of clay disk.
- Fig. 7 Propagation velocity and loss factor for dilational wave in clay disk at 75° F.: A, immediately after remolding specimen; B, two days later.
- Fig. 8 Small amplitude excitation of shearing oscillations in clay slab; (1) Plasticine slab with glass cover sheet, (2) ARA-20 slip table, (3) Ling V-50 Mk 1 shaker, (4) inertial mass driven by shaker, (5) strings to support weight of inertial mass.

- Fig. 9 Large amplitude excitation of shearing oscillations in clay slab; (1) Plasticine slab with glass cover sheet,
  (2) Calidyne Λ-174 shaker, (3) shaker armature (4) ARΛ-20 slip table, (5) connection points.
- Fig. 10 Plan view of clay slab and glass cover sheet placed on top of slip table. Accelerometer locations B-1 to B-4 on slip table and T-1 to T-5 on glass cover sheet.
- Fig. 11 Instrumentation chain for determining shear wave parameters of clay slab.
- Fig. 12 Propagation velocity and loss factor for shear wave in clay slab at 75° F.
- Fig. 13 Clay sandwich for alternating dilation and shear tests: A, axis of excitation for dilational deformation; B, axis of excitation for shear deformation.
- Fig. 14 Excitation of clay sandwich (a) for dilation, (b) for shear.
- Fig. 15. Instrumentation chain for recording corrected force amplitude, acceleration amplitude and phase difference as functions of frequency.
- Fig. 16 Force and acceleration signal amplitudes in dE re 1.0 volt for dilational test: corrected force signal (A); acceleration signal (B).

- Fig. 17 Phase angle by which acceleration signal leads corrected force signal for dilational test.
- Fig. 18 Force and acceleration signal amplitudes in dB re 1.0 volt for shear test: corrected force signal (A); acceleration signal (B).
- Fig. 19 Phase angle by which acceleration signal leads corrected force signal for shear test.
- Fig. 20 Lumped parameter models for clay sandwich (a) in dilation test, and (b) in shear test.
- Fig. 21 Shear propagation velocity of Plasticine at 75° F. as a function of time elapsed since remolding, calculated (A) by neglecting clay mass and (B) by apportioning all of clay mass to metal slabs.
- Fig. 22 Contours for fixed levels of rod propagation velocity crin frequency-temperature plane for 3" Plasticine rod. Dotted lines indicate loci of resonances and anti-resonances where measurements were made.
- Fig. 23 Contours for fixed levels of loss factor  $\eta$  in frequency-temperature plane for 3" Plasticine rod.
- Fig. 24 Rod propagation velocity of a Plasticine rod as a function of temperature.

- Fig. 25 Shear wave propagation velocity of a Plasticine slab as a function of temperature.
- Fig. 26 Loss factor  $\eta$  for shear of a Plasticine slab. Points plotted are averages of measured values at the temperatures indicated.
- Fig. 27 Rod propagation velocity of Plasticine rod at 75° F. due to time history of ambient pressure shown below.
- Fig. 28 Rod propagation velocity of four specimens as a function of longitudinal strain level.
- Fig. 29 Shear wave propagation velocity of clay slab with five different suspended masses as a function of shear strain level.
- Fig. 30 Time history of rod propagation velocity in a 6" Plasticine rod due to manual bending at A and calibrated bending at B.
- Fig. 31 Rod propagation velocity of a 3" Plasticine rod B, before, and A, after large-strain bending.
- Fig. 32 Shear wave propagation velocity as a function of shear strain level measured as strain level is decreased from three different maximum strain levels A, B, and C.
- Fig. 33 Rigid disk on viscoelastic half space vibrating vertically at frequency  $\omega$ : (a) complete system; (b) interaction force on half space; (c) interaction force on disk.

- Fig. 34 Viscoelastic half space functions for  $\nu = 0.5$  and  $\eta = 0.2$ .
- Fig. 35 Excitation of disk on surface of clay by Wilcoxon F-1 shaker driving through Wilcoxon Z-602 impedance head.
- Fig. 36 Instrumentation chain for measurement of admittance of disk on the surface of a tub of clay.
- Fig. 37 Comparison of predicted admittance of disk on viscoelastic half space (dashed curve) with measured admittance of disk on tub of Plasticine (solid curve).

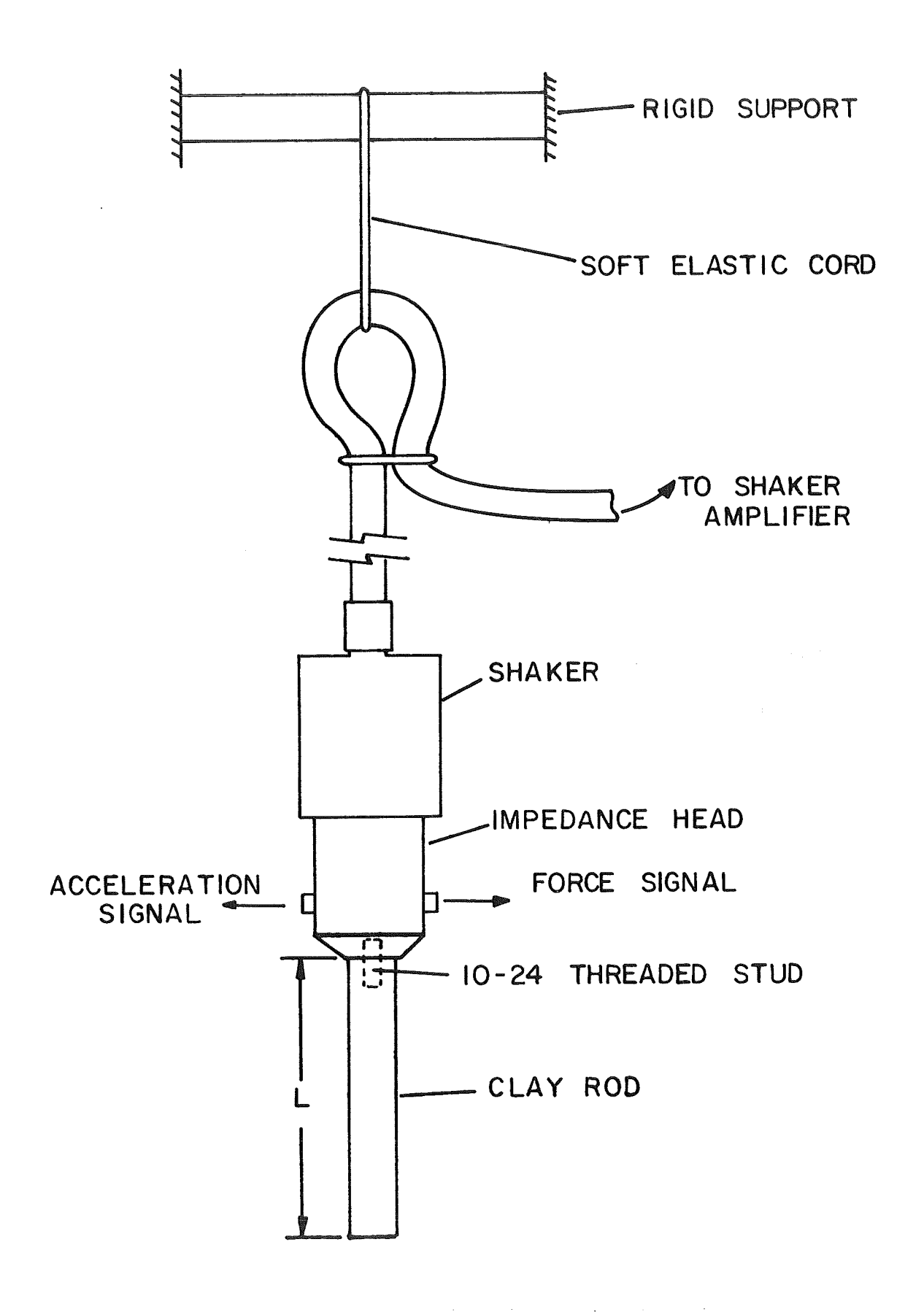


Fig. 1 Suspension configuration for longitudinal vibration of clay rods.

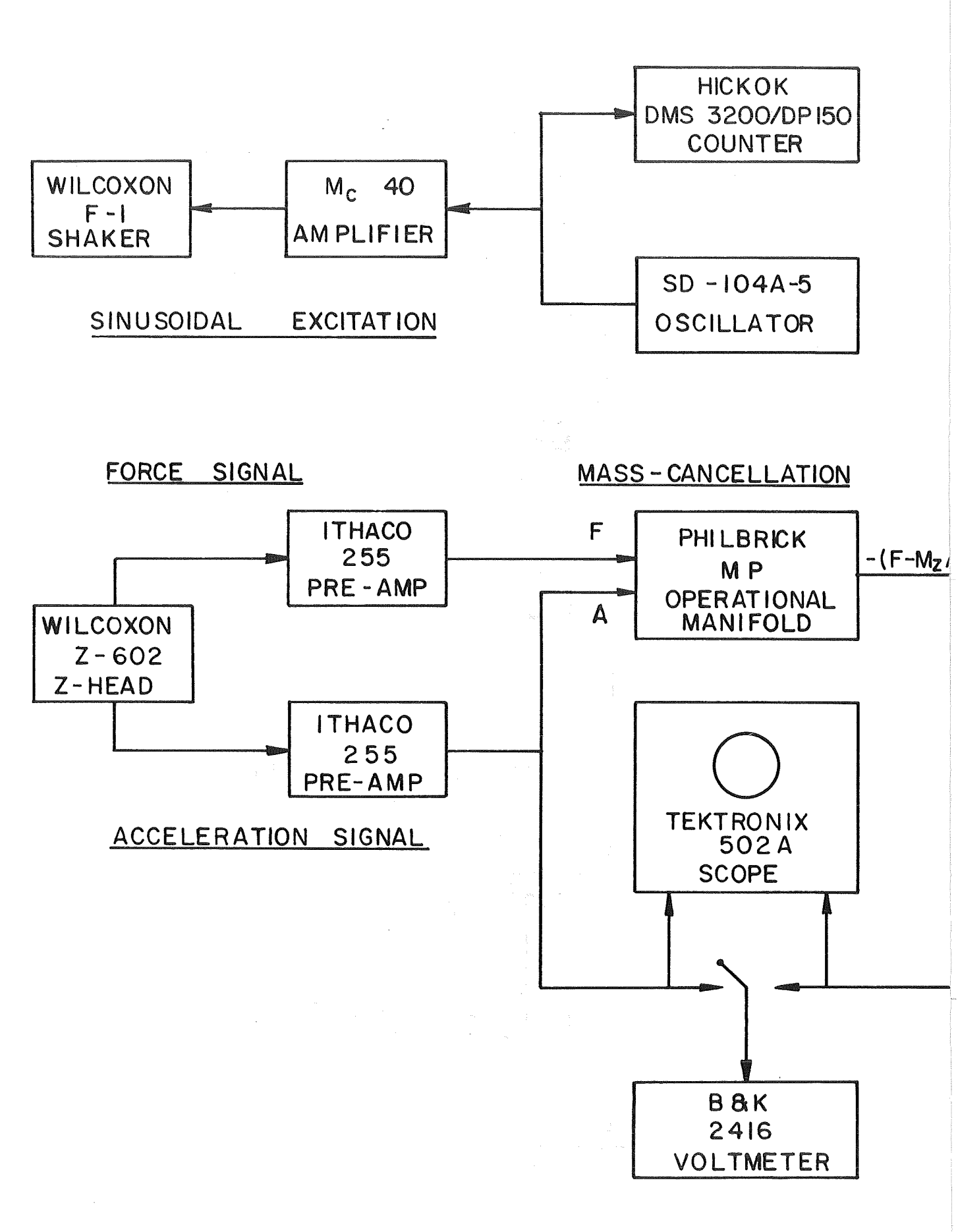


Fig. 2 Instrumentation chain for longitudinal vibration of rods

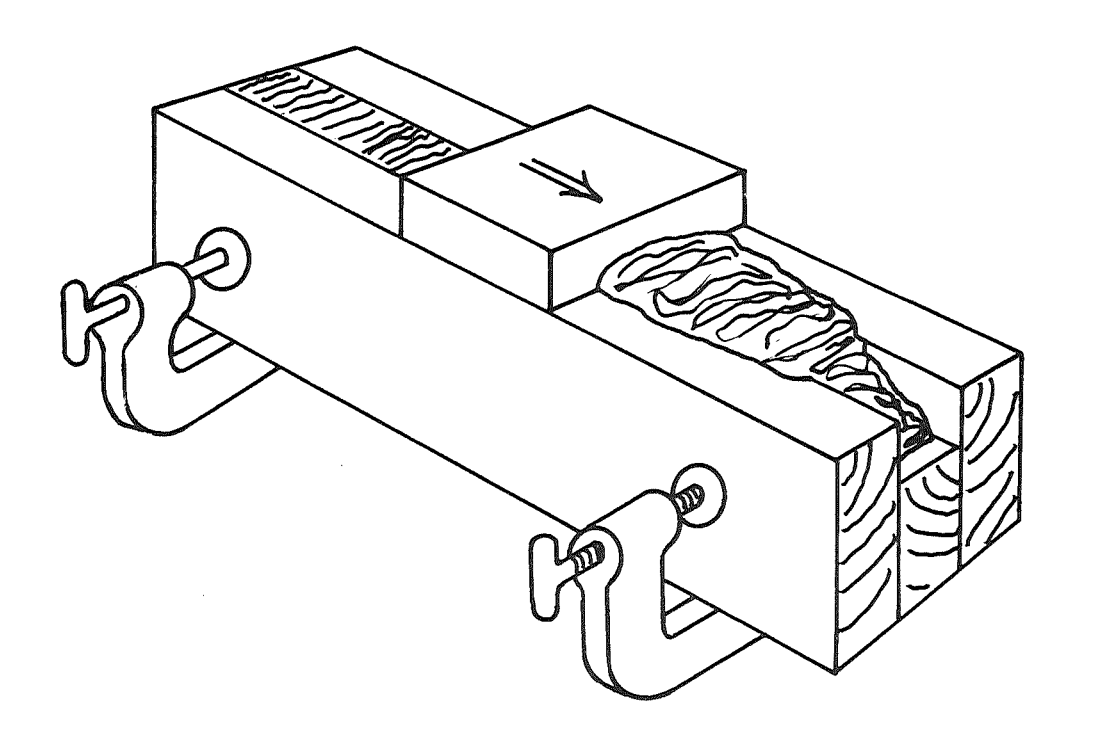


Fig. 3 Frame for forming clay rods

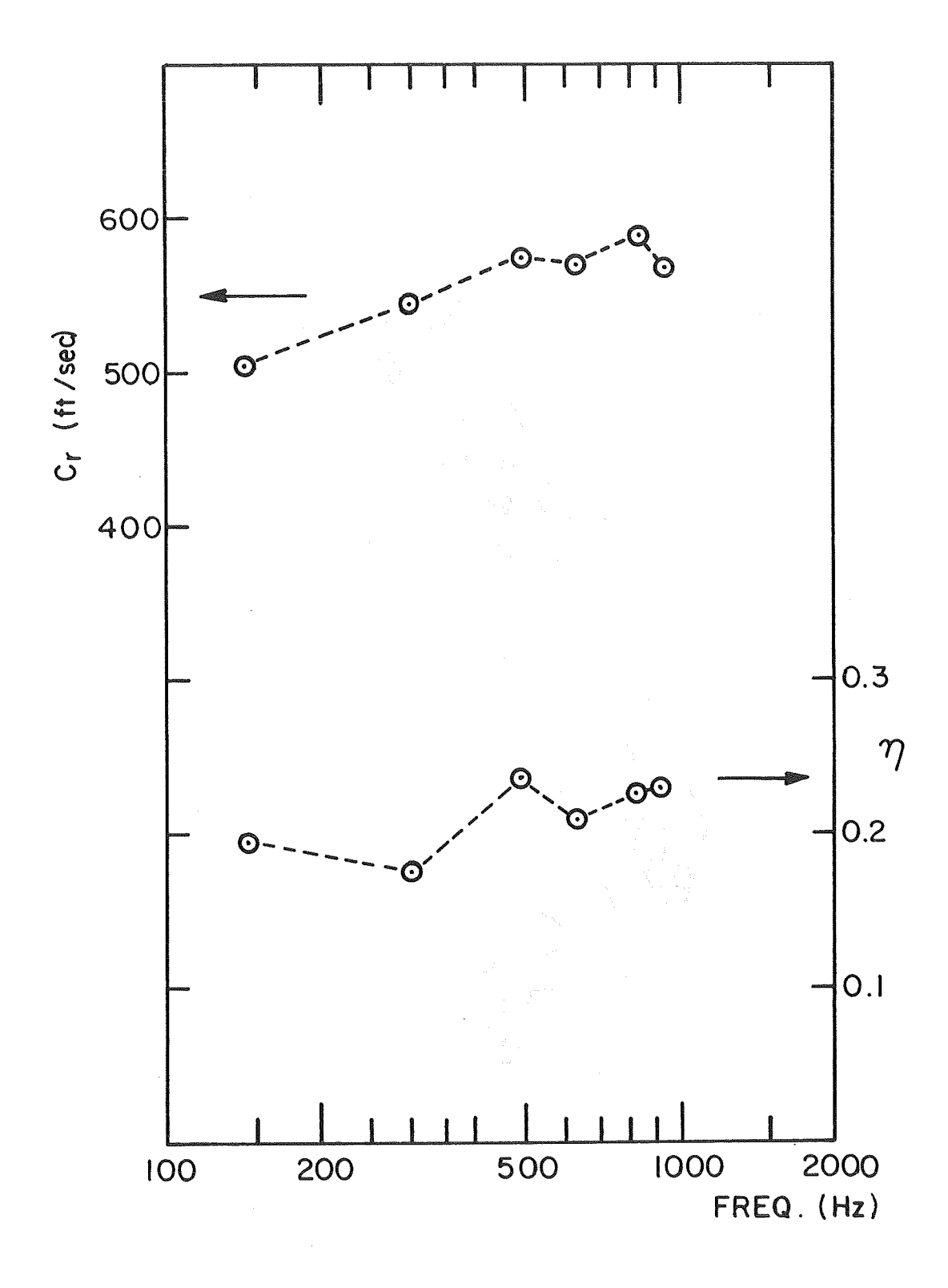
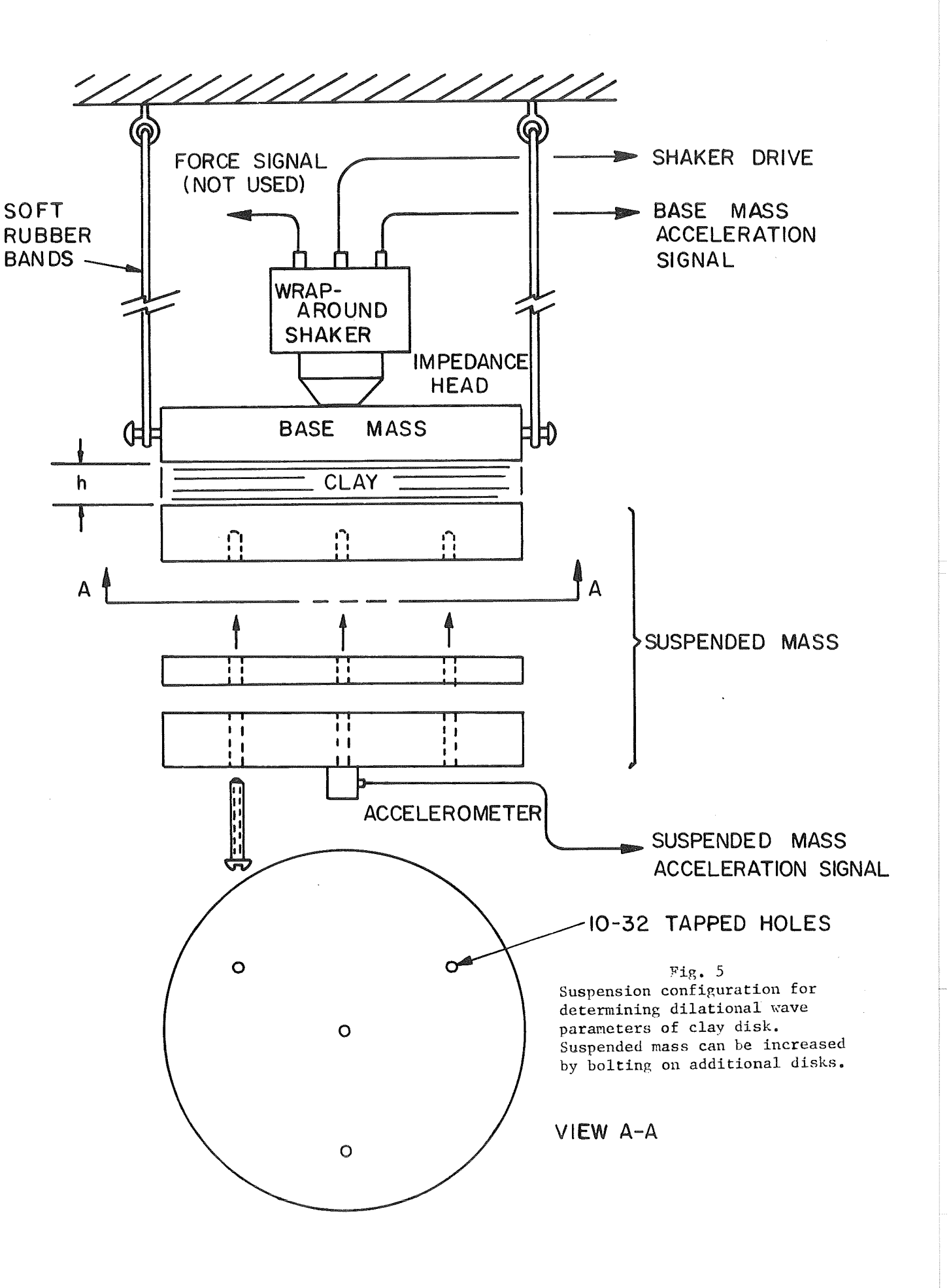
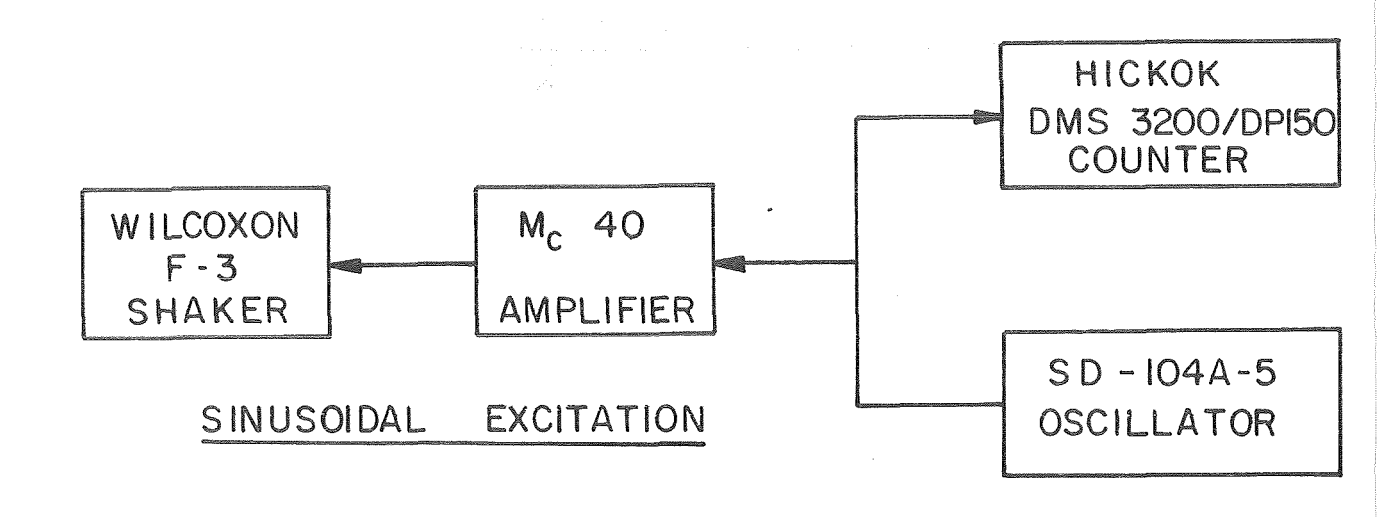


Fig. 4 Propagation velocity and loss factor for clay rod with L=9 in. at 75° F.





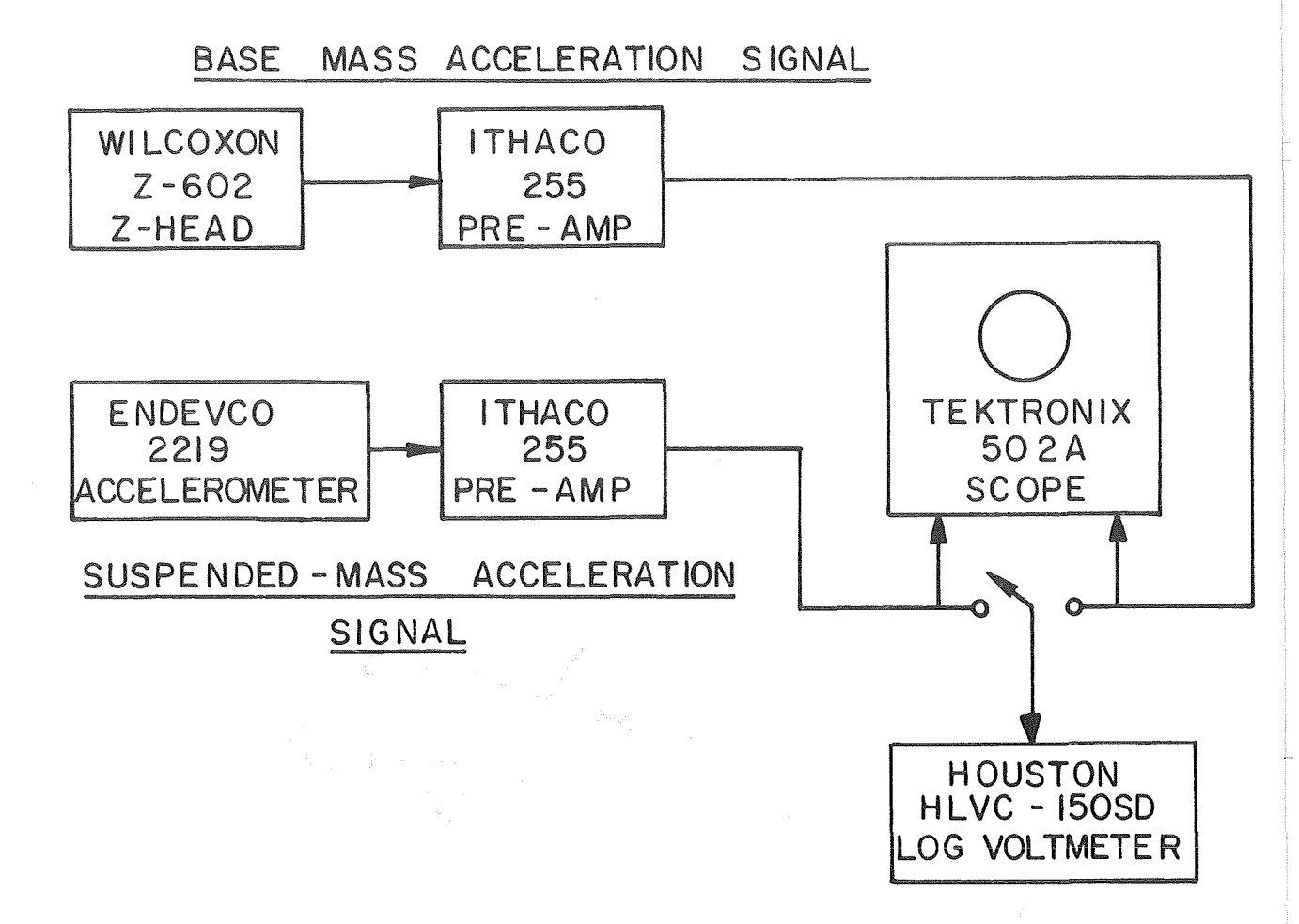


Fig. 6 Instrumentation chain for determining dilational wave parameters of clay disk.

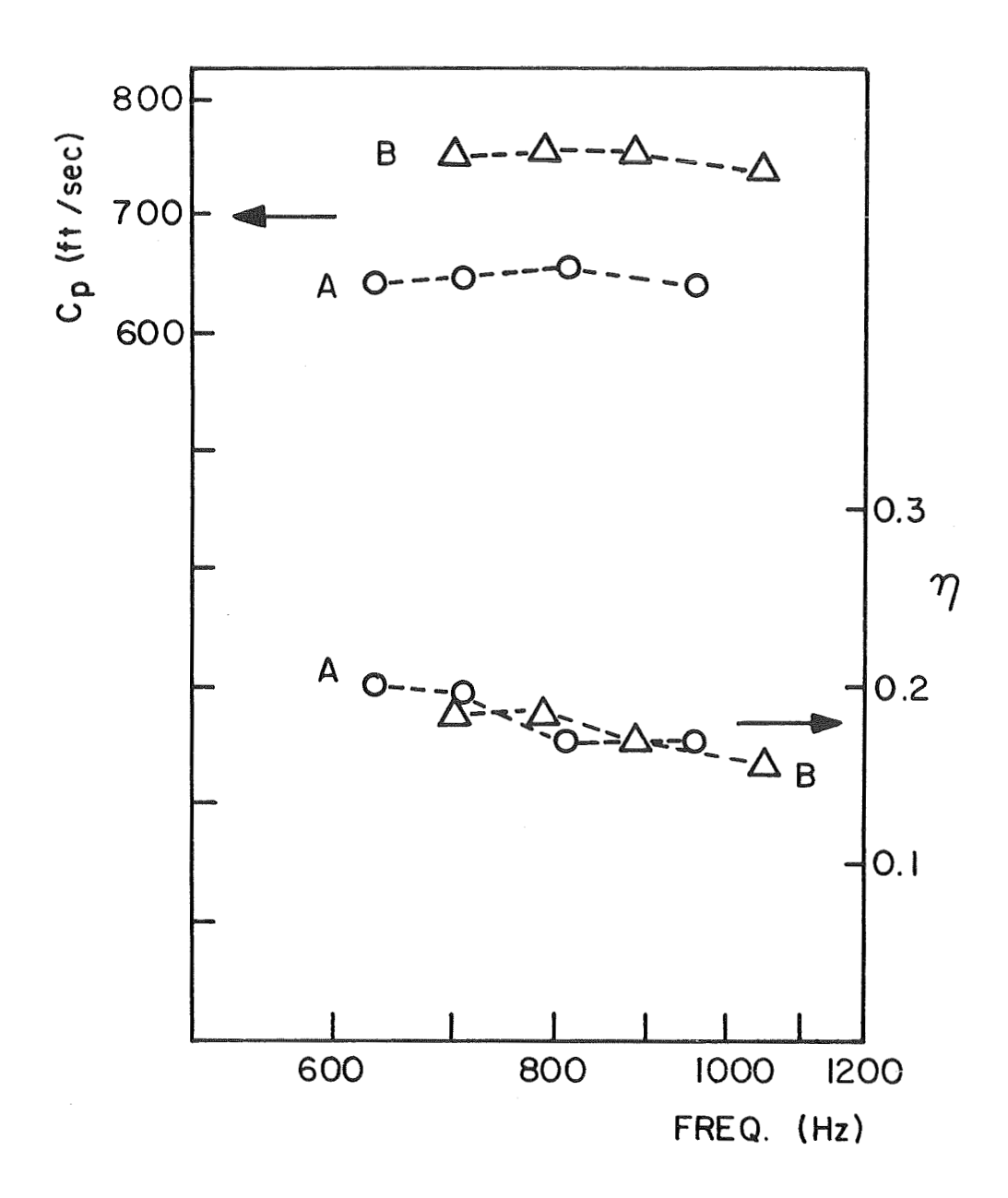


Fig. 7 Propagation velocity and loss factor for dilational wave in clay disk at 75° F.: A, immediately after remolding specimen b, two days later.

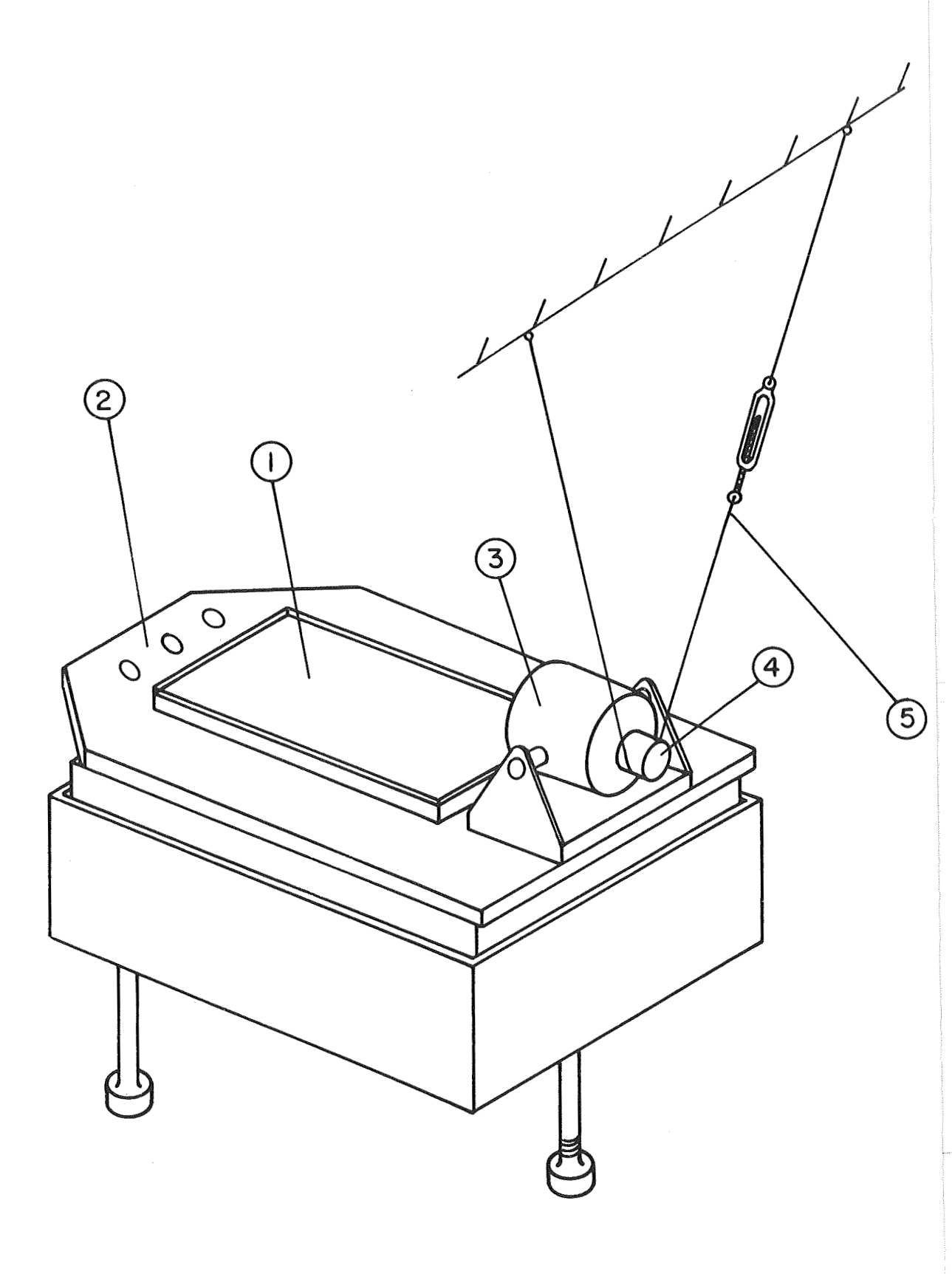


Fig. 8 Small amplitude excitation of shearing oscillations in clay slab;

- (1) Plasticine slab with glass cover sheet
- (2) ARA-20 slip table
- (3) Ling V-50 Mk 1 shaker
- (4) inertial mass driven by shaker
- (5) strings to support weight of inertial mass

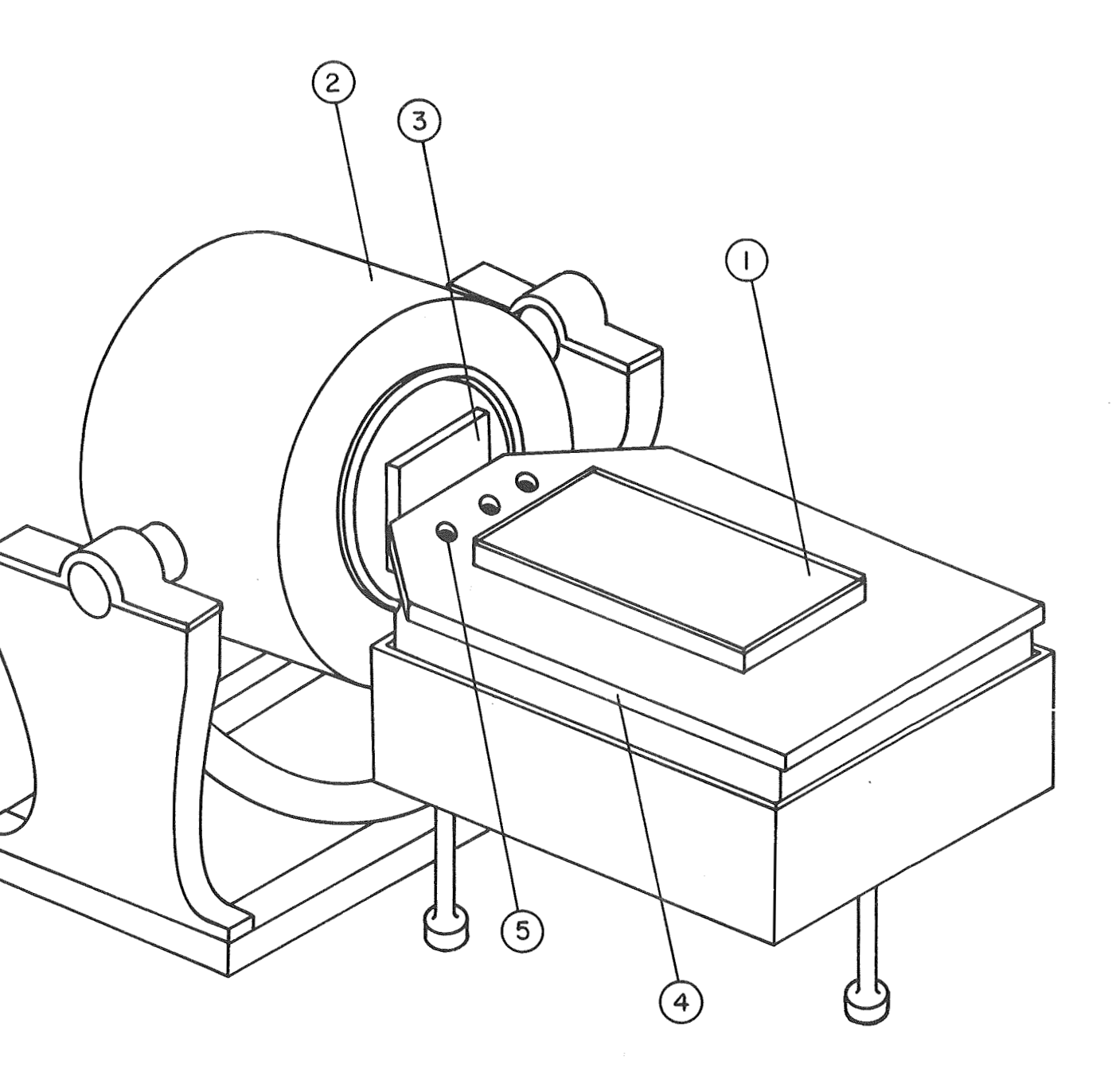


Fig. 9 Large amplitude excitation of shearing oscillations in clay slab; (1) Plasticine slab with glass cover sheet (2) Calidyne  $\Lambda$ -174 shaker (3) Shaker armature (4) ARA-20 slip table (5) connection points

- (5) connection points

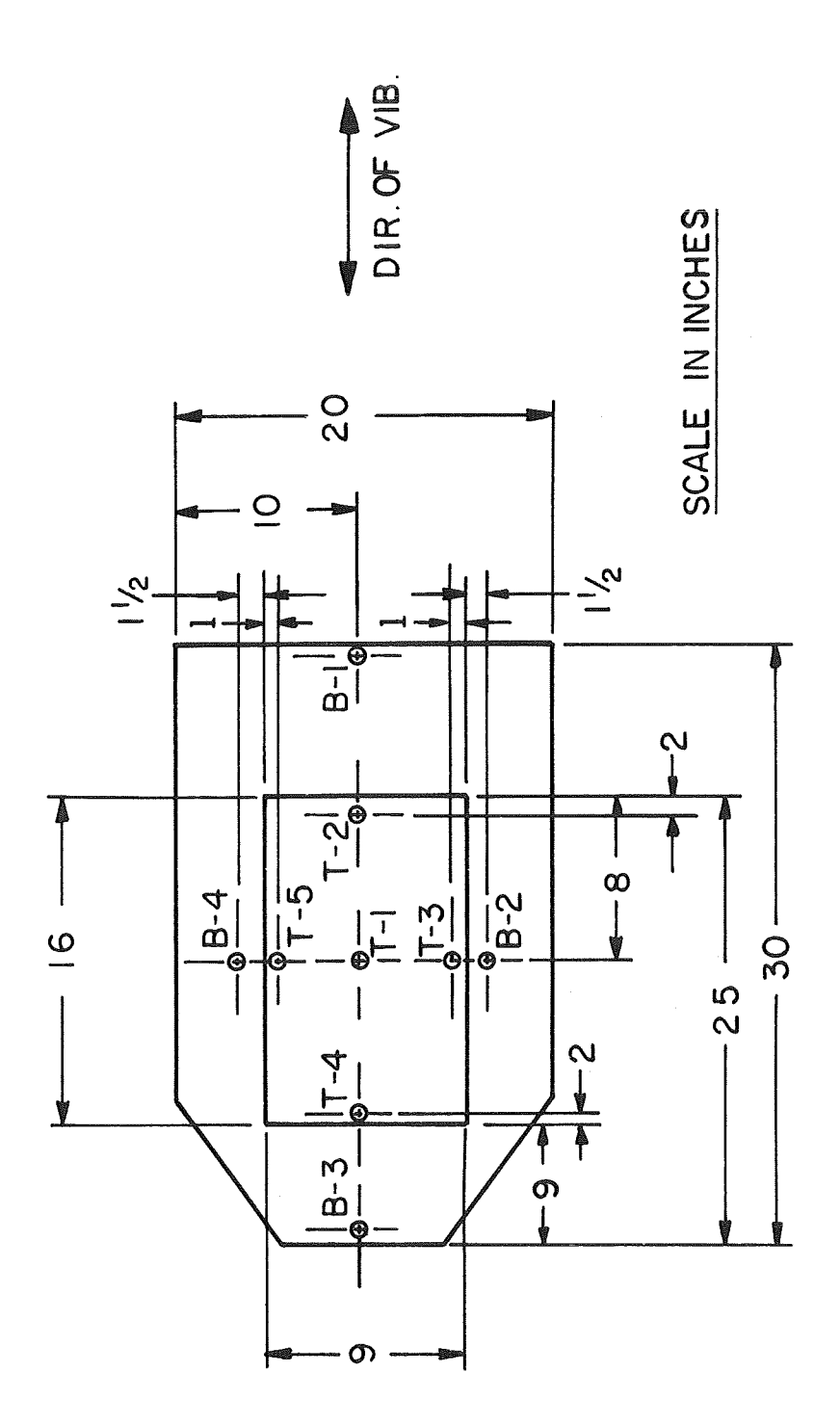


Fig. 10 Plan view of clay slab and glass cover sheet placed on top of slip table. Accelerometer locations B-1 to D-4 on slin table and T-1 to T-5 on glass cover sheet.

## SUSPENDED - MASS ACCELERATION SIGNAL

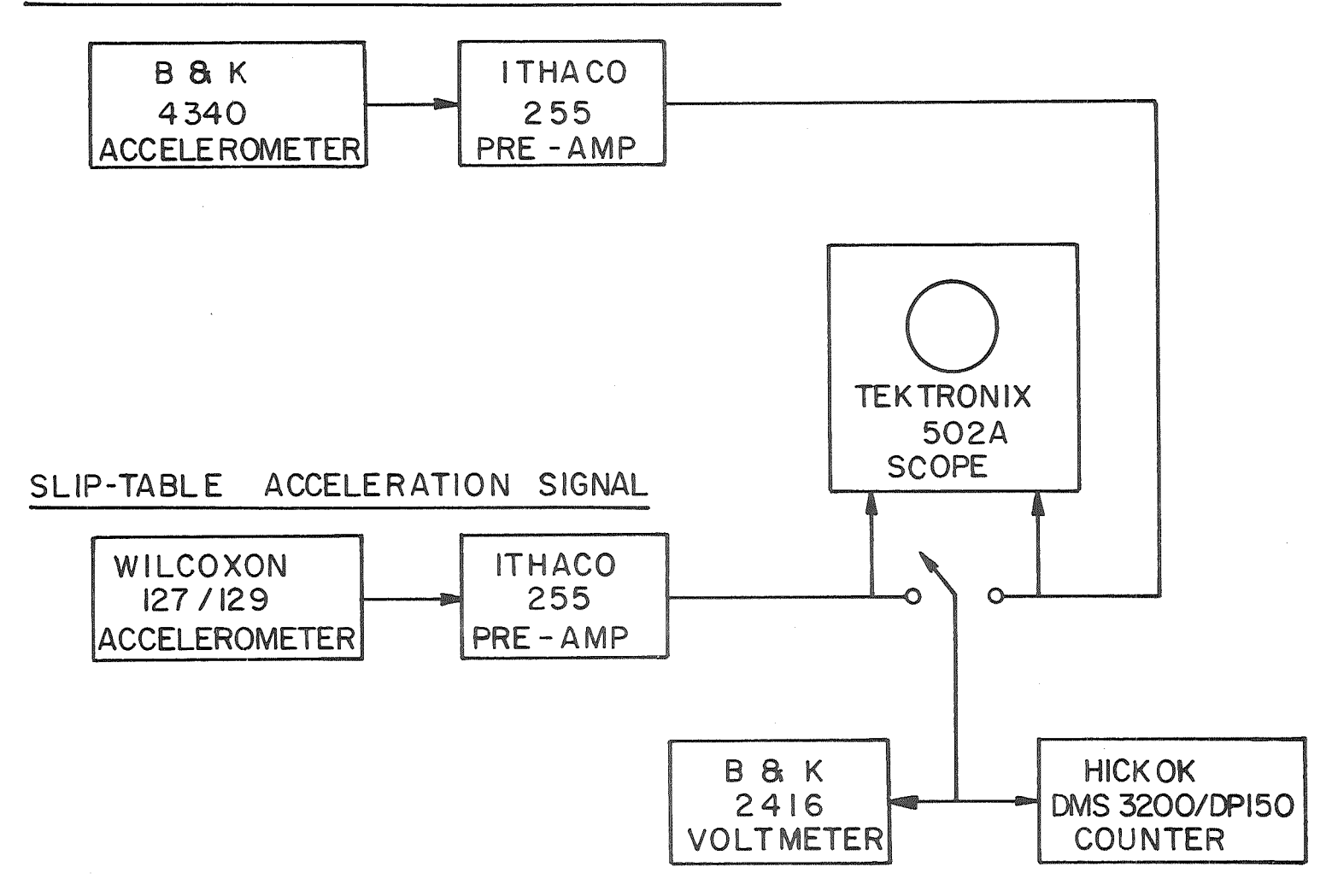


Fig. 11 Instrumentation chain for determining shear wave parameters of clav slab.

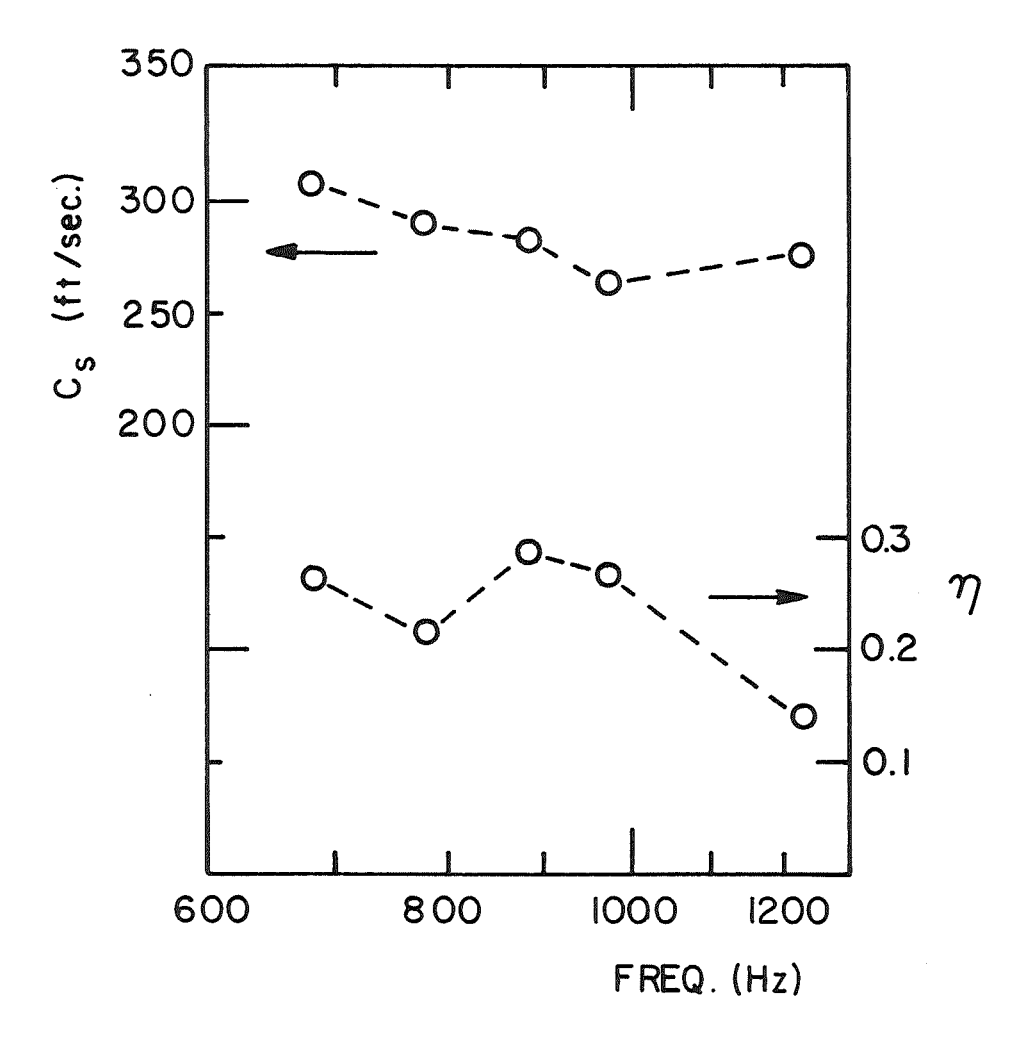


Fig. 12 Propagation velocity and loss factor for shear wave in clay slab at 75° F.

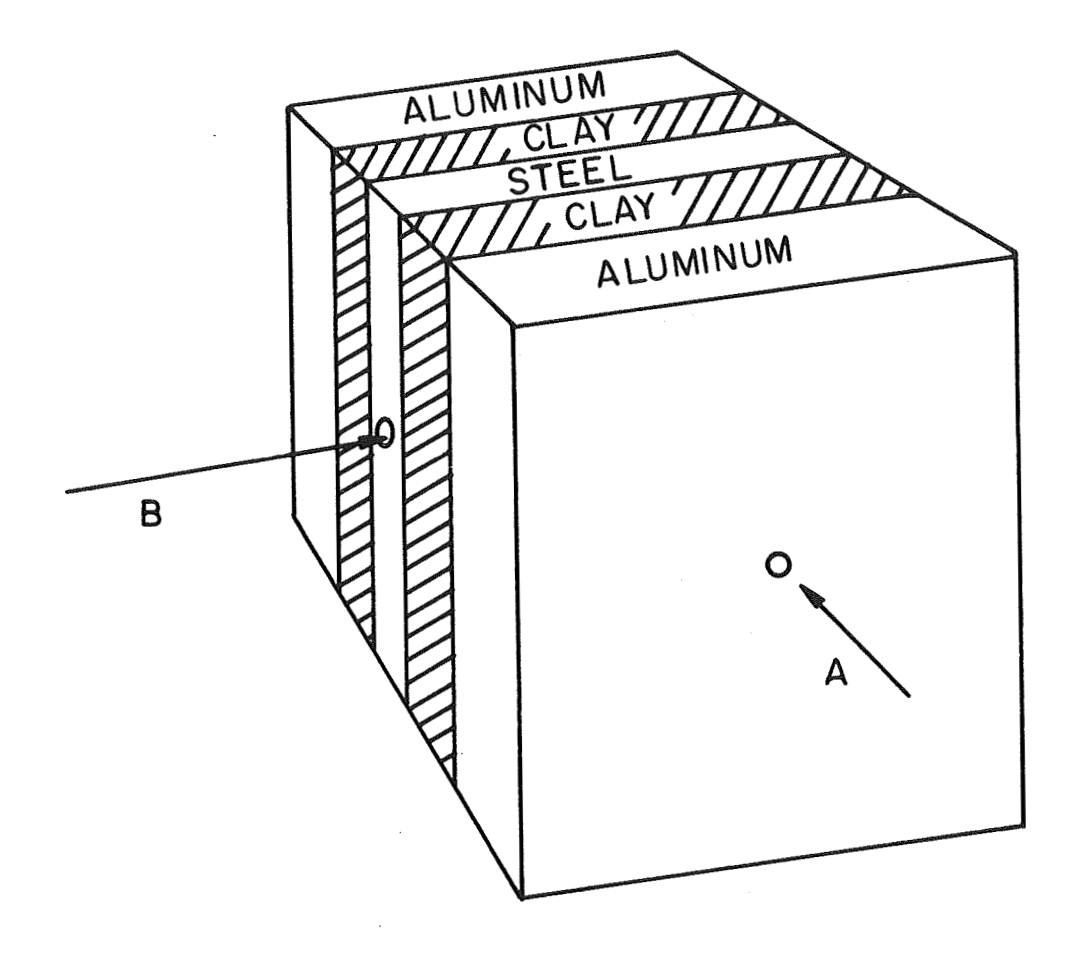


Fig. 13 Clay sandwich for alternating dilation and shear tests:
A, axis of excitation for dilational deformation
B, axis of excitation for shear deformation

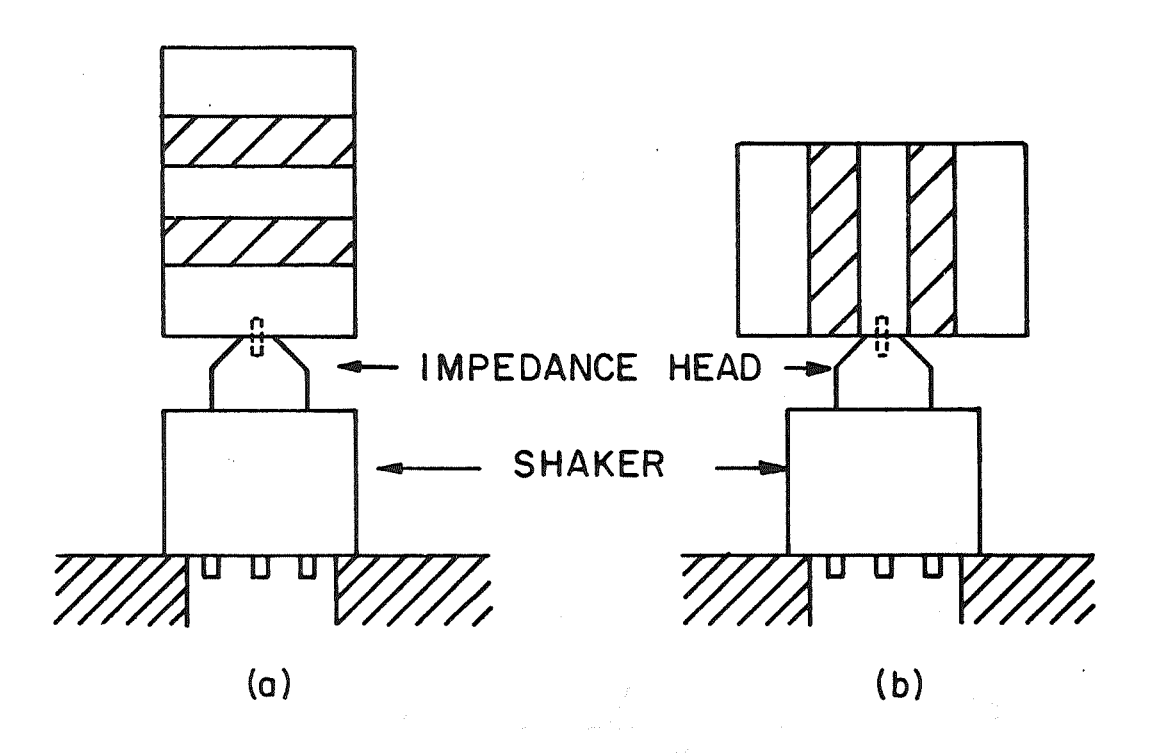
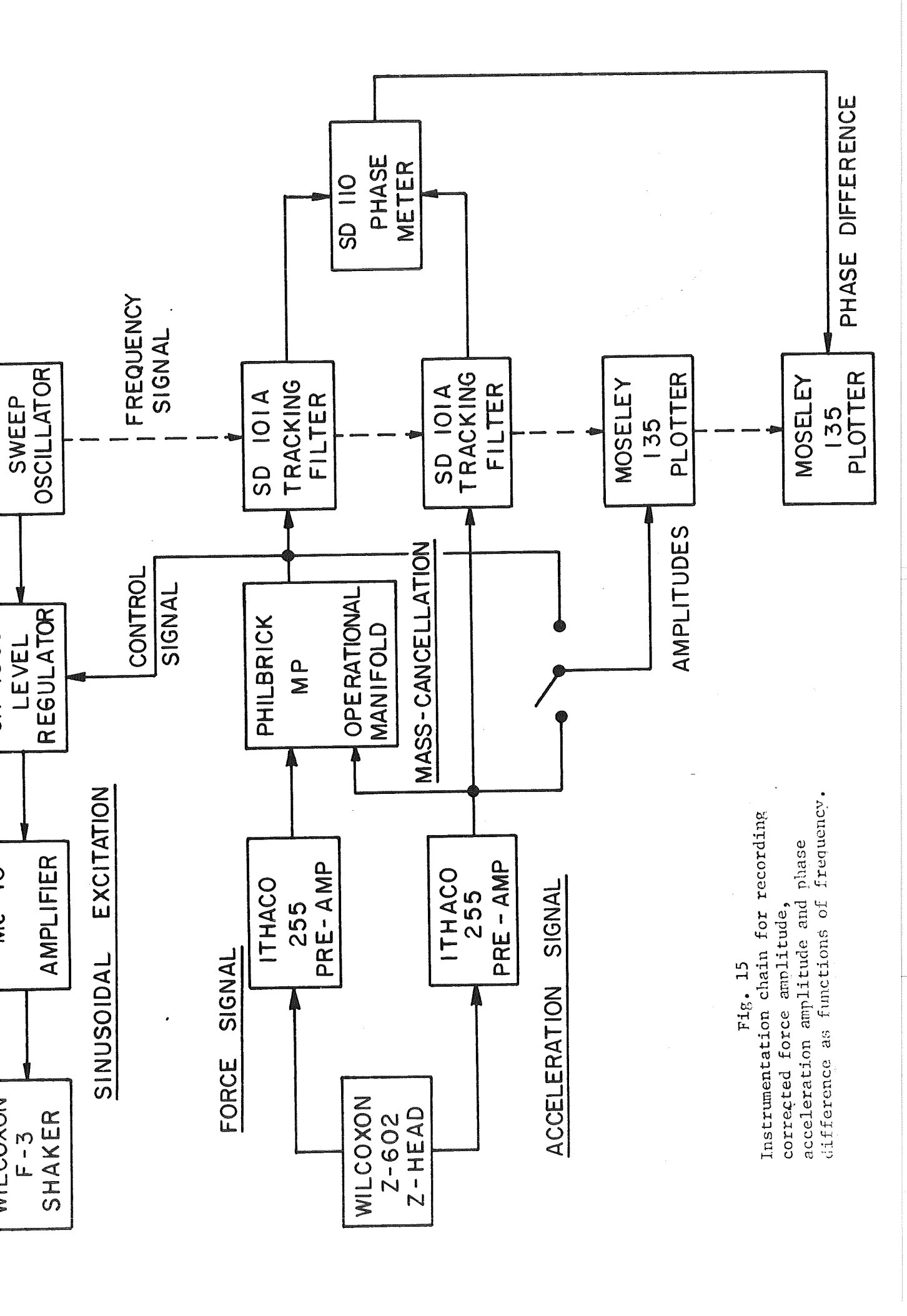


Fig. 14 Excitation of clay sandwich (a) for dilation (b) for shear



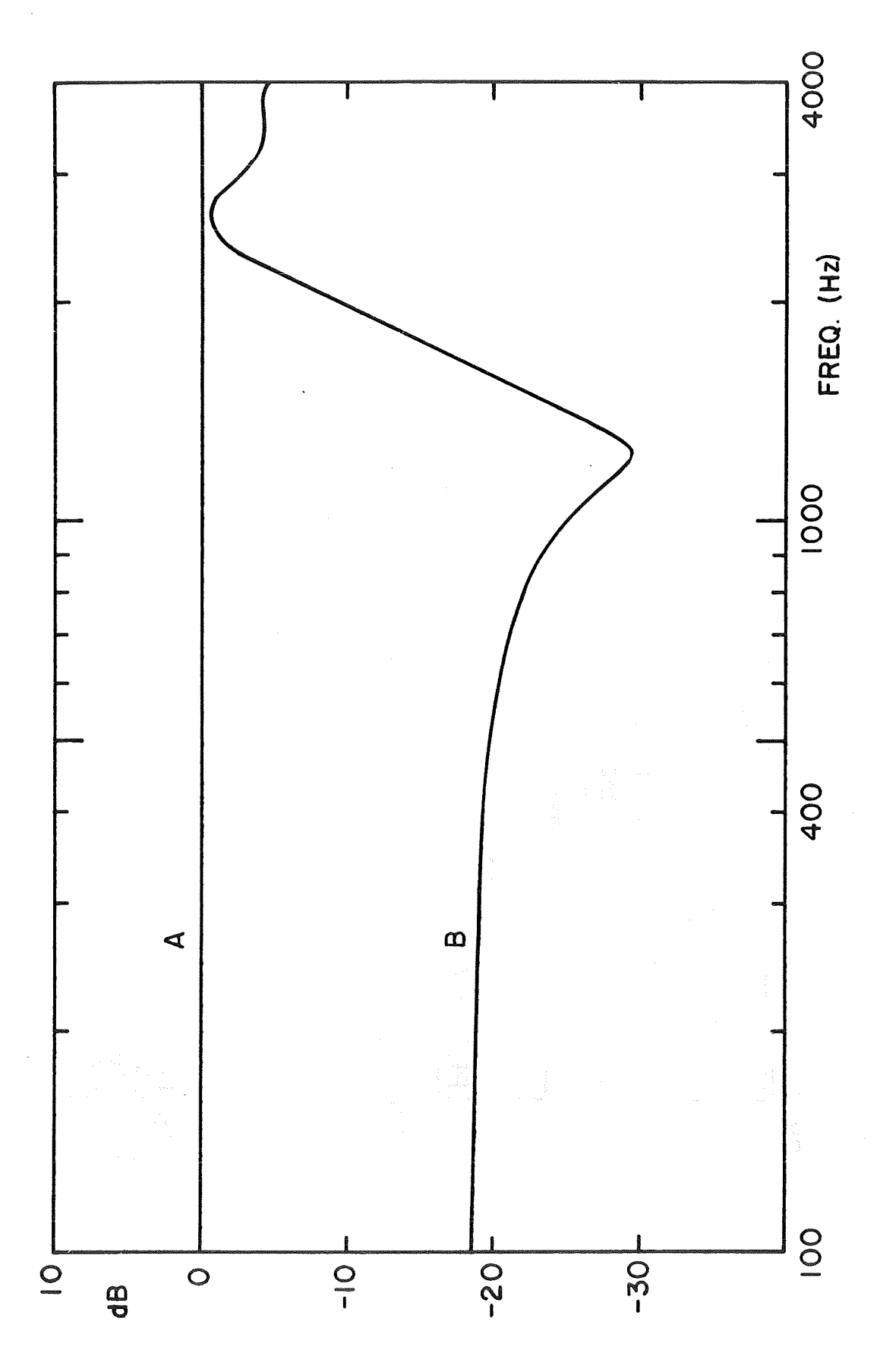


Fig. 16 Force and acceleration signal amplitudes in dB re 1.0 volt for dilational test: corrected force signal (A); acceleration signal (B).

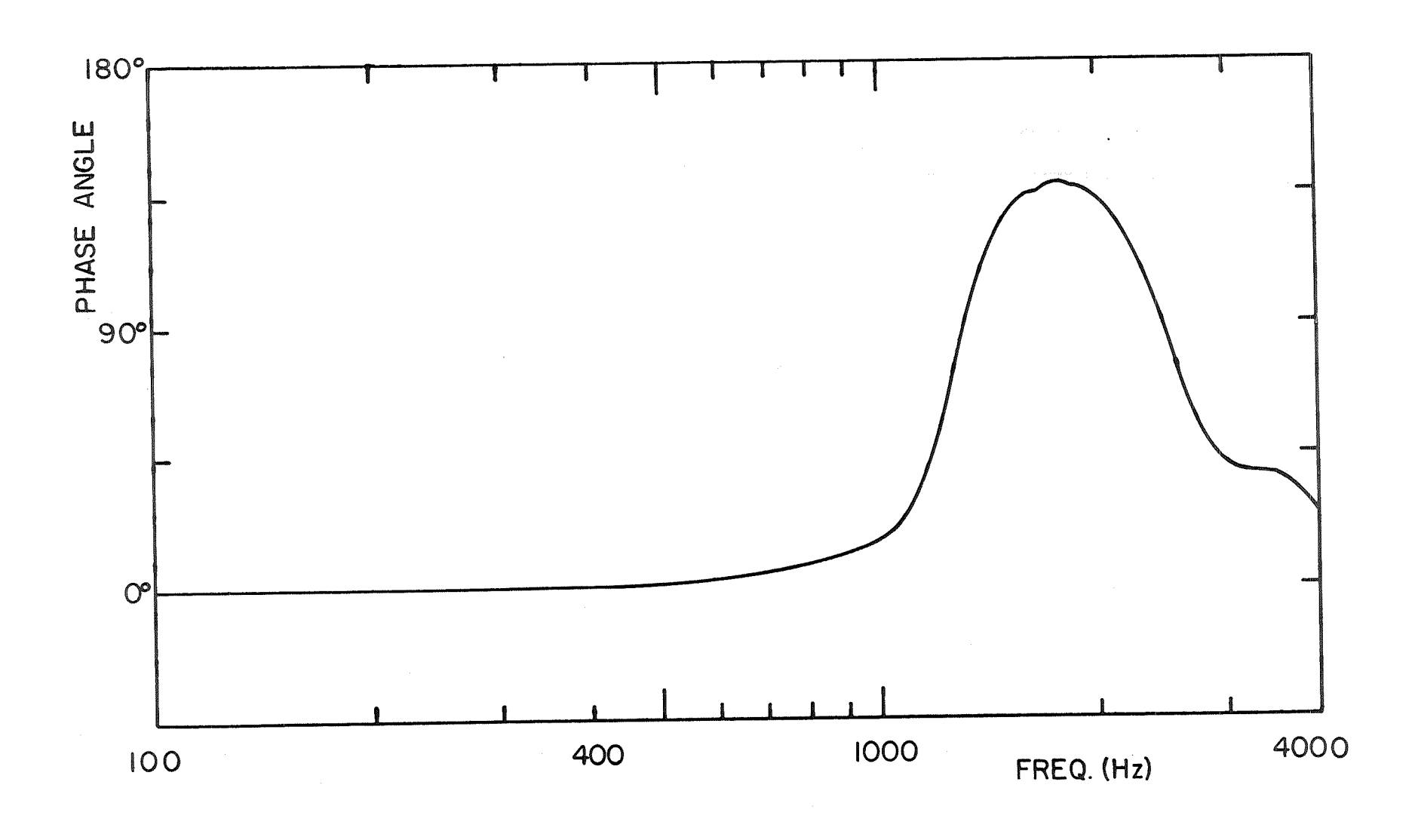


Fig. 17 Phase angle by which acceleration signal leads corrected force signal for dilational test

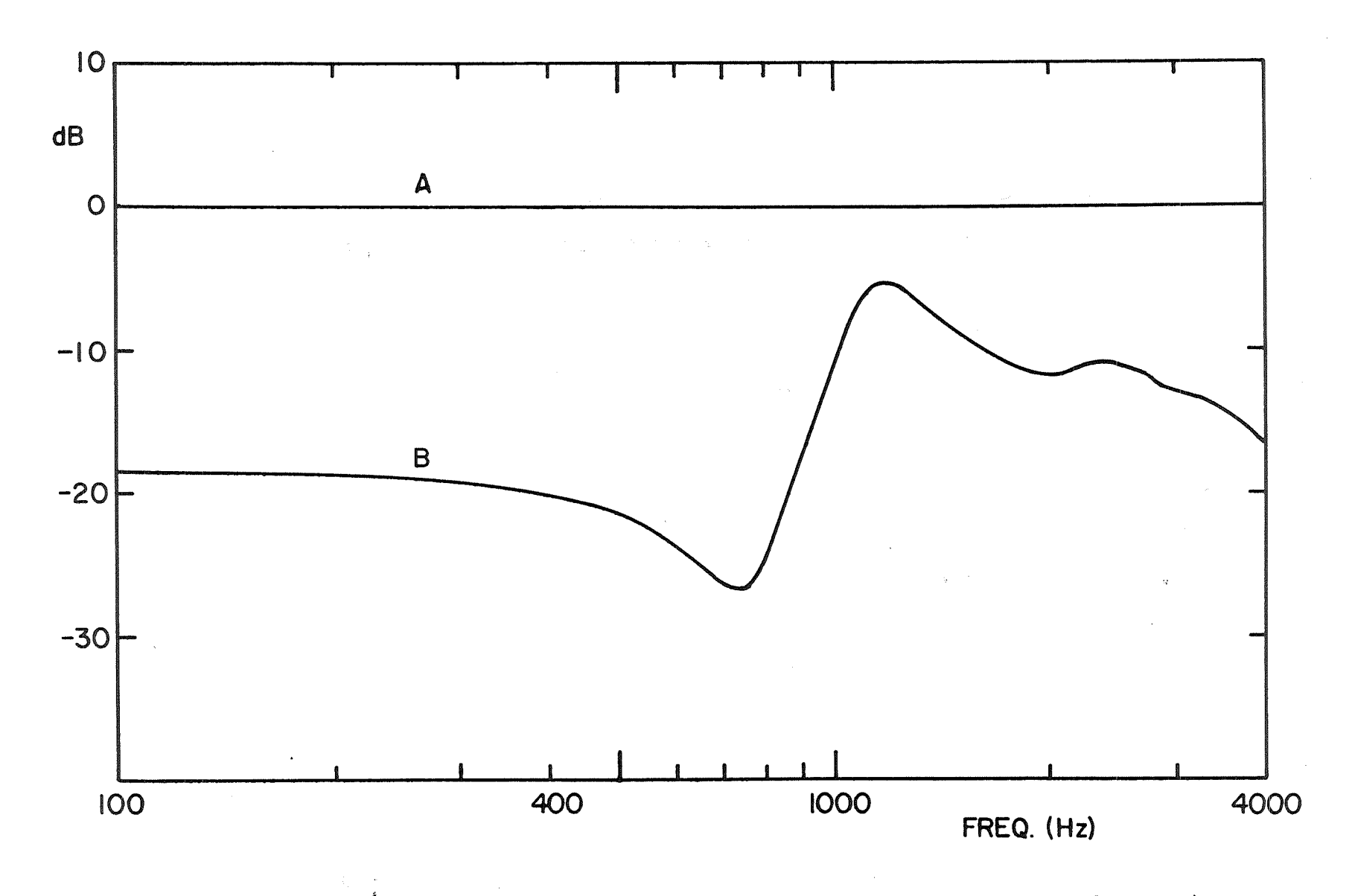


Fig. 18 Force and acceleration signal amplitudes in dB re 1.0 volt for shear test Corrected force signal (A); acceleration signal (B)

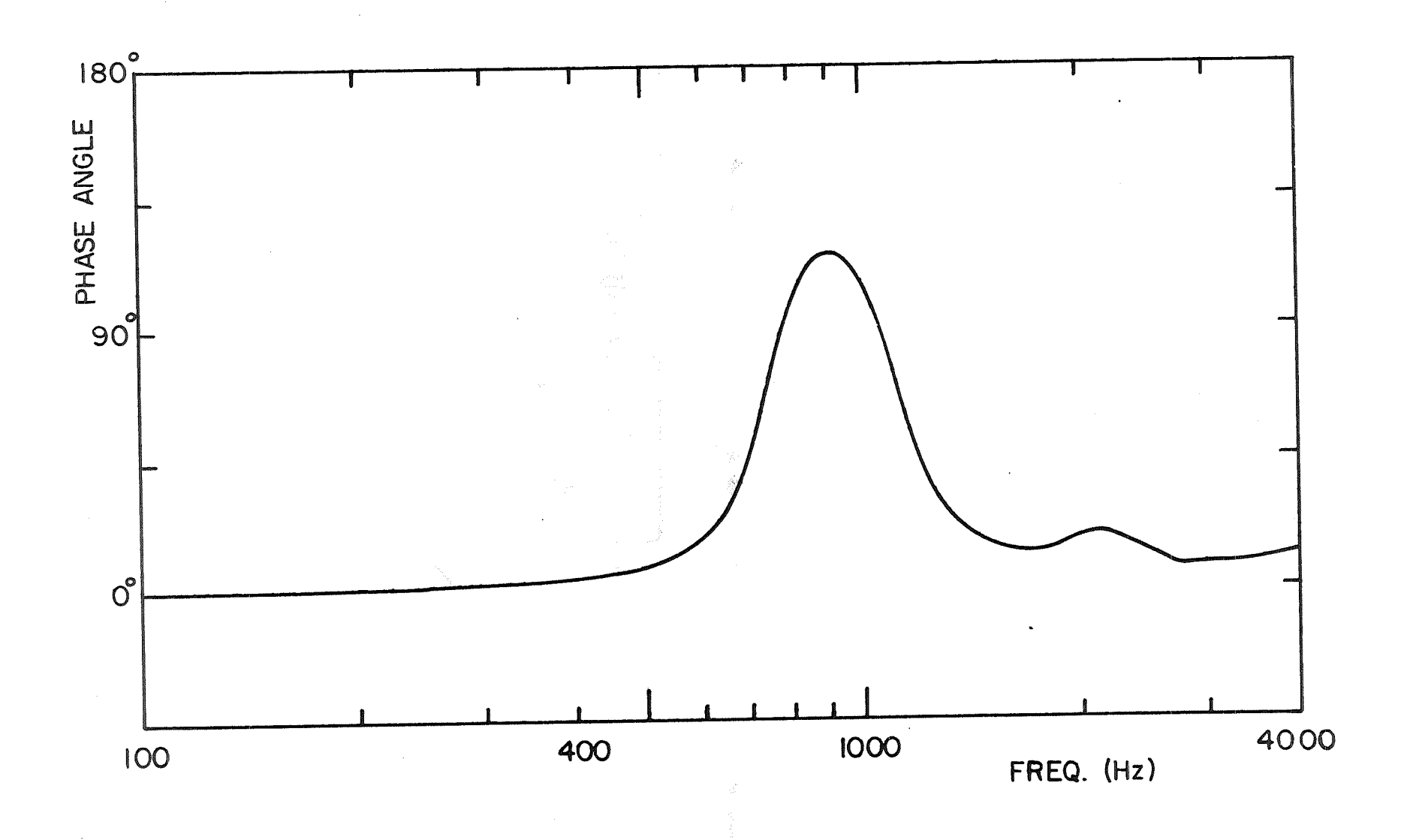
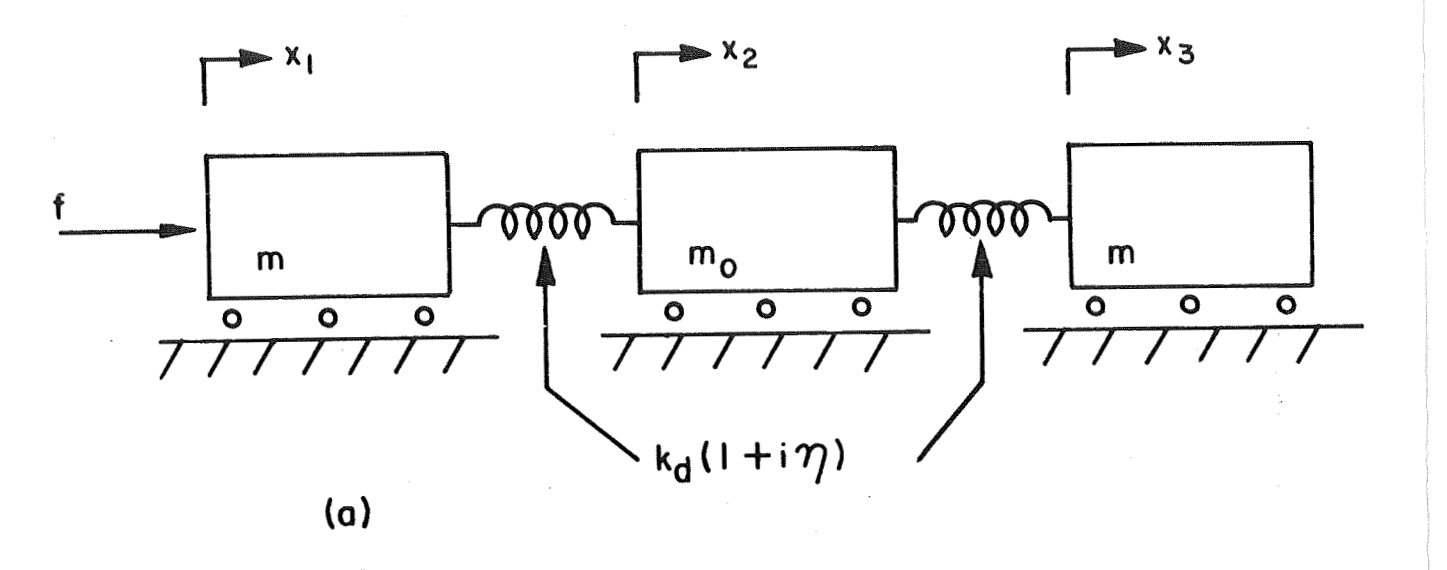


Fig. 19 Phase angle by which acceleration signal leads corrected force signal for shear test



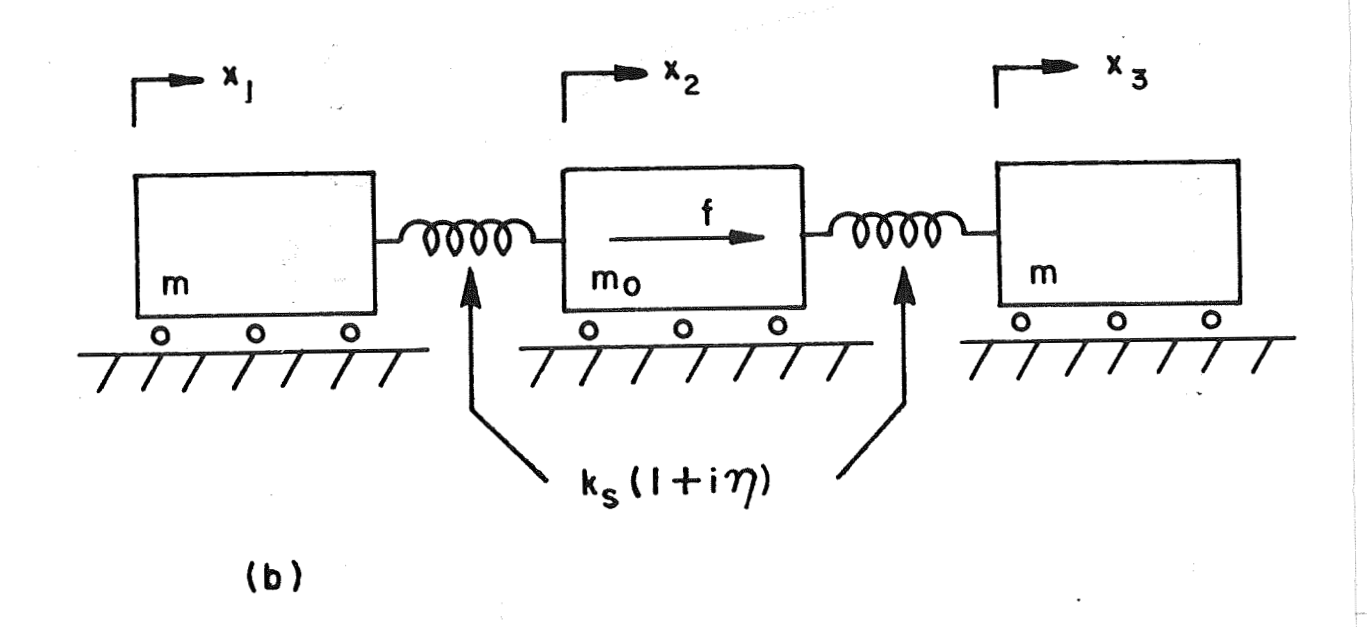


Fig. 20 Lumped parameter models for clay sandwich (a) in dilation test, and (b) in shear test.

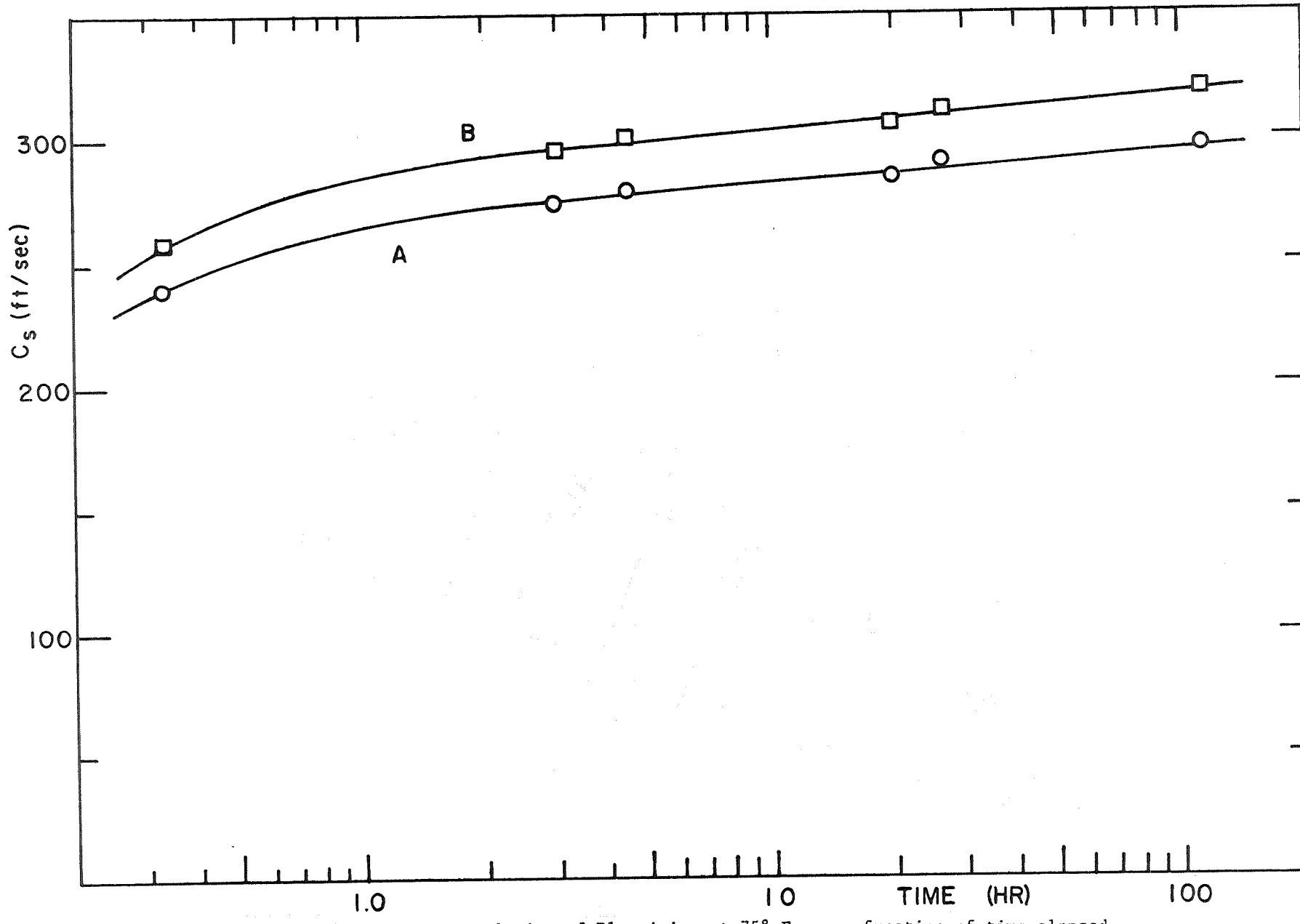


Fig. 21 Shear propagation velocity of Plasticine at 75° F. as a function of time elapsed since remolding, calculated (A) by neglecting clay mass and (B) by apportioning all of clay mass to metal slabs.

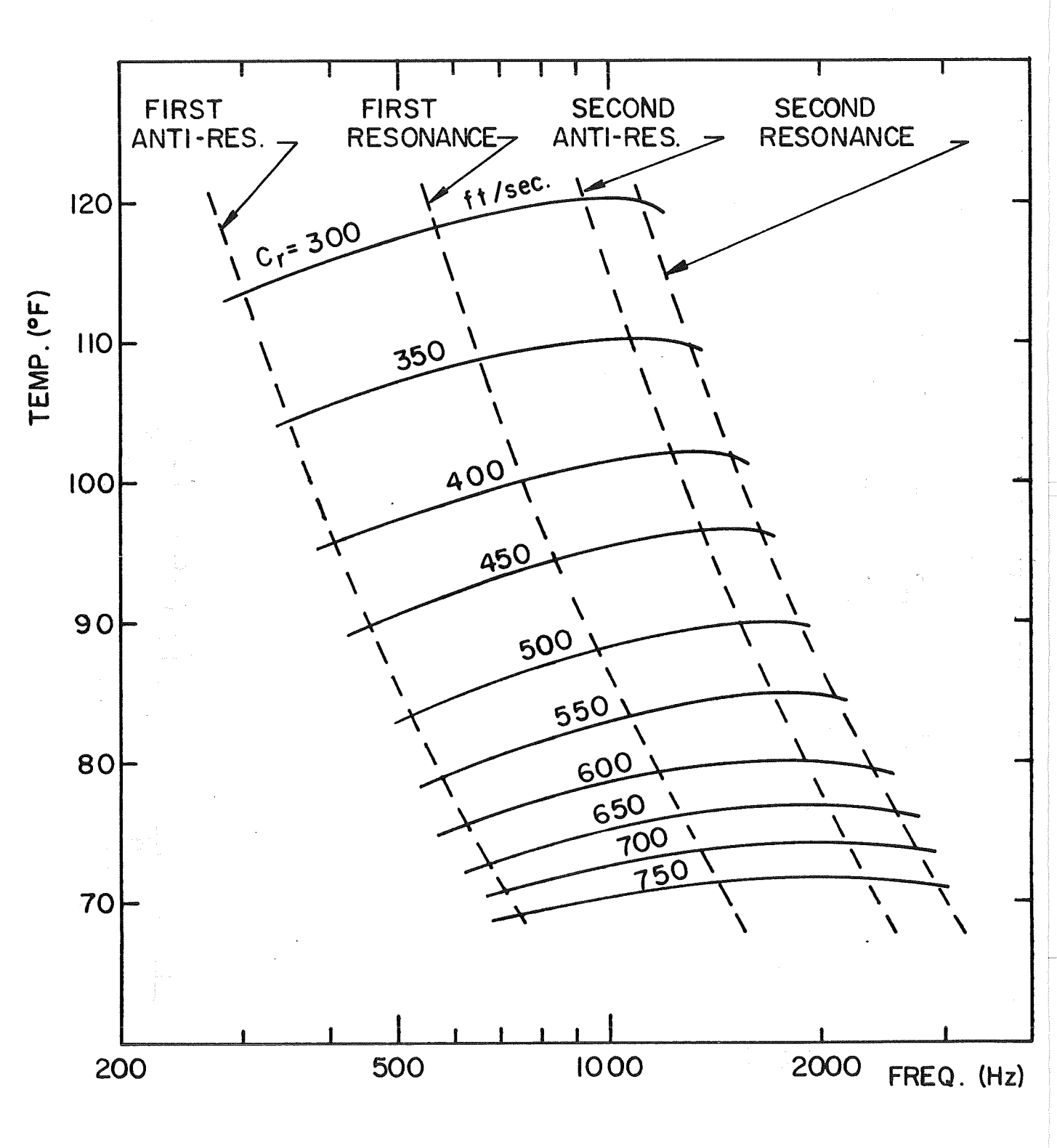


Fig. 22 Contours for fixed levels of rod promagation velocity  $\mathbf{c}_{\mathbf{r}}$  in frequency-temperature plane for 3" Plasticine rod. Dotted lines indicate loci of resonances and antiresonances where measurements were made.

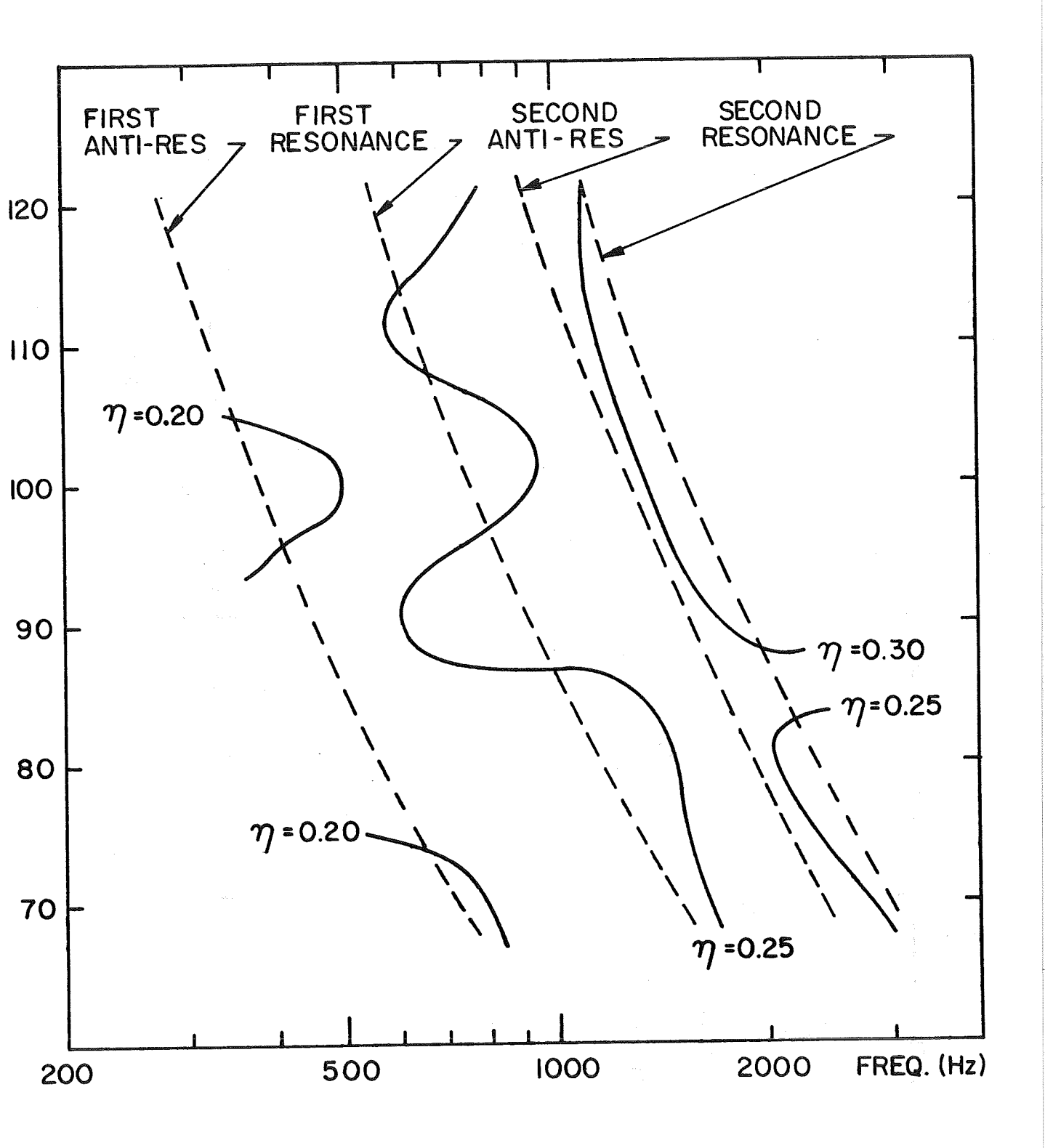


Fig. 23 Contours for fixed levels of loss factor  $\eta$  in frequency-temperature plane for 3" Plasticine rod.

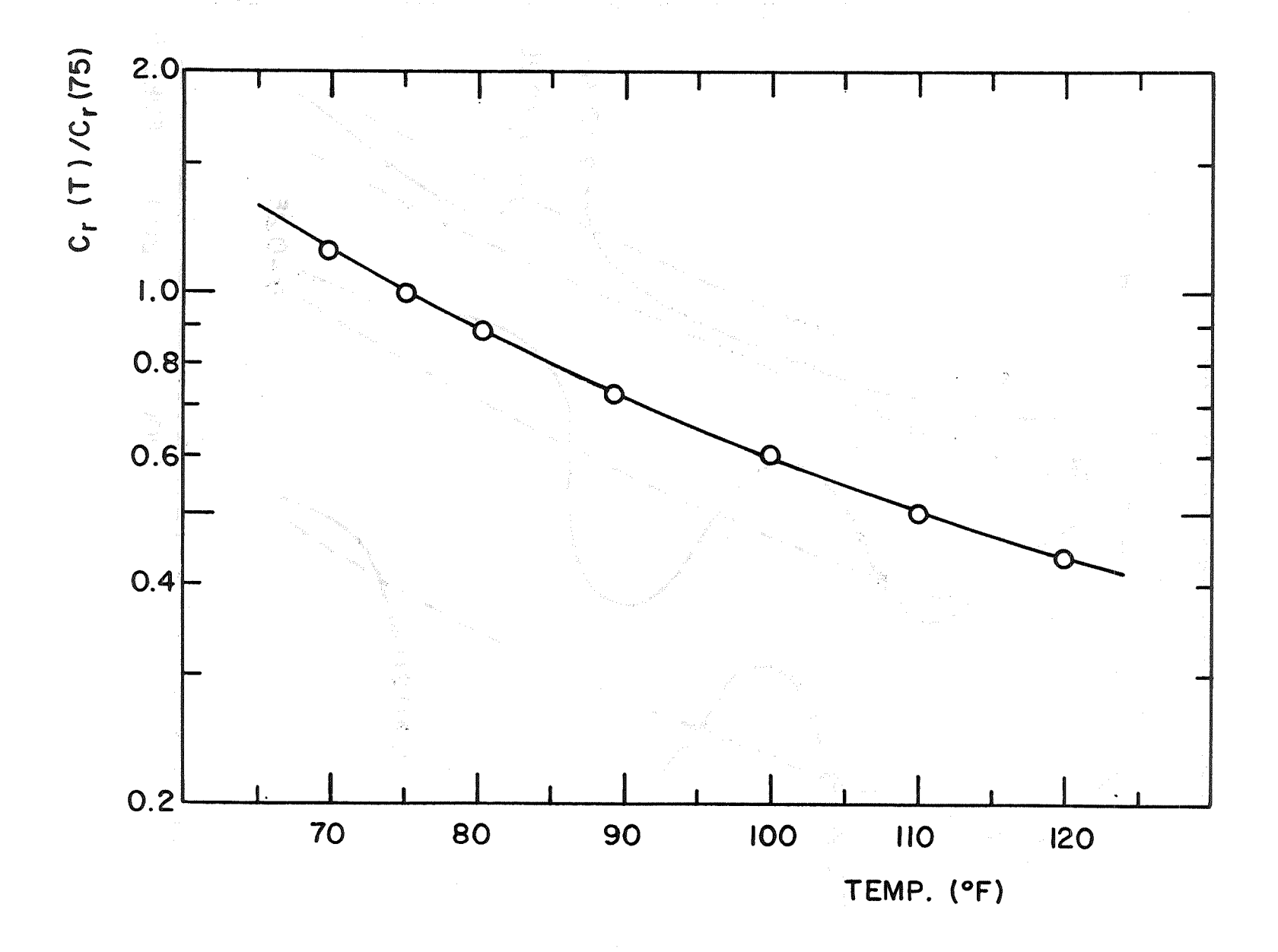


Fig. 24 Rod propagation velocity of a Plasticine rod as a function of temperature.

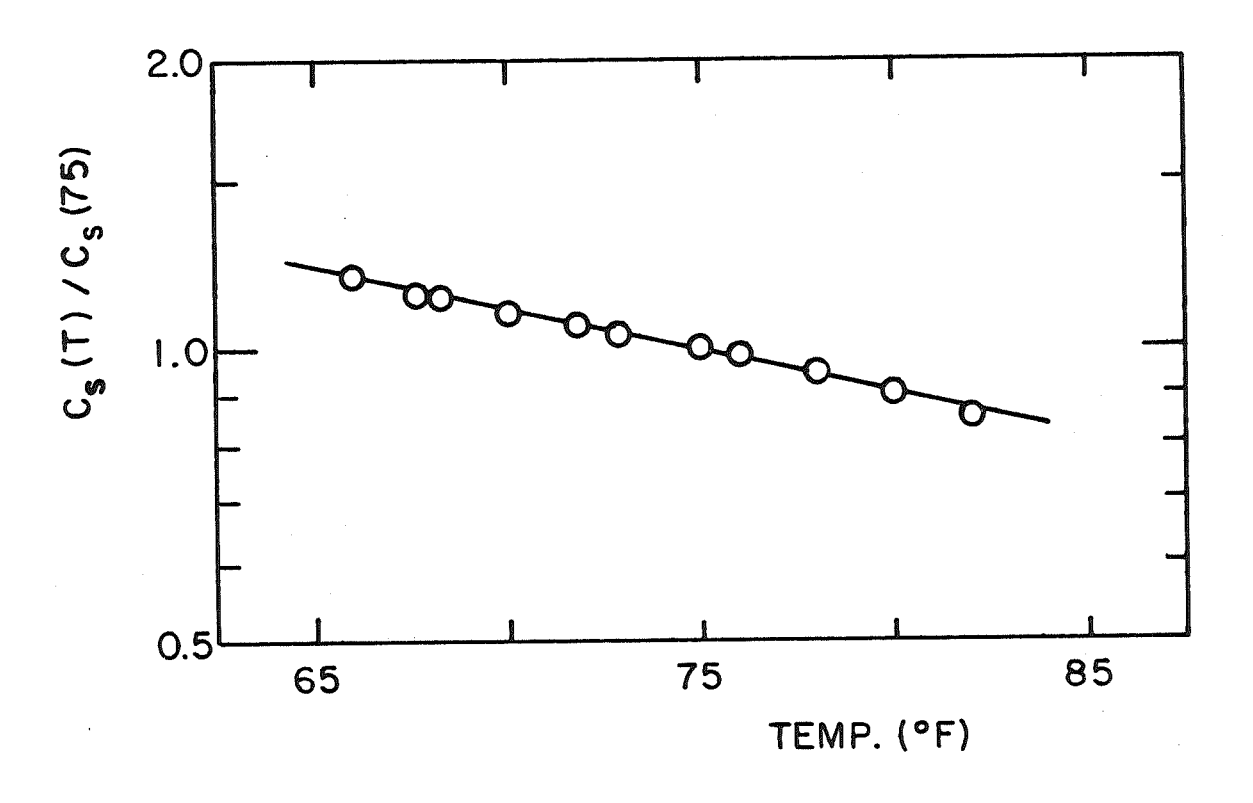


Fig. 25 Shear wave propagation velocity of a Plasticine slab as a function of temperature

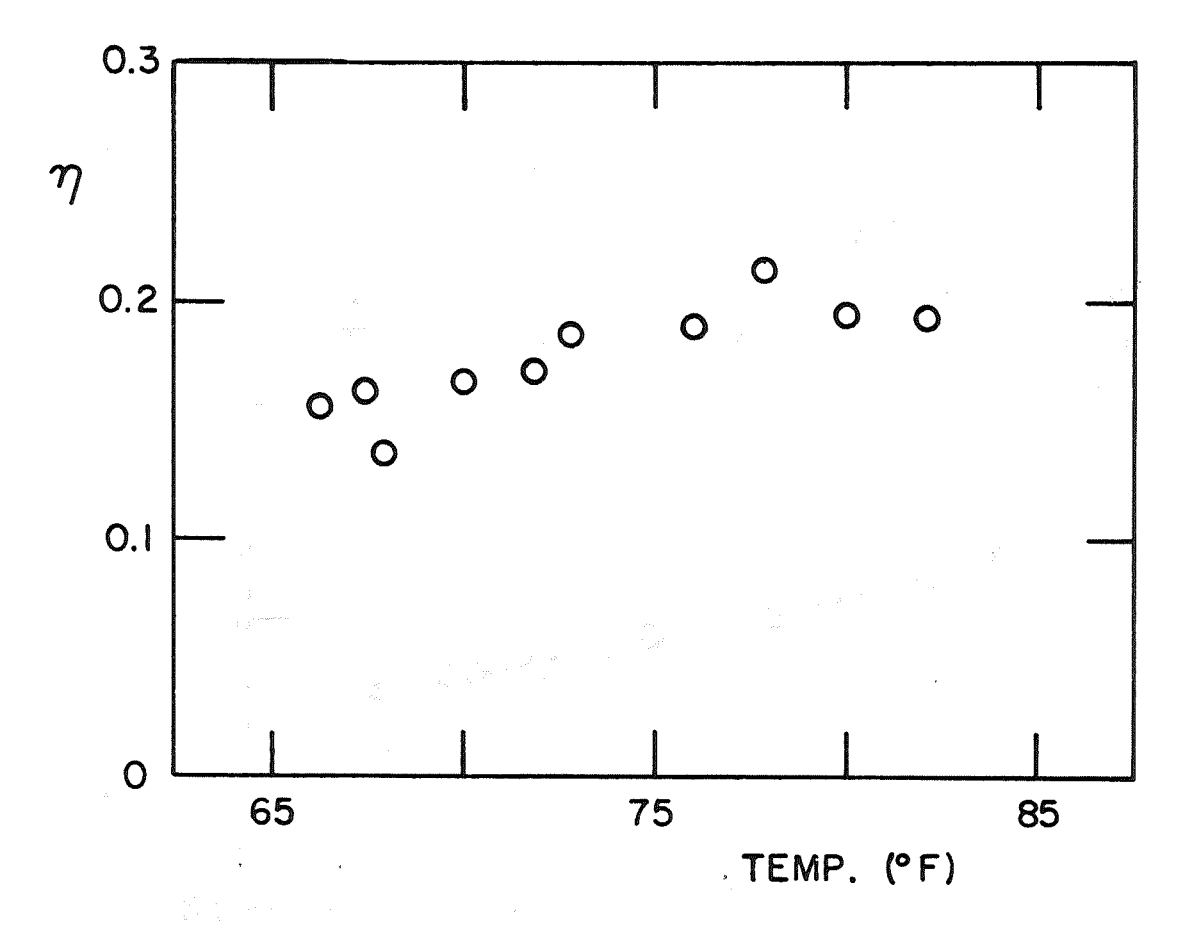


Fig. 26 Loss factor  $\eta$  for shear of a Plasticine slab. Points plotted are averages of measured values at the temperatures indicated.

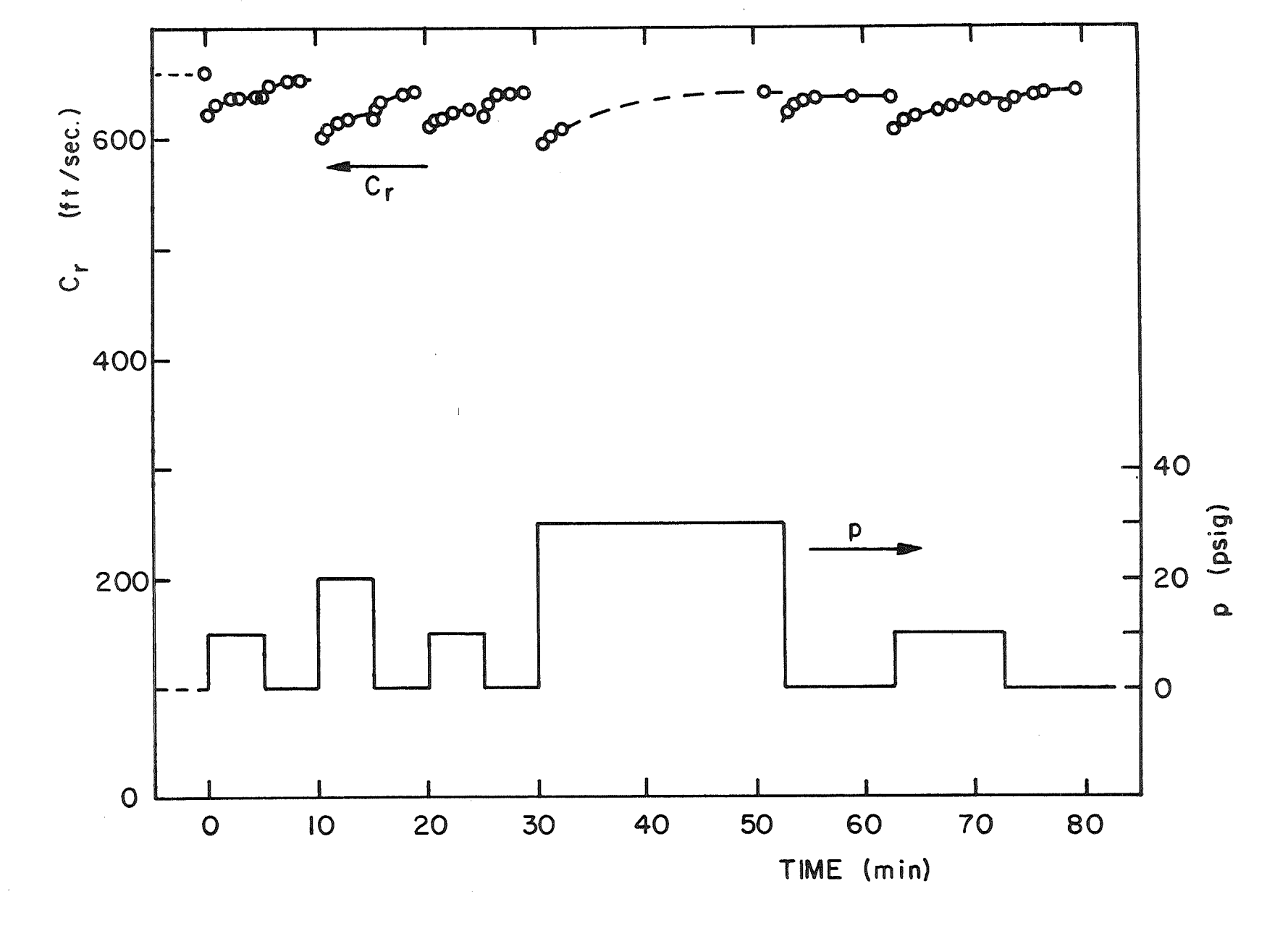


Fig. 27 Rod propagation velocity of a Plasticine rod at 75° F. due to time history of ambient pressure shown below.

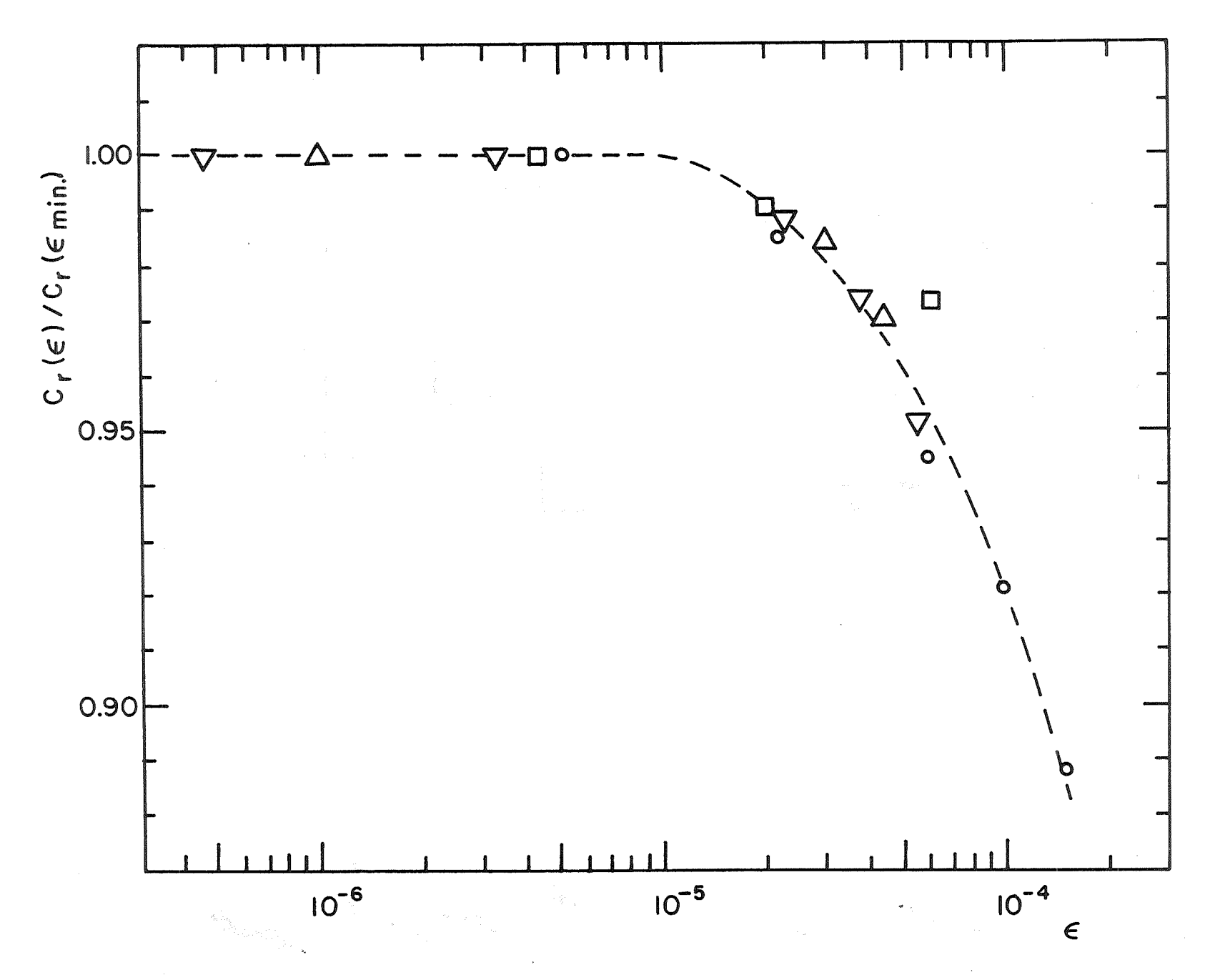


Fig. 28 Rod propagation velocity of four specimens as a function of longitudinal strain level.

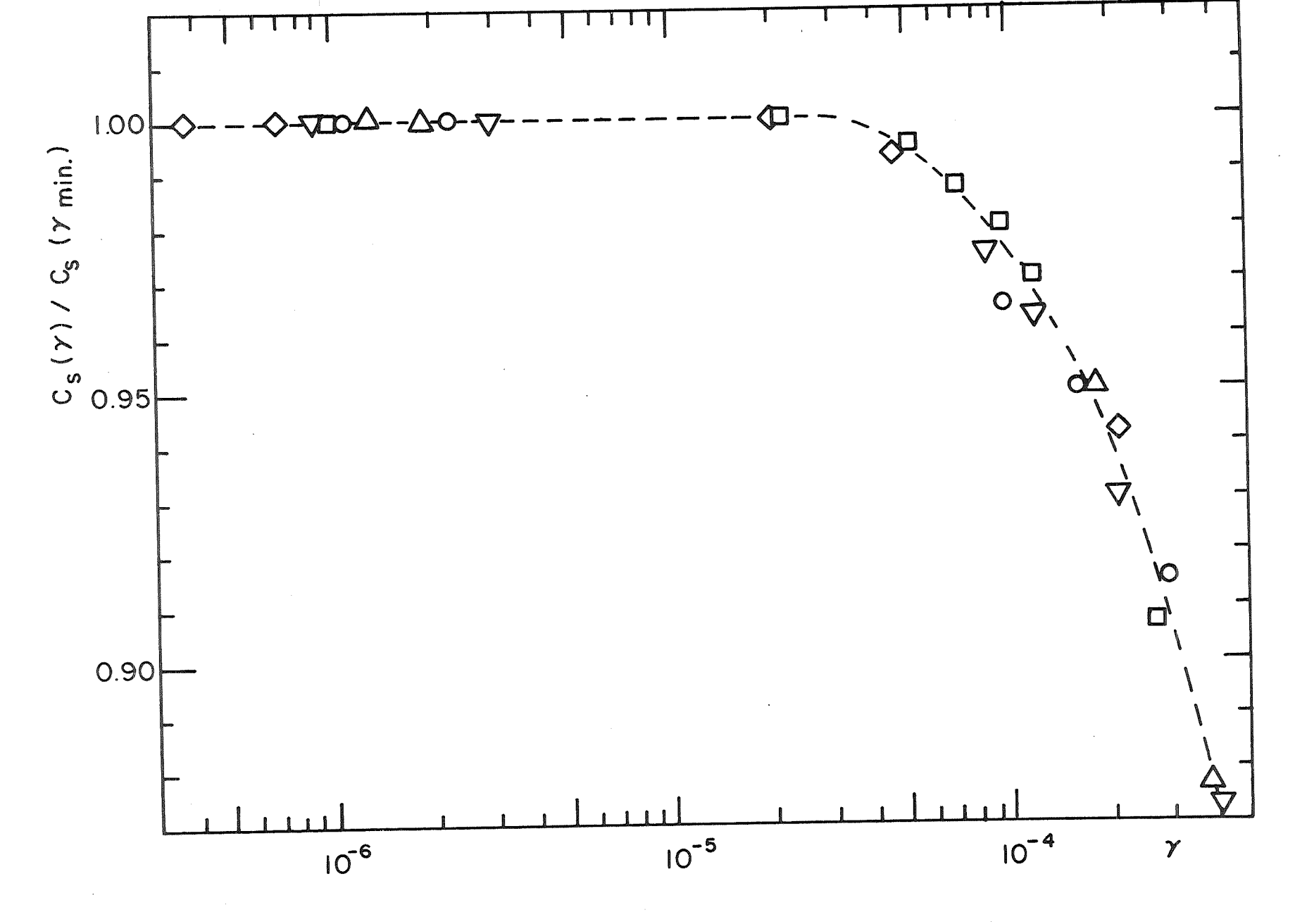


Fig. 29 Shear wave propagation velocity of clay slab with five different suspended masses as a function of shear strain level.

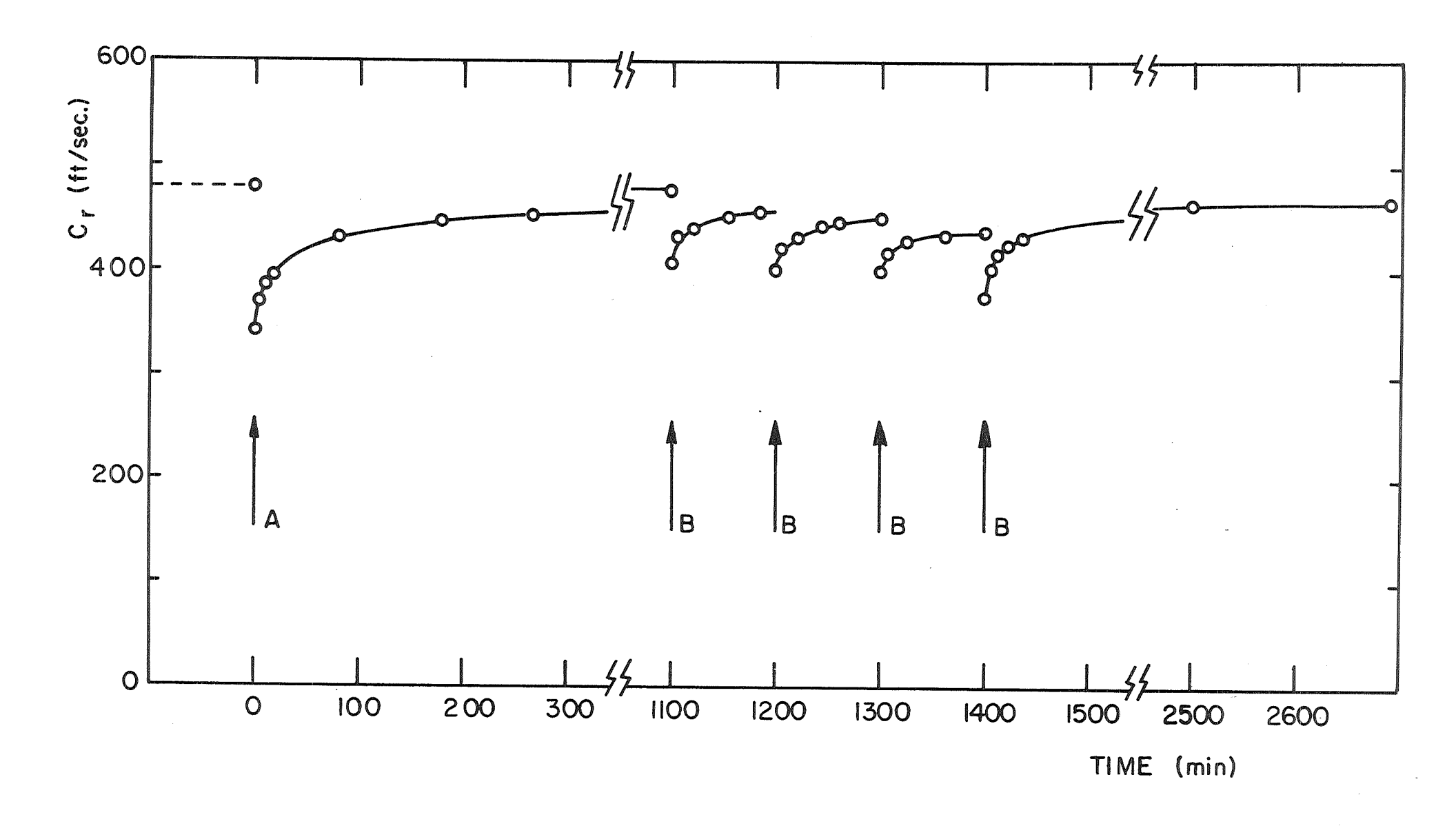


Fig. 30 Time history of rod propagation velocity in a 6" Plasticine rod due to manual bending at A and calibrated bending at B.

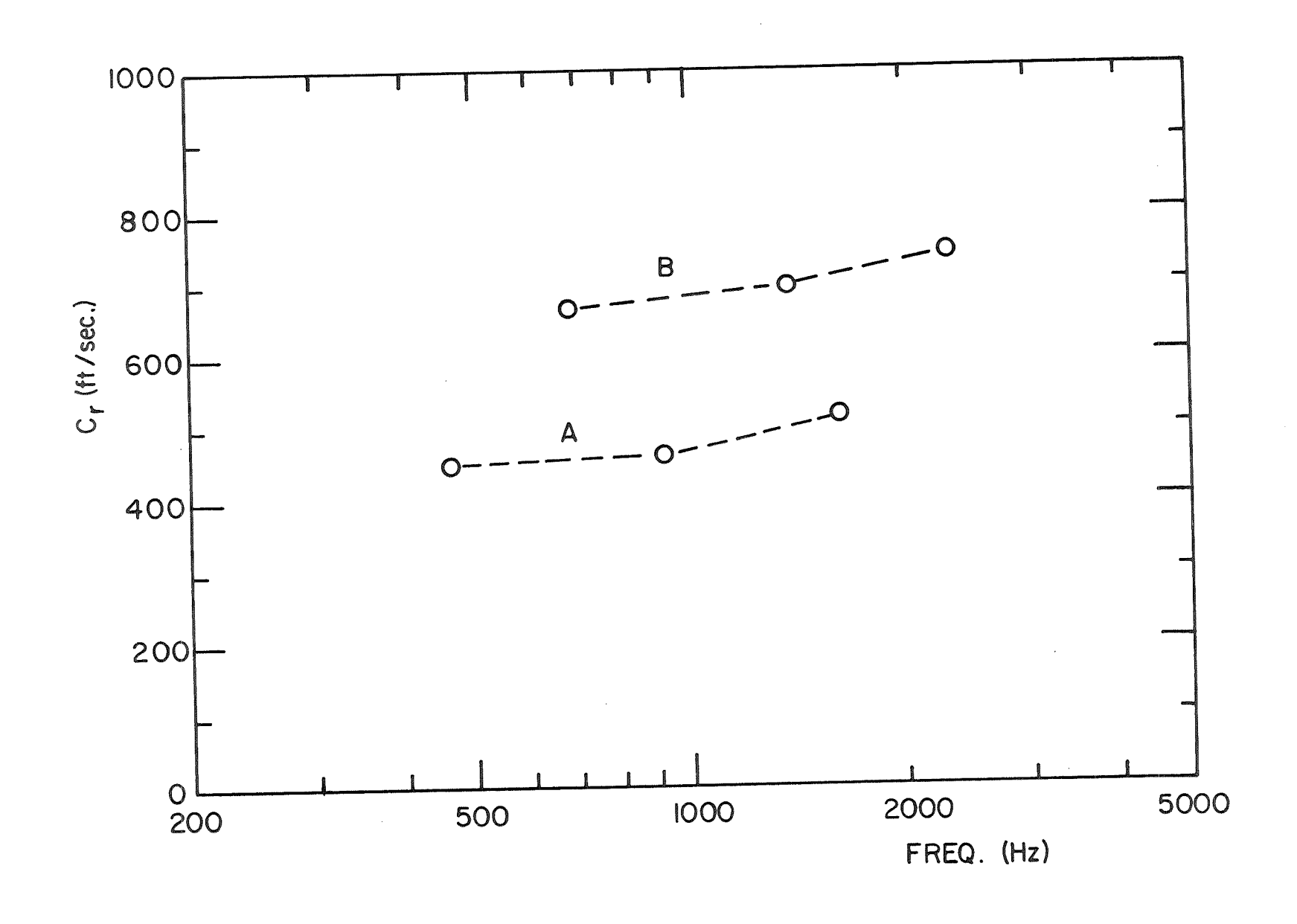


Fig. 31 Rod propagation velocity of a 3" Plasticine rod B, before and A, after large-strain bending.

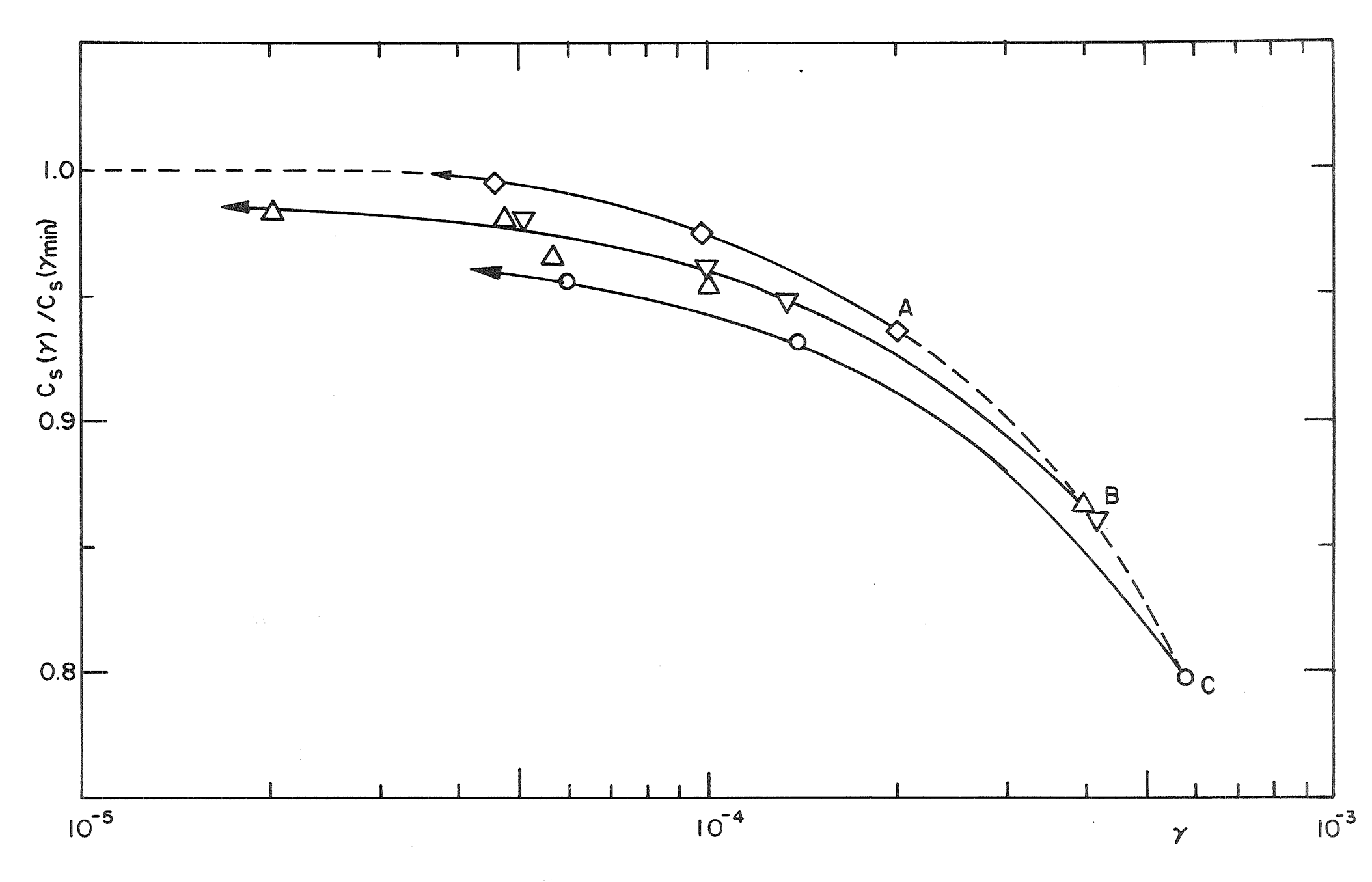


Fig. 32 Shear wave propagation velocity as a function of shear strain level measured as strain level is decreased from three different maximum strain levels A, B, and C.

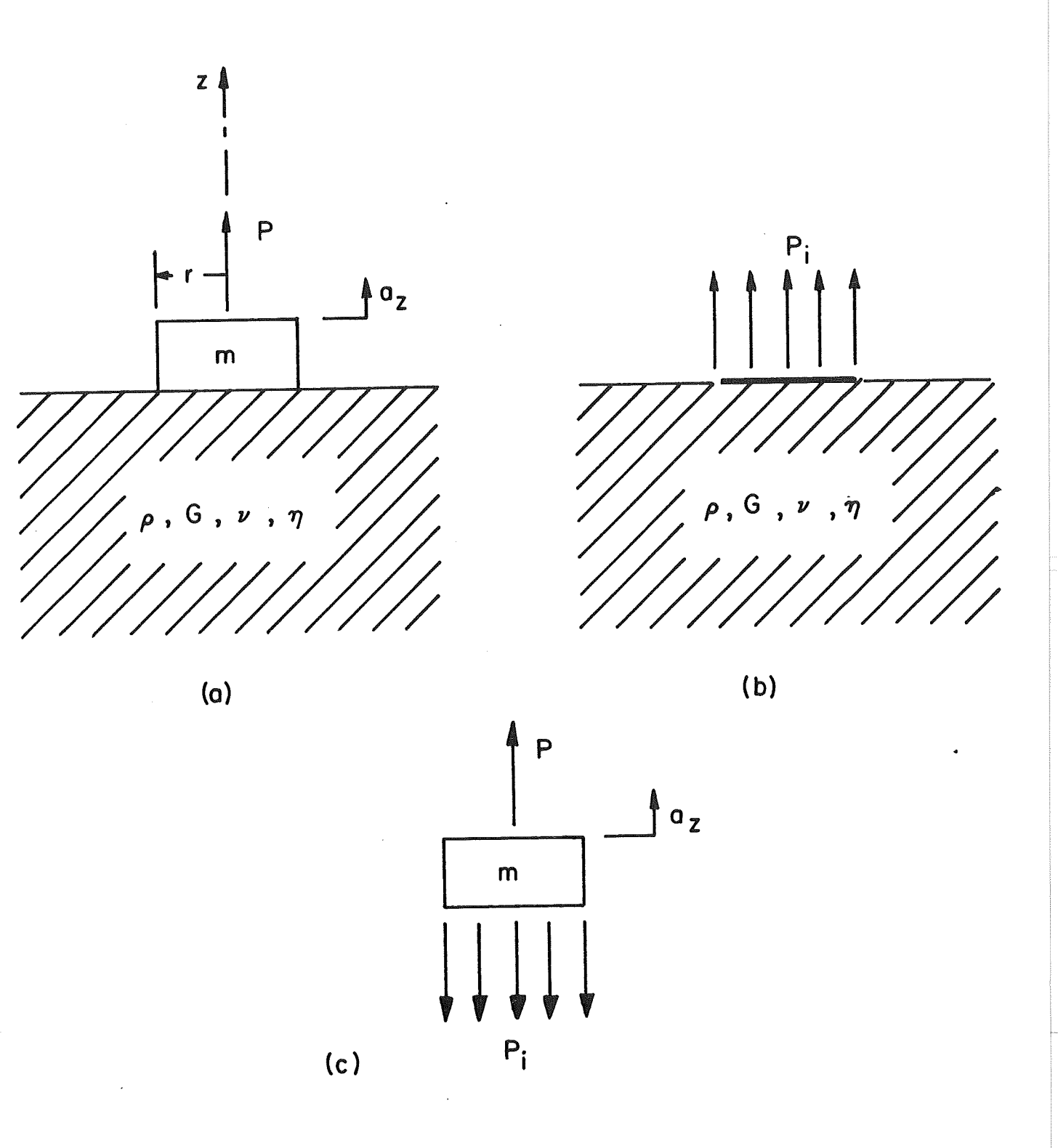


Fig. 33 Rigid disk on viscoelastic half space vibrating vertically at frequency  $\omega$ : (a) complete system (b) interaction force on half space (c) interaction force on disk

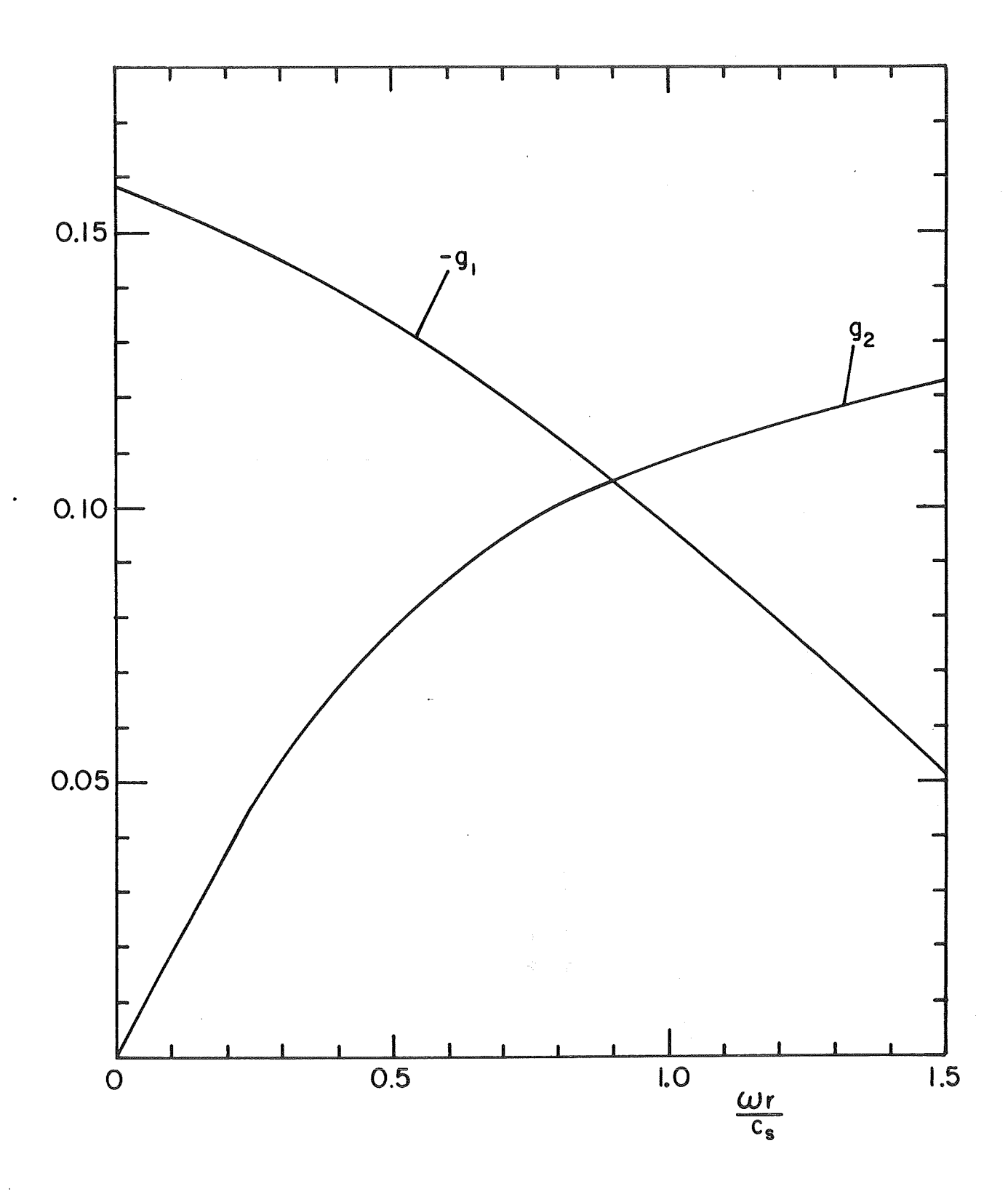


Fig. 34 Viscoelastic half space functions for v = 0.5 and  $\eta = 0.2$ 

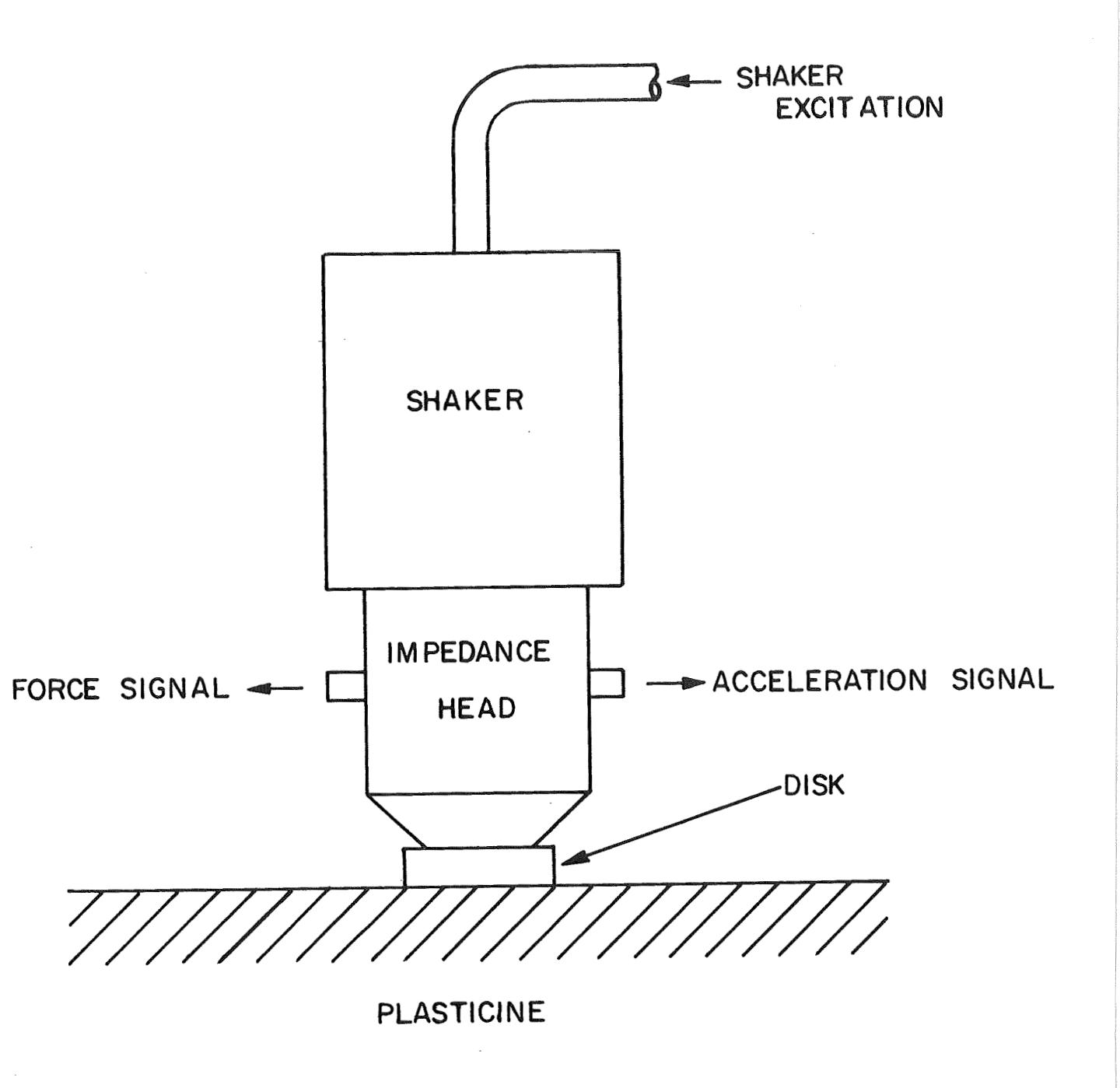


Fig. 35 Excitation of disk on surface of clay by Wilcoxon F-1 shaker driving through Wilcoxin Z-602 impedance head

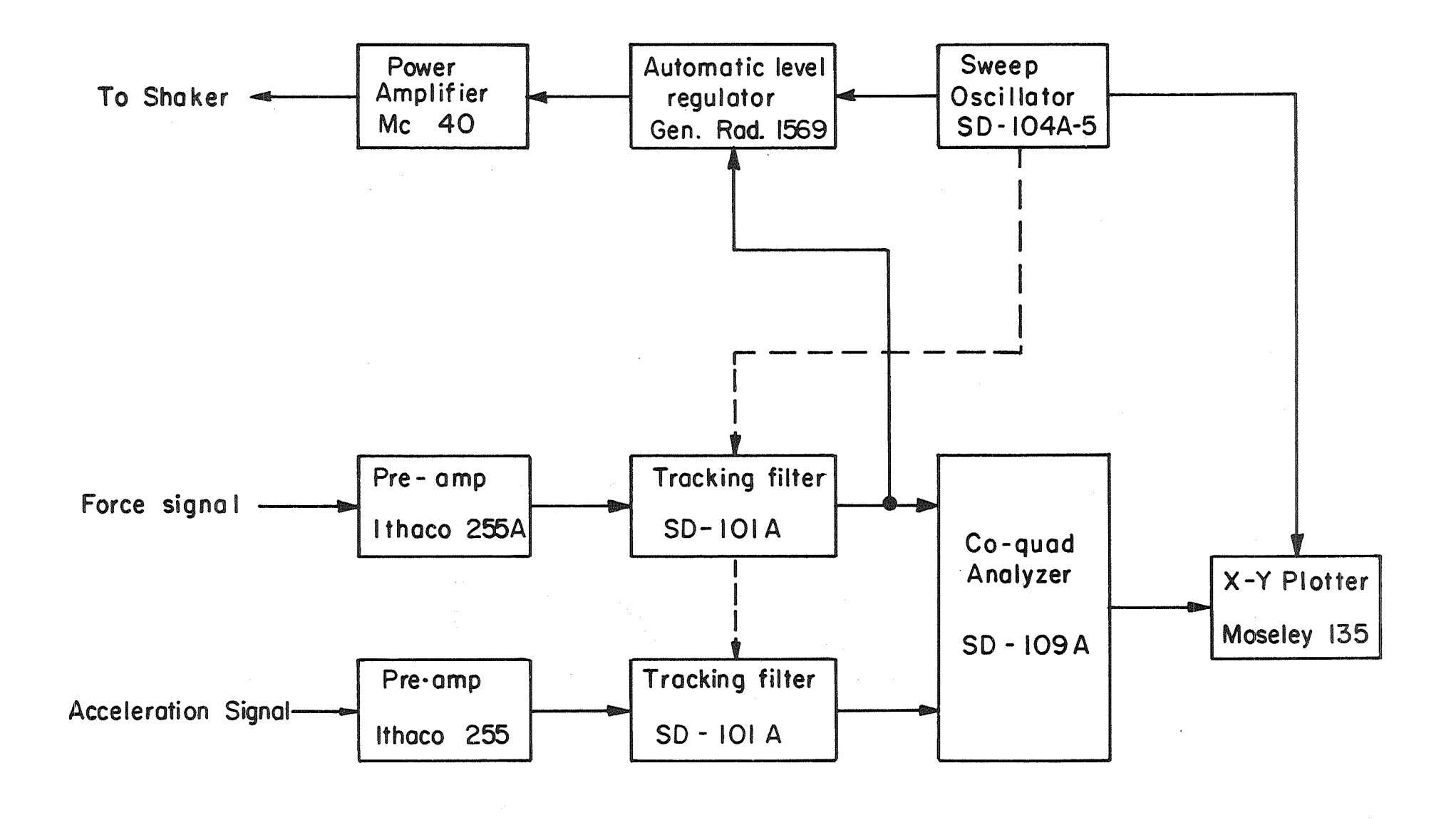


Fig. 36 Instrumentation chain for measurement of admittance of disk on the surface of a tub of clay

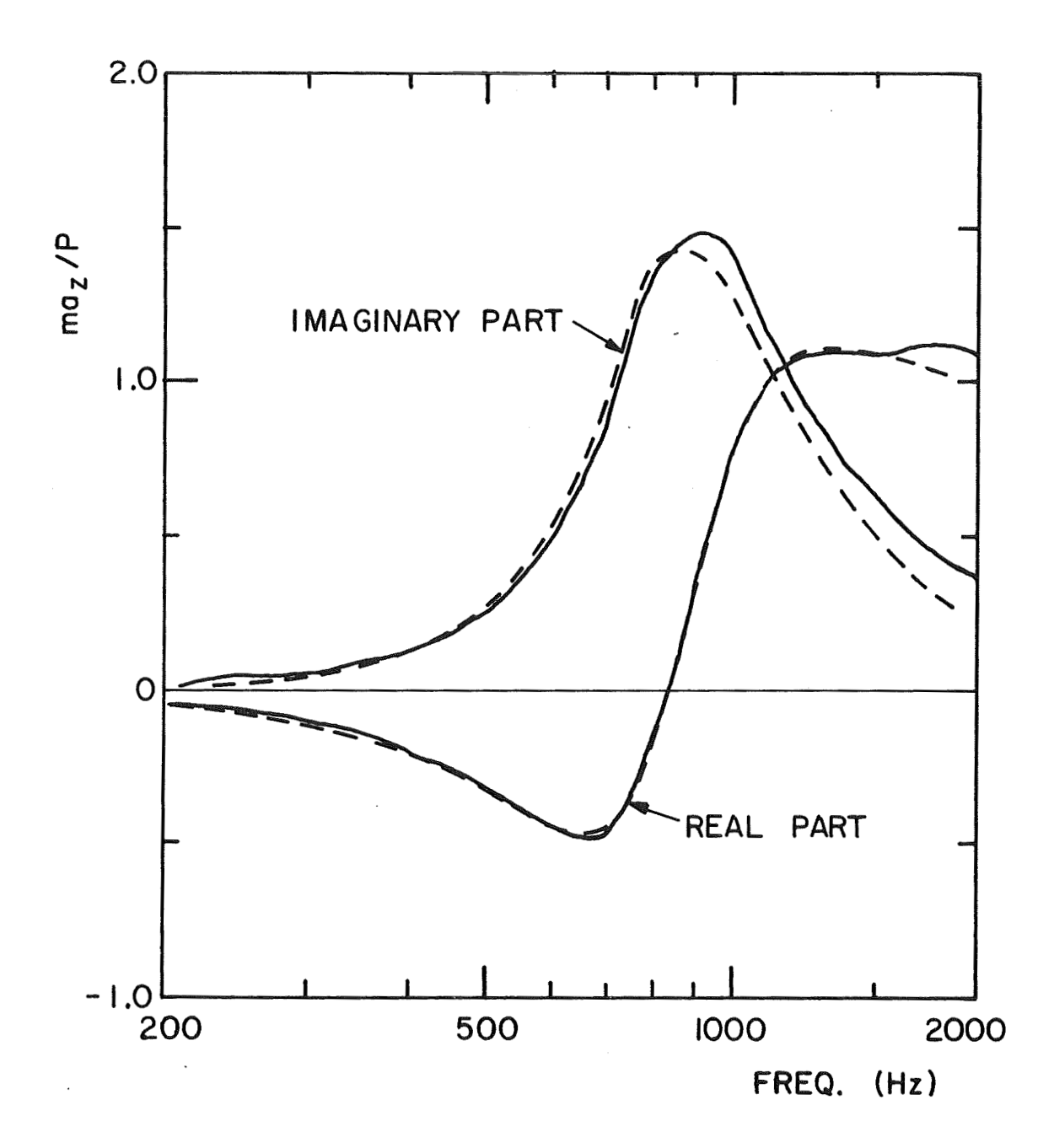


Fig. 37 Comparison of predicted admittance of disk on viscoelastic half space (dashed curve) with measured admittance of disk on tub of Plasticine (solid curve).